Thesis submitted in fulfillment of the requirements for the degree of Doctor (PhD)
in Engineering and Architecture from the Public University of Navarre

Evaluation of topographic correction algorithms on satellite images

Ion Sola Torralba

November 2015

Supervisors:
Jesús Álvarez Mozos
María González de Audícana Amenábar

upna Universidad Pública de Navarra Nafarroako Unibertsitate Publikoa

upna Universidad Pública de Navarra Nafarroako Unibertsitate Publikoa

ACKNOWLEDGEMENTS

First, I would like to thank my supervisors Professor Jesús Álvarez Mozos and Professor María González de Audícana Amenábar from the Department of Projects and Rural Engineering of the Public University of Navarre for helping and advising me throughout this challenging process. I would like to acknowledge Professor Jose Luis Torres Escribano from the Public University of Navarre because his indications considerably helped to improve this work.

Also, I am very grateful to the Institute for Applied Remote Sensing of the European Academy of Bozen (EURAC) for hosting me and sponsoring my studies there. I want to specifically acknowledge Doctor Ruth Sonnenschein and Ruben Remelgado for opening new lines of research on which we worked during the summer of 2014. I also want to express my gratitude to Abraham Mejia for being the perfect guide in our field trips across the Dolomites.

I would like to thank all external reviewers and members of the Doctoral Thesis Jury.

And of course, I would like to acknowledge my family, especially my parents for their unconditional support and trusting in me completely, and my grandmother who is always proud of me ; my friends and teammates of Hiru Herri, for helping me to disconnect after work; and especially Susana, for her unquestionable support day after day.

And anyone who has played any role during these years. Thanks to all of you!

TABLE OF CONTENTS

LIST OF ACRONYMS

Abbreviature	Meaning
RS	Remote Sensing
LU/LC	Land use / Land cover
TOC	TOpographic Correction
SPOT	Satellite Pour l'Observation de la Terre
SCS+C	Sun-Canopy-Sensor+C method
CC	C-correction method
SE	Statistic-Empirical method
COS	Cosine method
2SN	Two Stage Normalization method
MIN	Minnaert method
BRDF	Bidirectional Reflectance Distribution Function
DEM	Digital Elevation Model
EMIN	Enhanced Minnaert method
SM	Slope-Matching technique
sCC3	smooth C-Correction method (Smoothing factor = 3)
PBM	Pixel-Based Minnaert correction method
MM	Modified Minnaert method
VECA	Variable Empirical Coefficient Algorithm
AC	Atmospheric Correction
IRC	Integrated Radiometric Correction
FM3DR	Forward-Mode 3 Dimension Reflectance model
ASC	Adaptive Shade Compensation
ATCOR3	Atmospheric/Topographic CORrection for Mountainous Terrain
MFMTOPO	Multiple Forward Mode TOPOgraphic Correction method
PBCC	Pixel Based C-Correction method
ROT	ROTation model

SCOS	Smooth COSine correction
BC	B-Correction method
EKS	EKStrand topographic correction
MINSCS	Minnaert-Sun-Canopy-Sensor method
3F	Three-Factor correction
ADVCC	ADVanced C-Correction
ADVMIN	ADVanced MINnaert method
ICOS	Improved COSine method
BR	Band Ratioing
IGN	Instituto Geográfico Nacional
DN	Digital Number
TOARD	Top-Of-Atmosphere RaDiance
RMSE	Root Mean Square Error
LIDAR	Light Detection And Ranging
SD	Standard Deviation
CV	Coefficient of Variation
RMSD	Root Mean Square Deviation
SR	Synthetic Real image
SH	Synthetic Horizontal image
NIR	Near infrared
SWIR	Short Wave Infrared
SRF	Spectral Response Function
IEEE	Institute of Electrical and Electronics Engineers *(Journal)*
SPIE	Society of Photo-Optical Instrumentation Engineers *(Conference)*
RSE	Remote Sensing of Environment *(Journal)*
AET	Asociación Española de Teledetección *(Conference)*
ETRS89	European Terrestrial Reference System 1989
UTM30N	Universal Transverse Mercator. Zone 30 North
SSIM	Structural SIMilarity index
LTOC	Lambertian TOpographic Correction
NLTOC	Non-Lambertian TOpographic Correction

DIRSIG	Digital Imaging and Remote Sensing Image Generation
ASHRAE	American Society of Heating, Refrigerating, and Air-Conditioning Engineers
SMARTS2	Simple Model of the Atmospheric Radiative Transfer of Sunshine 2
AOD	Aerosol Optical Depth
UQI	Universal Quality Index
MSSIM	Mean Structural SIMilarity index
UTC	Coordinated Universal Time
ASTER	Advanced Spaceborne Thermal Emission and Reflection Radiometer
USGS	United States Geological Survey
HRG2	High Resolution Geometric 2
DOS	Dark Object Subtraction method
RGB	Red Green Blue
GN	Gobierno de Navarra /Government of Navarre
GV	Gobierno Vasco / Basque Government
IQR	InterQuartile Range
NDVI	Normalized Difference Vegetation Index
STOC	Stratified TOpographic Correction
SRC	Spectral Rule Classifier
CLC	Corine Land Cover
EEA	European Environmental Agency
MDE	Modelo Digital de Elevaciones

PARAMETER GLOSSARY

Symbol	Explanation
γ_i	Solar incidence angle
β	Terrain slope
θ_s	Solar zenith angle
φ_n	Pixel's aspect angle
φ_s	Solar azimuth angle
$E_{e,g}$	Global horizontal irradiance
$E_{e,s}$	Direct horizontal irradiance
$E_{e,d}$	Diffuse horizontal irradiance
x_1, x_2, x_3	% of irradiance corresponding to 0.5-0.9 μm
E_{ESNO}	Extraterrestrial normal irradiance
$T_{eL\ (2)}$	Linke's turbidity factor
a_{er}	Optical thickness of a Rayleigh atmosphere
m	Relative optical air mass
$E_{\beta,g}$	Global tilted irradiance
$E_{\beta,s}$	Direct tilted irradiance
$E_{\beta,r}$	Ground-reflected irradiance
$E_{\beta,d}$	Sky diffuse irradiance
Θ	Binary factor to model cast shadows
AI	Anisotropy index
V_d	Sky View Factor
V_t	Terrain View Factor
$E_{e,g\ adj}$	Global average horizontal irradiance
$\rho_{\ adj}$	Average reflectance
L_{sen}	At-sensor radiance
L_p	Path radiance
ρ	Land cover reflectance

T_u	Upward atmospheric transmittance
d	Sun-to-Earth distance correction factor
ρ'_a	Atmospheric albedo
θ_0	Viewing angle of the satellite
$l_{(x,y)}$	Luminance component of SSIM index
$c_{(x,y)}$	Contrast component of SSIM index
$s_{(x,y)}$	Structure index of SSIM index
$\alpha, \varepsilon, \omega$	Parameters to adjust the SSIM index
μ_x	Mean radiance of reference image
μ_y	Mean radiance of corrected image
σ_x	Standard deviation of reference image
σ_y	Standard deviation of corrected image
σ_{xy}	Covariance of reference and corrected image
c_1, c_2	are two user-defined constants included to avoid unstable results
h	Terrain altitude (m.)
L_e	Direct radiance
k_λ	Constant of Minnaert for band λ
c_λ	Empirical coefficient used by CC, sCC3 and SCS+C methods for band λ
A, B	Slope and intercept of the regression between $\cos\gamma_i$ and radiance/reflectance
$L_{sen,\lambda}$	At-sensor radiance for band λ
$L_{sen,corr,\lambda}$	Corrected at-sensor radiance for band λ
$\overline{L_{sen,\lambda}}$	Mean radiance of the image for band λ
$\Delta\hat{\sigma}$	Normalized standard deviation difference
$L_{p,\lambda}$	Path radiance for band λ
ρ_λ	Land cover reflectance
$T_{u,\lambda}$	Upward atmospheric transmittance for band λ
$E_{\beta,g,\lambda}$	Global tilted irradiance for band λ
$E_{e,s,\lambda}$	Direct horizontal irradiance for band λ
$E_{e,d,\lambda}$	Diffuse horizontal irradiance for band λ
$E_{e,g,\lambda\ adj}$	Global average horizontal irradiance for band λ
$\rho_{\lambda,adj}$	Average reflectance for band λ

r^2	Coefficient of determination for band λ
L	Dynamic range
k_1, k_2	Constants used by SSIM index
γ'_i	Solar incidence angle obtained from smoothed slope
k_λ *	Pixel-based k_λ of band λ obtained stratifying the image by terrain slope ranges
$L_{LAMB,\lambda}$	Radiance of band λ after a Lambertian correction, i.e., COS method
G	Correction factor to avoid the overcorrection (MM method)
μ_k	Mean value of the scaled (0–255) cosγ_i for the main cover type
X_{ij}	Scaled (0–255) cosine of γ_i for pixel ij for the main cover type
$c_{2sn,\lambda}$	Empirically-derived calibration coefficient of band λ (2SN method)
$L_{sen,max,\lambda}$ /$L_{sen,min,\lambda}$	Maximum and minimum radiance value for main cover type
μ_w	Mean value of the scaled cosγ_i the main cover type on sunny slopes
$c_{sm,\lambda}$	Modified correction coefficient of band λ (SM technique)
β_t	Threshold angle introduced by MM correction

LIST OF FIGURES

LIST OF TABLES

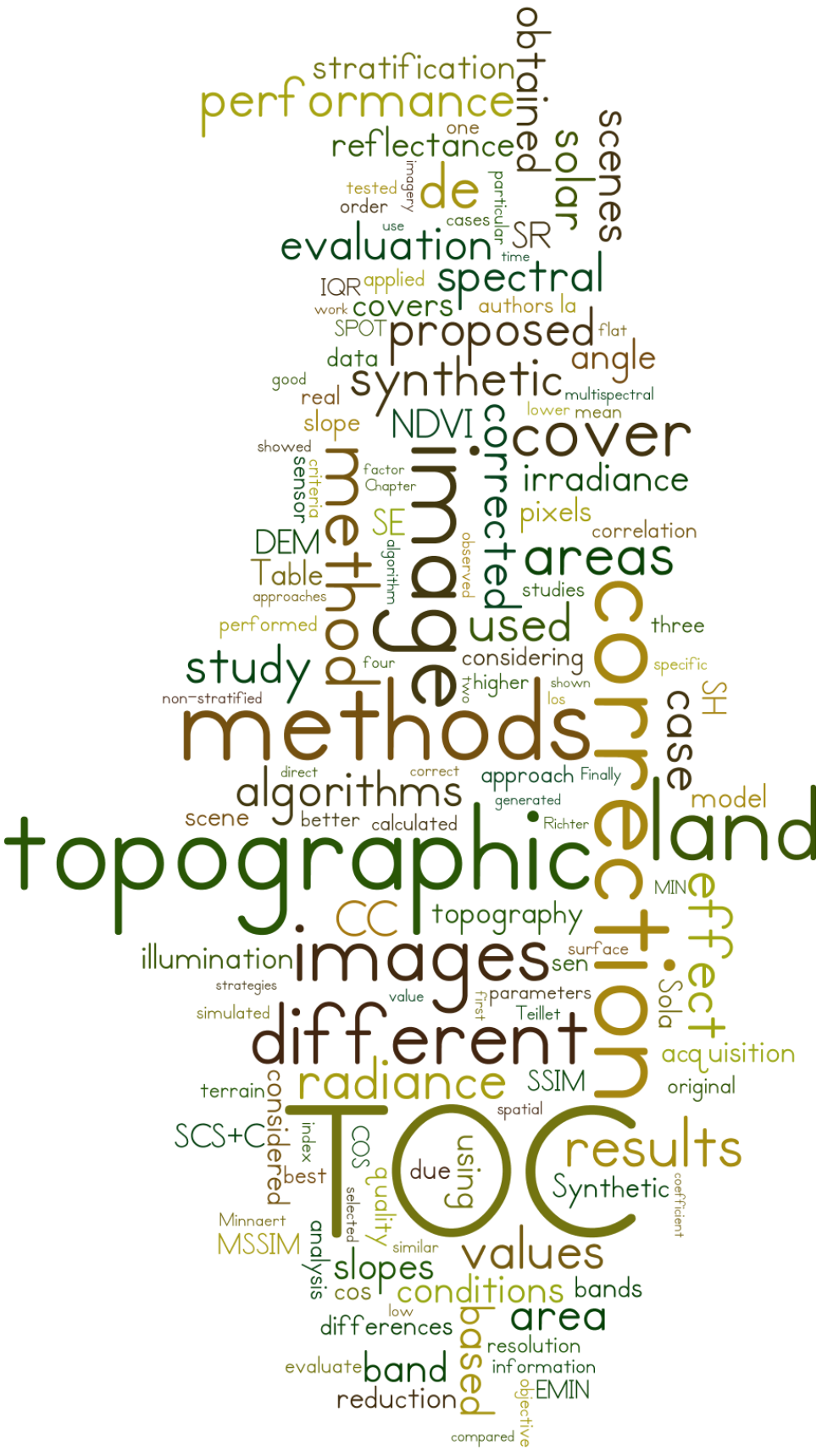

ABSTRACT

The use of Remote Sensing data in mountainous areas is hampered by the radiometric distortions introduced by the topography. These distortions impact the spectral signatures of land covers and thus the radiance values detected by the sensor. This effect, so called topographic effect, has a negative influence on the quality of products derived from Remote Sensing data in several applications, such as land use or land cover cartography, change detection or retrieval of biophysical parameters.

In the last decades different topographic correction methods have been proposed in order to solve this problem, but there is not a single correction method that outperforms the rest in every situation. In fact, the performance of topographic correction algorithms depends not only on the study site, its local topography, illumination conditions and land cover distribution but also on the selected evaluation criteria.

Different evaluation strategies have been proposed in the literature to assess the quality of the topographic correction, but each has its own limitations and a simple and objective procedure is missing. The objective of this thesis is to analyze and assess the existing topographic correction methods considering the main factors involved in the scene acquisition

process, that is, the sensor's characteristics, the acquisition date and time, the solar geometry, the Earth surface relief and the spatial distribution of land covers on the study site.

Our findings contribute to the previously limited knowledge regarding the quality of topographic correction by proposing a new methodology based on synthetic images. This new methodology has been tested on SPOT 5 scenes in different study sites over mountainous regions of Northern Spain, for different acquisition dates and solar geometries. Therefore, the performance of topographic correction algorithms has been evaluated on different conditions. Moreover, this new methodology has been combined with other evaluation criteria proposed in the literature to perform a multi-criteria analysis of the most popular correction methods. The thesis has focused in the semi-empirical topographic correction methods due to their simplicity, ease of implementation and good performance. Finally, the quality of topographic correction has been assessed in combination with a priori land cover stratification.

Our results suggest a good performance of semi-empirical methods, especially Sun-Canopy-Sensor+C, C-Correction, and Statistic-Empirical methods, in most situations. Nevertheless, no method achieved to correct areas where the cosine of solar incidence angle was close to zero or negative (shadows), and some methods showed problems of overcorrections, such as the Cosine method, the Two Stage Normalization method or the Minnaert method. Unlike other studies that tested stratified topographic correction, our findings with this regard suggest only a minor improvement when compared to a non-stratified strategy. This work is expected to be a contribution to the limited knowledge of this effect and to the adequate implementation of these techniques on topographic correction.

RESUMEN

La utilización de información remota en relieves montañosos se ve fuertemente afectada por las distorsiones radiométricas que introduce la topografía. Estas distorsiones hacen variar la firma espectral de las cubiertas y por tanto los valores de radiancia que detecta el sensor. Este efecto, conocido como efecto topográfico, tiene una influencia negativa en los productos derivados de imágenes de satélite en distintas aplicaciones, tales como cartografía de usos y cubiertas, detección de cambios o estimación de parámetros biofísicos.

En las últimas décadas un gran número de métodos de corrección topográfica han sido propuestos para resolver este problema, pero no existe un único método que funcione mejor que el resto en cualquier situación. De hecho, el rendimiento del método de corrección topográfica depende no sólo del área de estudio, su topografía, las condiciones de iluminación y la distribución de cubiertas, sino también del criterio de evaluación empleado.

Se han propuesto diferentes estrategias de evaluación en la literatura que permiten cuantificar la calidad de la corrección topográfica, pero la mayoría de ellas tienen limitaciones y faltaba un procedimiento simple y objetivo de evaluación. El objetivo de esta tesis es analizar y evaluar los métodos de corrección topográfica existentes considerando los

principales factores que influyen en el proceso de adquisición de la imagen, tales como las características propias del sensor, la fecha y hora de adquisición, la geometría solar, el relieve de la superficie terrestre y la distribución espacial de las cubiertas en la zona de estudio.

Este trabajo contribuye al previamente limitado conocimiento acerca del rendimiento de los métodos de corrección topográfica proponiendo una nueva metodología de evaluación basada en imágenes sintéticas. Esta nueva metodología ha sido testada en imágenes SPOT 5 en diferentes zonas de estudio, principalmente en regiones montañosas del norte de España, considerando diferentes fechas y horas de adquisición, y por tanto diferentes geometrías solares. Por tanto, el rendimiento de los métodos de corrección topográfica ha sido evaluado en diferentes condiciones. Además, esta nueva metodología ha sido combinada con otros criterios de evaluación para llevar a cabo un análisis multi-criteria de los métodos más populares, centrándonos principalmente en los métodos semi-empíricos debido a su sencillez, facilidad de aplicación, operatividad y buenos resultados. Por último se ha evaluado la calidad de la corrección topográfica en combinación con una estratificación de cubiertas previa.

Los resultados obtenidos demuestran el buen rendimiento de los métodos semi-empíricos, principalmente Sun-Canopy-Sensor+C, C-Correction y el método Estadístico Empírico, en la mayoría de situaciones. Sin embargo, ninguno de los métodos testados alcanza a corregir las zonas sombreadas donde el coseno del ángulo de incidencia solar es próximo a cero o negativo, y algunos métodos muestran signos evidentes de sobrecorrección. Este es el caso de los métodos del Coseno, Two Stage Normalization Method o del método de Minnaert, entre otros. A diferencia de otros estudios que demostraron un rendimiento superior de la corrección topográfica estratificada, los resultados obtenidos en nuestra zona de estudio reflejan una mejora insignificante de la calidad fruto de la estratificación. Se espera que este trabajo contribuya al entendimiento de este efecto y a la adecuada implementación de técnicas para su corrección.

PUBLICATIONS

The dissertation is presented as a compendium of publications about topographic correction of satellite images. This set of articles has recently been published or are being published following the same line of research:

- Sola, I.; González-Audícana, M.; Álvarez-Mozos, J.; Torres, J.L. (2014). Synthetic images for evaluating Topographic Correction Algorithms. *IEEE Transactions on Geoscience and Remote Sensing*, vol. 52, issue 3, pp. 1799 - 1810. doi: 10.1109/TGRS.2013.2255296. Impact factor: 3.514. Subject category: Remote Sensing (rank 2 out of 28). Received 5 March 2012 / Revised 27 November 2012 and 12 February 2013 / Accepted 12 March 2013 / Published: 15 May 2013.

- Sola, I.; González-Audícana, M.; Álvarez-Mozos, J. (2015). Validation of a Simplified Model to Generate Multispectral Synthetic Images. *Remote Sensing*, vol. 7, pp. 2942-2951. doi:10.3390/rs70302942. Impact factor: 3.180. Subject category: Remote Sensing (rank 5 out of 28). Received: 23 December 2014 / Revised: 20 February 2015 / Accepted: 4 March 2015 / Published: 12 March 2015.

- Sola, I.; González-Audícana, M.; Álvarez-Mozos, J.; Torres, J.L. (2014). Evaluación multitemporal de métodos de corrección topográfica mediante el uso de imágenes sintéticas multiespectrales. *Revista Teledetección* vol. 41, pp. 71-78. doi: http://dx.doi.org/10.4995/raet.2014.2246, Available in: http://polipapers.upv.es/index.php/raet/article/view/2246. Published: June 2014.

- Sola, I.; González-Audícana, M.; Álvarez-Mozos, J. (2015). Multi-criteria evaluation of topographic correction methods. Remote Sensing of Environment. Submitted: 31st July 2015. Impact factor: 6.393. Subject category: Remote Sensing (rank 1 out of 28).Pending review.

- Sola, I.; González-Audícana, M.; Álvarez-Mozos, J. (2015). On the added value of stratified topographic correction of multispectral images. *Remote Sensing*. Impact factor: 3.180. Subject category: Remote Sensing (rank 5 out of 28). Submitted: 20st November 2015.

CHAPTER 1

INTRODUCTION

1.1. State of the art

The availability of satellite data has grown exponentially in the last years and their applications in different fields, such as land resource planning, LU/LC cartography, change detection, retrieval of biophysical parameters or studies of environmental change and biodiversity conservation, have increased accordingly. Thus, the demand for land cover information has increased, and consequently this topic became probably the most widely applied in Remote Sensing (RS) (Cihlar 2000). Land cover is a critical variable that links many parts of the human and physical environments. Accurate and updated information on land cover is required for a plethora of applications, including forest monitoring and change detection, retrieval of land cover biophysical parameters, agriculture, or risk assessment, and in terms of cost-effectiveness RS data provides the most efficient alternative to obtain it (Foody and Mathur 2004).

Distortions of the radiance measured by sensors are inherent to any image acquisition process, yet they can substantially affect the quality of RS data; hence, pre-processing operations have to be performed. These operations are becoming more and more important to extract accurate information from satellite imagery in RS applications, such as classification and image interpretation, LU/LC mapping, change detection or retrieval of biophysical parameters. Summing up, the capability of satellite images to provide reliable information is restricted by radiometric effects caused by: 1) the intensity of solar irradiance, 2) the atmospheric effects, 3) the bidirectional reflectance distribution function (BRDF) of the surface, and 4) the spectral response functions of the sensor spectral bands (Sandmeier and Itten 1997).

In mountainous areas, special emphasis has to be put on the influence of topography on solar irradiance, which seriously affects any quantitative analysis based on RS data. Therefore, topographic correction, which eliminates the terrain effect caused by the topographic relief, becomes one of the fundamental steps in pre-processing high-resolution RS data (Tan et al. 2013), since it is responsible for the same land cover having a different spectral signature due to the topographic characteristics (Gao and Zhang 2009b). In particular, the radiance detected by sensors can significantly vary depending, not only on the reflectance of land

covers, but also on the slope and aspect of the areas where they are located (Riaño et al. 2003). This phenomenon, normally referred to as the topographic effect, has negative consequences on the interpretation and extraction of accurate information from RS scenes, particularly in environmental and forestry applications, frequently related to areas with very significant topography.

The aim of topographic correction (TOC) is thus to compensate differences in solar irradiance between areas with differing slope and aspect and, ultimately, to obtain the radiance values the sensor would have obtained in case of a perfectly flat surface.

1.1.1. TOC algorithms

The topographic effect has long been recognized as an important problem for quantitative analyses of remotely sensed data (Zhang et al. 2015). During the last two decades, several procedures have been proposed to correct or attenuate the topographic effects on the radiance measured by satellites. This radiance depends on the direct, diffuse and reflected irradiance impinging on the Earth surface, being the direct component directly related to the cosine of solar incidence angle, $\cos\gamma_i$.

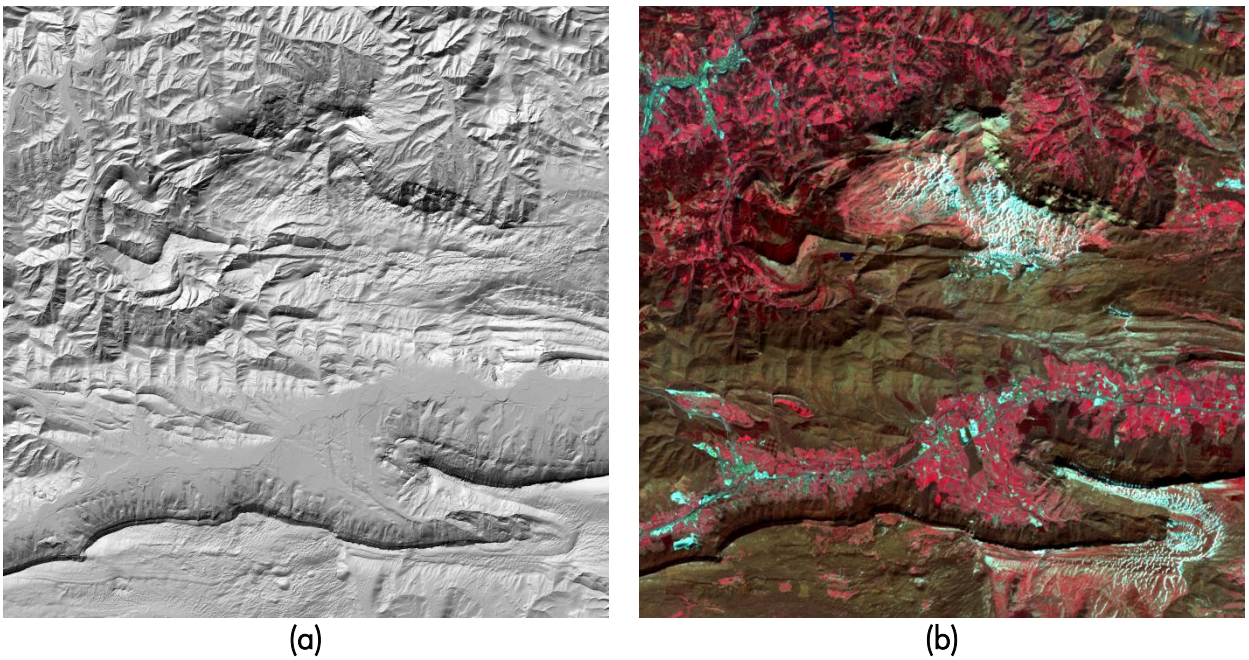

(a) (b)

Fig. 1.1. (a) Image of illumination ($\cos\gamma_i$) and (b) RGB composition of Landsat 8 subscene of a mountainous area.

This angle defines the illumination conditions for each pixel, and can be calculated based on the solar geometry at the acquisition time, and the terrain slope and aspect of these pixels (Eq. 1.1).

$$cos\gamma_i = cos\beta cos\theta_s + sin\beta sin\theta_s cos(\varphi_s - \varphi_n) \qquad (1.1)$$

where, β is the terrain slope, θ_s the solar zenith angle, φ_s the solar azimuth angle and φ_n the terrain aspect. Both β and φ_n are pixel-based values computed from the DEM.

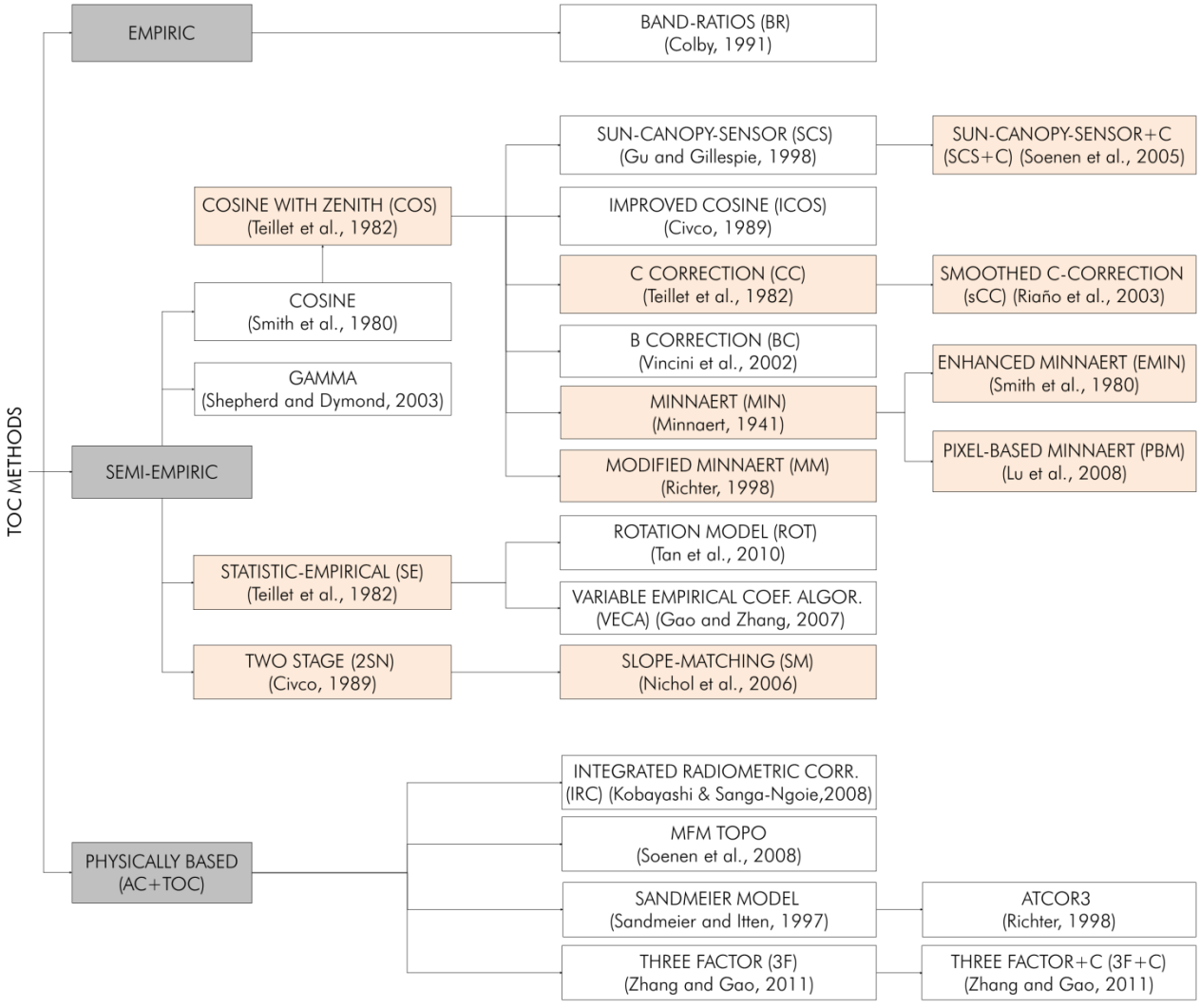

Fig. 1.2. Scheme of the most widely-used TOC algorithms

According to Balthazar (2012), TOC methods can be grouped into three subcategories (see Fig. 1.2): Empirical methods, semi-empirical methods, and physically based methods. The first category integrates simple empirical methods, such as band ratioing, that does not require additional auxiliary data (Balthazar et al. 2012). These simple operations are based on the assumption that radiometric distortions introduced by the topographic effect on reflectance values are proportional in all bands. These procedures are easily implemented, but Colby (1991) concluded that they only partially removed the topographic effect, whereas Mulder (1988) claimed their output did not have a physical meaning.

The second group consists of semi-empirical methods that require a DEM to model the variations introduced by the topography on the solar irradiance impinging on the surface (Ghasemi et al. 2013; Hantson and Chuvieco 2011).

Early in the 1980s, Smith et al. (1980) originally proposed the simplest and probably the most popular semi-empirical method, i.e., the Cosine method (COS), later modified by Teillet et al. (1982). This method normalized the radiance/reflectance of any pixel based on the assumption that the total irradiance received at any tilted surface was directly proportional to its $\cos\gamma_i$, but it did not take into account diffuse irradiance from atmospheric or terrain sources (Conese et al. 1993; Proy et al. 1989) and relied upon the Lambertian assumption, which is not always applicable to natural surfaces (Soenen et al. 2005). As a result, many authors reported problems of overcorrection on areas that are weakly illuminated by direct irradiance (Ghasemi et al. 2013; Law and Nichol 2004; Twele et al. 2006).

To overcome these limitations, several non-Lambertian methods were developed, including band dependent parameters to simulate other radiative components, such as the sky diffuse irradiance, terrain reflected irradiance or BRDF of the ground objects (Dymond and Shepherd 1999; Gu and Gillespie 1998; Lu et al. 2008; Richter and Schläpfer 2002; Wen et al. 2009).

The most used semi-empirical TOC algorithm is probably the Minnaert correction method (MIN), originally developed by Minnaert (1941), that included a k_λ constant to characterize surface anisotropic properties of each land cover for every spectral band. Several alternative algorithms were proposed based on the Minnaert method, such as the Enhanced Minnaert (EMIN) proposed by Smith et al. (1980) including the terrain slope in the equation, or the

Pixel-based Minnaert (PBM) (Lu et al. 2008) based on a relationship established between Minnaert k_λ coefficients and topographic slopes. Similarly, Richter (1998) proposed a modified Minnaert (MM) approach that minimized the overcorrection of Lambertian correction on weakly illuminated slopes reducing the corrected radiance/reflectance values according to a set of empirical rules in those areas where the solar incidence angle exceeded an established threshold.

Another widely used semi-empirical method is the C-Correction (CC), which introduced a parameter c_λ, in order to reduce the effects from diffuse irradiance and terrain reflected irradiance (Karathanassi et al. 2000). Besides, Riaño et al. (2003) proposed a modification of this method based on slope-smoothing to improve its performance.

To take into account specific attributes of arboreal land covers, Gu and Gillespie (1998) proposed a method for forested areas based on subpixel Sun–Canopy–Sensor geometry, so called SCS. This method was later modified by Soenen et al. (2005) to account for diffuse atmospheric irradiance and terrain reflected irradiance by introducing the previously mentioned parameter c_λ, i.e., SCS+C correction.

Furthermore, other simple semi-empirical approaches have also been proposed based on statistical relationships between the radiance/reflectance of each band before correction and $\cos\gamma_i$. The Statistic-Empirical method (SE) of Teillet et al. (1982), assumed that this relationship was linear. Similarly Gao and Zhang (2007) proposed the Variable Empirical Coefficient Algorithm (VECA) that used an empirically estimated adjustment factor, while Tan et al. (2010; 2013) introduced an empirical rotation model that removed the dependency of the radiance/reflectance on illumination according to the same linear relationship used in the SE method of Teillet et al. (1982).

Lastly, the third category of TOC methods comprises physically-based topographic corrections, which physically model illumination and directional reflectance in mountainous terrain to produce standardized reflectance for each spectral band. Some of the most popular methods are the Sandmeier model (Sandmeier and Itten 1997), the integrated radiometric correction (IRC) of Kobayashi and Sanga-Ngoie (2008), or the Three Factor Correction Model proposed by Zhang and Gao (2011). A thorough modelling of the radiance components on a physical basis is expected to give the best results but has important data

requirements (Balthazar et al. 2012) rarely available. Related to this, Couturier et al. (2013) evaluated the efficiency of TOC methods by quantifying the number of parameters needed for each method in terms of their degrees-of-freedom. The authors claimed a simple semi-empirical method such as Minnaert correction needed just 5 parameters, while a complex physically-based method (i.e., the FM3DR model) used approximately 375.

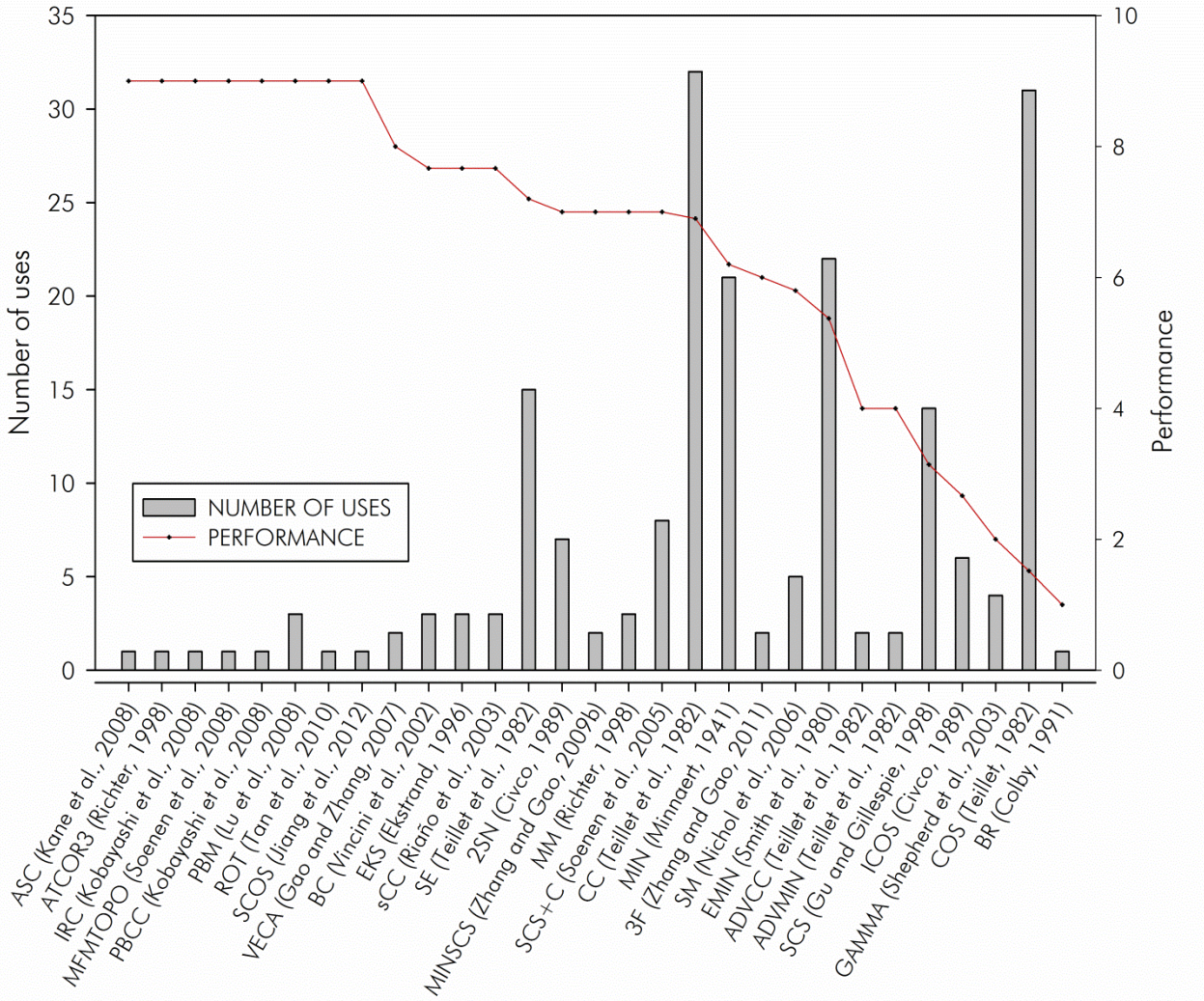

Fig. 1.3. Performance and times TOC algorithms were used in the literature

Summing up, after a thorough revision of the literature, a group of topographic correction algorithms were evaluated based on their popularity, i.e., times used and performance reported by other authors (see Fig. 1.3). Some of these methods have been widely used in the literature but most authors reported limitations. This is the case of Lambertian methods such

as COS or SCS. On the contrary, some others performed well but were only tested in one case study, and thus more research might be necessary to fully prove their goodness.

1.1.2. Considerations for the practical implementation of TOC algorithms

As explained above, topographic correction is an important part of the pre-processing of RS scenes in mountain areas. When TOC algorithms need to be implemented, there are a number of issues upon which no clear agreement exists in the literature. These issues and the alternatives proposed by different authors are briefly reviewed in this section.

Firstly, it can be noted that some authors applied TOC algorithms directly to raw digital numbers (DN) or atmospherically non-corrected top-of-atmosphere radiance (TOARD) (Hoshikawa and Umezaki 2014; Törmä and Härmä 2003; Wu et al. 2008). But some others, rather applied atmospheric corrections prior to the topographic correction (Balthazar et al. 2012; Roupioz et al. 2014; Vanonckelen et al. 2013; Gao and Zhang 2009a, 2011), that is, they converted TOARD to surface reflectance (ρ_t) and then corrected the topographic effect to obtain horizontal reflectance (ρ_h). Finally, some other authors claimed it was better to apply a coupled correction of both atmospheric and topographic effects (Kobayashi and Sanga-Ngoie 2008; Zhang et al. 2015). As far as we know, no one has specifically assessed the impact of using DN, radiance or reflectance units on the results of TOC algorithms. As a result, there is no clear recommendation with this regard, but this issue seems to have only a minor impact in TOC results.

Another important issue is the calculation of the parameters required by each TOC algorithm (i.e., k_λ, c_λ, etc.). On the one hand, Reese and Olsson (2011) examined the precision and accuracy of the empirical parameters obtained (e.g., c_λ of CC correction) as a function of the sample from which they were derived. They compared three different sampling strategies (random, stratified by aspect and stratified by $\cos\gamma_i$,) and their results showed that as sample size decreased, the precision of c_λ also decreased, with the lowest precision obtained from the smallest sample. On the other hand, different studies demonstrated that semi-empirical methods in combination with a previous stratification approach provided better results in correcting topographic effects of satellite imagery (Szantoi and Simonetti 2013). This a priori stratification was used to split the image in different land cover types that were

assigned to several strata and corrected separately with the selected TOC method. Therefore, it enabled a more precise estimation of the empirical parameters (that a priori depend on the physical characteristics of land covers), required to achieve better reduction of the topographic effect. Generally, the stratification was based on the different spectral response of the land covers on the image to be corrected (Bishop and Colby 2002; Bishop et al. 2003; Hantson and Chuvieco 2011; Richter 1998; Tokola et al. 2001), although, this stratification was limited by the need for a priori knowledge of structural landscape characteristics (Baraldi et al. 2010).

In any case, no empirical nor semi-empirical method provided effective correction under conditions of low or negative $\cos\gamma_i$ (i.e., pixels where the illumination was low and therefore no spectral information could be extracted from them), though such conditions can often be found during some periods of the year. In particular, the correction introduced by TOC algorithms that require division by $\cos\gamma_i$ (i.e., COS, SCS, CC or MIN) results in an asymptotical increase as the latter approaches 0. Furthermore, some of these methods even return negative radiances/reflectances when $\cos\gamma_i$ is negative, which is obviously impossible (Goslee 2012).

Related to this, the performance of TOC methods and its evaluation was strongly affected by the masking of shadowed pixels (i.e., low or negative $\cos\gamma_i$ values). The use of an illumination threshold to exclude some pixels affects both the calculation of correction parameters and the statistics of the resultant corrected image. For instance, Baraldi et al. (2010) decided to exclude pixels with $\gamma_i > 85°$. Similarly, Goslee (2012) excluded pixels where $\gamma_i > 78°$ (i.e., $\cos\gamma_i < 0.2$). In areas of rough terrain and periods of low solar elevation angle, this threshold could leave uncorrected too many pixels. On the contrary, attempts to correct these extreme pixels might provide unreliable results.

As previously explained, TOC methods usually require a DEM of the study area from which illumination conditions of each pixel are derived. If the selected DEM has artifacts, these will be transferred to the topographically corrected image. This problem frequently occurs when DEM is resampled to higher resolution (i.e., the original DEM resolution of 30 m is resampled to a 5 m pixel size). Artifacts can also be due to an integer coding of the height values of the DEM instead of float data, which would have smoother transitions. A simple way to smoothen

these effects is through the use of a kernel window with a large enough size for the slope/aspect calculation (i.e., kernel=5 or 7 instead of the default kernel=3 pixels), but this approach causes a reduction of the high frequency spatial information (Richter and Schläpfer, 2015).

For rugged terrain, the success of topographic correction relies on two standard requirements of a DEM: 1) The exact orthorectification of the multispectral image to be draped over the DEM and 2) An adequate spatial resolution of the DEM. For the former, some authors claimed that RMSE co-registration error should be lower than 0.5 pixels (Lunetta and Elvidge 1999; Baraldi et al. 2010), or even lower than 0.2 pixels for change detection applications (Xiaolong and Khorram, 1998). Regarding to the spatial resolution, many studies suggested that a DEM with an inadequate spatial resolution would result in an incorrect removal of topographic effects. Specifically, DEM's spatial resolution was best recommended to be a quarter of the sensor's spatial resolution, or at least the same resolution of the sensor (Richter 1998). In line with the findings of Richter, Zhang et al. (2015) suggested that, in general, for 30-m resolution RS images, it would be desirable to have a DEM of a spatial resolution of at least 10 m, whereas for 90 to 500-m resolution RS images, a 30-m DEM could achieve the required topographic correction accuracy.

In the last years, due to the increase of LIDAR data available, new scenarios in the creation of high-resolution DEM appeared. Consequently, the derived terrain-related parameters can be calculated with a level of detail never imagined before, which enables to correct not only the topographic effect controlled by viewing and solar geometry, but also the shadowing due to objects (e.g., trees) within a pixel, i.e., self-shadowing (Kane et al. 2008). Thus, in a close future LIDAR data will feasibly enhance the performance of TOC.

1.1.3. Evaluation of TOC-corrected images

As outlined in Section 1.1.1, plenty of empirical, semi-empirical and physically-based TOC methods were proposed in the last years, so it becomes essential to assess their performance over different sensor, terrain and temporal configurations. Several authors have proposed different strategies for the accuracy assessments of topographic correction methods (Civco 1989; Hantson and Chuvieco 2011; Lu et al. 2008; Richter et al. 2009). Generally, the first

indicator on the quality of the correction is through visual evaluation of the removal of the topographic effect (Civco 1989; Conese et al. 1993; Gu and Gillespie 1998; Itten and Meyer 1993). Notwithstanding that, the results of TOC methods must be quantitatively evaluated (Balthazar et al. 2012).

One of the most widely used procedures to quantitatively assess the goodness of TOC is the decrease in the dependence between $\cos\gamma_i$ and the radiance/reflectance of each spectral band after TOC. Some authors measured this decrease through the slope of the linear regression (Vanonckelen et al. 2014), whereas others used the correlation coefficient (Gao et al. 2014), or both (Gao et al. 2014; Goslee 2012; Szantoi and Simonetti 2013; Gao and Zhang 2009a). The lower the dependence between $\cos\gamma_i$ and the corrected radiance/reflectance, the better the performance of topographic correction. Nonetheless, in many ecosystems, land cover is influenced by the orientation of the slope, and therefore this criterion would not be valid, as a complete removal of the correlation of radiance/reflectance against $\cos\gamma_i$ would hide real and important radiometric differences. On the contrary, in these areas a residual correlation between radiance/reflectance and $\cos\gamma_i$ should be expected, even after a successful topographic correction (Hantson and Chuvieco 2011).

On the other hand, an ideal topographic correction should not change substantially the spectral characteristics (i.e., mean radiance/reflectance value) of land covers (Riaño et al. 2003; Richter et al. 2009). Ideally, image-wide per-class mean values should be maintained before and after TOC, otherwise the TOC method would have introduced a bias. Some authors applied this to the complete corrected image (Ghasemi et al. 2013; Goslee 2012), while others measured these variations per land covers (Goslee 2012; Moreira and Valeriano 2014). All the same, this strategy should not be considered a pure criterion to evaluate the quality of TOC, but rather a measure of the stability of the TOC (Baraldi et al. 2010). Another criterion to evaluate the performance of TOC algorithms is the quantification of the reduction of land cover class variability. As some authors suggested (Fan et al. 2014; Gao et al. 2014; Moreira and Valeriano 2014), land covers should become more homogenous after the correction, due to the removal of the radiometric variations caused by the topographic effect. This criterion was normally measured through the SD or the CV of reflectance within each land cover class. However, this evaluation relies on *a priori* knowledge of land cover

distribution. Hence, some authors measured this by stratifying the image in broad land cover classes based on vegetation index thresholds (i.e., vegetation/no vegetation (Szantoi and Simonetti 2013) or forest/pastures (Goslee 2012; Lu et al. 2008)) and quantifying the variability of these strata.

Many authors have studied the effects of TOC (sometimes along with atmospheric correction) on land cover classification accuracy (Füreder 2010; Hoshikawa and Umezaki 2014; Moreira and Valeriano 2014; Vanonckelen et al. 2013). TOC corrected images should provide an increase on classification accuracy compared to the results obtained using uncorrected data, and this could be used as a quality indicator of the TOC algorithm used. However, the degree of improvement provided by TOC algorithms is not easy to account for, as the topographic effect is only one of the several factors that contribute to land cover classification accuracy (Hoshikawa and Umezaki 2014). In fact, classification results depend also on the study site, land cover distribution, field data used for training and the selected classification algorithm, among other factors. By the same token, the improvement in change detection accuracy (Tan et al. 2013; Vanonckelen et al. 2015) or in biophysical parameter retrievals (Ekstrand 1996; Tokola et al. 2001) after topographic correction has been considered. However, these assessments are unable to directly quantify the degree to which the topographic effect has been reduced, due to the inherent uncertainties entailed by classification, change detection and retrieval algorithms.

Furthermore, some authors suggested a different evaluation criteria based on the selection of pixels of a pseudo-invariant land cover, such as conifer forests of the same density. This assessment required the extraction of random samples for North-facing and South-facing slopes of that land cover (Notarnicola et al. 2014; Vicente-Serrano et al. 2008). On these samples the differences of radiance/reflectance values between North and South facing slopes were compared before and after topographic correction. An ideal TOC should remove this difference and consequently make North and South samples more similar. The terms North/South-facing slopes were substituted by sunlit/shaded slopes (Fan et al. 2014; Riaño et al. 2003; Vicente-Serrano et al. 2008) or pixels facing the sun/facing away from the sun (Civco 1989) in comparable studies. Schulmann et al. (2015) applied a similar procedure but

substituted the mean difference by the RMSD, whereas other authors applied this evaluation criteria to different land covers, such as snow (Singh et al. 2015) or pastures (Goslee 2012).

There is an issue that negatively affects the performance of several TOC methods, and that is the generation of abnormal reflectance values, so called statistical outliers, after the correction. Following Tukey's (1977) indications, Balthazar et al. (2012) considered reflectance values lower than the 25th percentile minus 1.5 times the inter-quartile-distance (IQR), and values greater than the 75th percentile plus 1.5 times the same distance as statistical outliers. Consequently, these pixels were identified and their number or proportion was measured.

Finally, a new methodology based on synthetic images was proposed by Sola et al. (2014a) to evaluate topographic correction algorithms in a simple and objective way. These images represent the radiance an optical sensor would receive under specific geometric and temporal acquisition conditions and assuming a certain land cover type. In particular, a pair of images was generated: A Real Synthetic image (SR) considering the real topography of the study site, and a Synthetic Horizontal image (SH) where a completely flat relief was simulated. Subsequently, the SR image was corrected with different TOC algorithms and a comparative analysis between these corrected SR images and the ideal situation in absence of topographic effect (i.e., the SH image) was performed. This comparison provided a sound, objective and clear method for the quantitative assessment of TOC algorithms.

To summarize, many TOC algorithms have been proposed in the last decades, but most of them have not been fully evaluated, since most studies only tested TOC methods on a single image, generally acquired under favorable illumination conditions and considering only one or two evaluation criteria.

1.2. Objectives

As it has been pointed out in Section 1.1.1, many topographic correction methods have been proposed in the last decades, but there is no agreement on which one is the most adequate for each setting. The general objective of this thesis is to analyze and assess the existing topographic correction methods considering the main factors involved in the scene acquisition process, that is, the sensor's characteristics, the acquisition date and time, the

solar geometry, the Earth surface relief and the spatial distribution of land covers on the study site. In order to achieve this general objective, some particular objectives were established as well:

- To analyze the physical and empirical base of the TOC methods proposed up to now, specially focusing on semi-empirical methods due to their simplicity, ease of implementation and effectiveness in an automated preprocessing chain.
- To assess the performance of TOC methods considering the quality assessment strategies described in the literature, and eventually proposing additional evaluation strategies.
- To evaluate the behavior of different TOC methods when correcting images acquired at different dates and times, that is, with different solar illumination conditions.
- To combine different evaluation criteria in order to perform a multi-criteria analysis of topographic correction algorithms.
- To implement and apply the TOC algorithms proposed in the literature to satellite images in combination with a previous stratification approach and compare the results with the performance of a traditional non-stratified TOC.

A key issue to reach the objectives formulated is the analysis of the quality of the corrected scenes obtained. So far, the strategies used to evaluate the quality of the corrected scenes have clear limitations since they often require land cover information, which is normally not available. Therefore, and in order to approach the assessment of topographic correction algorithms in a throughout and objective manner, the use of simulated scenarios based on synthetic images was proposed in this thesis as a new objective. For that purpose some additional specific objectives were set up:

- To define a physically based protocol to generate synthetic images.
- To validate the model to generate synthetic images with real imagery.

1.3. Structure of the thesis

Each chapter of this thesis responds to the specific objectives established, ordered with a thematic unity as explained below. 1) This first chapter consists of an introduction and state of the art, supporting literature, objectives and justification of the thesis. 2) The second chapter describes the scenes, study sites and methodology used in the thesis. 3) The third chapter answers to the particular objective of proposing an additional evaluation strategy to assess the performance of TOC methods, and presents a new methodology to evaluate topographic correction algorithms based on panchromatic synthetic images. In particular, the physically based protocol to generate synthetic images is defined. 4) The fourth chapter responds to the specific objective of validating the model to generate synthetic images with real imagery. Specifically, the model to generate panchromatic synthetic scenes was extended to the multispectral case and validated with real SPOT 5 images. 5) The fifth chapter fulfills the particular objective based on the evaluation of the behavior of different TOC methods when correcting images acquired with different solar illumination conditions. This chapter performs a multitemporal analysis of topographic correction algorithms on multispectral images based on the methodology proposed in the previous chapter. 6) Chapter 6 combines different evaluation criteria so as to perform a multi-criteria analysis of ten widely used topographic correction algorithms. And finally, 7) in Chapter 7 the performance of the best TOC method of Chapter 6 is assessed in combination with a previous stratification approach and the results are compared with the performance of a traditional non-stratified TOC.

CHAPTER 2

MATERIALS AND METHODS

2.1. Satellite images

In this thesis multispectral scenes of Satellite Pour l'Observation de la Terre 5 (SPOT 5) sensor have been used. The main reasons for selecting this sensor were that it offered an optimum combination of resolution and coverage, with resolutions of 20 m to 2.5 m (see Fig. 2.1), while covering vast areas in a single pass (i.e., a single SPOT scene covers a footprint of 3600 km^2). In particular, we have worked with four spectral bands (i.e., green: 0.50 – 0.59 μm, red: 0.61 – 0.68 μm, NIR (near infrared): 0.78 – 0.89 μm and SWIR (short-wave infrared): 1.58 – 1.75 μm) at a spatial resolution of 10 m for the first three bands, and 20 m for SWIR. Such spatial resolution is ideal for applications such as medium-scale mapping, urban and rural planning or change detection, in line with newer satellites such as Sentinel constellation. The temporal resolution is also high, as the revisit interval can be as high as 2 to 3 days (1 day with full constellation of SPOT satellites).

The images were acquired as level 1A, that is, a radiometric correction of distortions due to differences in sensitivity of the elementary detectors of the viewing instrument was performed. The image was orthorectified by the National Geographic Institute (IGN) based on ground control points and a DEM, and DN were converted to top of atmosphere radiance (W m^{-2} sr^{-1} μm^{-1}) by using the gain and offset values provided in the metadata file for each spectral band. The panchromatic band was not included in this work.

Table 2.1. SPOT 5 bands

Band	Description	Wavelength (μm)	Resolution (m)
PAN	Panchromatic	0.48-0.71	2.5/5
1	Green	0.50-0.59	10
2	Red	0.61-0.68	10
3	Near Infrared	0.78-0.89	10
4	Shortwave Infrared	1.58-1.75	20

As seen in Table 2.2, different acquisition date and times (i.e., corresponding to scenes acquired across the whole year) have been considered in the thesis. The date and time of the acquisition determines the solar geometry, essential to correct or attenuate the topographic effect. A wide range of solar geometries have been considered in order to assess the

performance of TOC under different illumination conditions. The lower the sun is (solar elevation angle closer to zero) the stronger the topographic effect. Particularly, solar elevation angle in our case studies ranged from 21° to 64°, whereas azimuth angles did from 132° to 168° (SE direction). The influence of the time of the day was not assessed, considering only the typical acquisition times of SPOT 5 satellite, around 10-11 a.m. Finally, the effect introduced by the sensor geometry when acquisition was no-nadiral was not considered in this study.

Table 2.2. Geometry and acquisition date of study sites used in the thesis

Paper	SPOT 5 scene	Solar Azimuth	Solar elevation	Acquisition date	Acquisition time
Sola et al. (2014a) (Chapter 3)	37264*	153.04	30.60	15/02/2009	10:45
Sola et al. (2015a) (Chapter 4)	36263**	167.58	37.66	15/10/2009	11:13
	37264**	140.70	56.44	15/08/2009	10:45
	38264**	152.54	57.97	19/08/2009	11:08
	35263**	155.01	53.53	30/08/2008	11:11
Sola et al. (2014b) (Chapter 5)	36263*	150.01	40.80	15/03/2009	10:45
		132.98	64.35	15/06/2009	10:45
		141.12	55.78	15/09/2009	10:45
		161.34	21.70	15/12/2009	10:45
Sola et al. (2015b) (Chapter 6)	37264	140.70	56.44	15/08/2009	10:45
	36263	167.58	37.66	15/10/2009	11:13
	35263	165.15	21.91	26/12/2006	11:07
Sola et al. (2015d) (Chapter 7)	35263	155.02	53.53	30/08/2008	11:11

** Synthetic scenes were used, based on data obtained from SPOT 5 real images ** Both synthetic and real SPOT 5 images were used*

In this work, besides of real imagery, synthetic images have been used to assess the performance of TOC. The model to generate these images was firstly developed for a single panchromatic scene considering a constant ground reflectance of 0.2, in order to consider only the parameters involved in the topographic effect. Afterwards, a more complex model was developed, extracting reflectances from local LU/LC cartography and spectral libraries, and simulating atmospheric effects such as atmospheric upward transmittance and path radiance. This model was published in Sola et al. (2014a) and it is included in Chapter 3. Later, the model was adapted to the multispectral case, simulating SPOT-like scenes and using ground reflectances extracted from real images, atmospheric and topographically

corrected. This model was presented and validated with real images in Sola et al. (2015a), and it is included in Chapter 4.

2.2. Case studies

Different study sites have been considered in this thesis, with sizes ranging from 13 x 13 km to 44 x 44 km. All the study sites in this thesis were located in mountainous regions of Northern of Spain due to the presence of the Pyrenees, were the topographic effect is important. Summing up, regions of Basque Country, Navarre and Aragón were covered by at least one of our study sites. In Fig. 2.1 the different study sites used in the thesis are displayed. All of them are sub-scenes of SPOT 5 images, with two basic requirements: high resolution DEM available and area fully covered by a SPOT 5 scene.

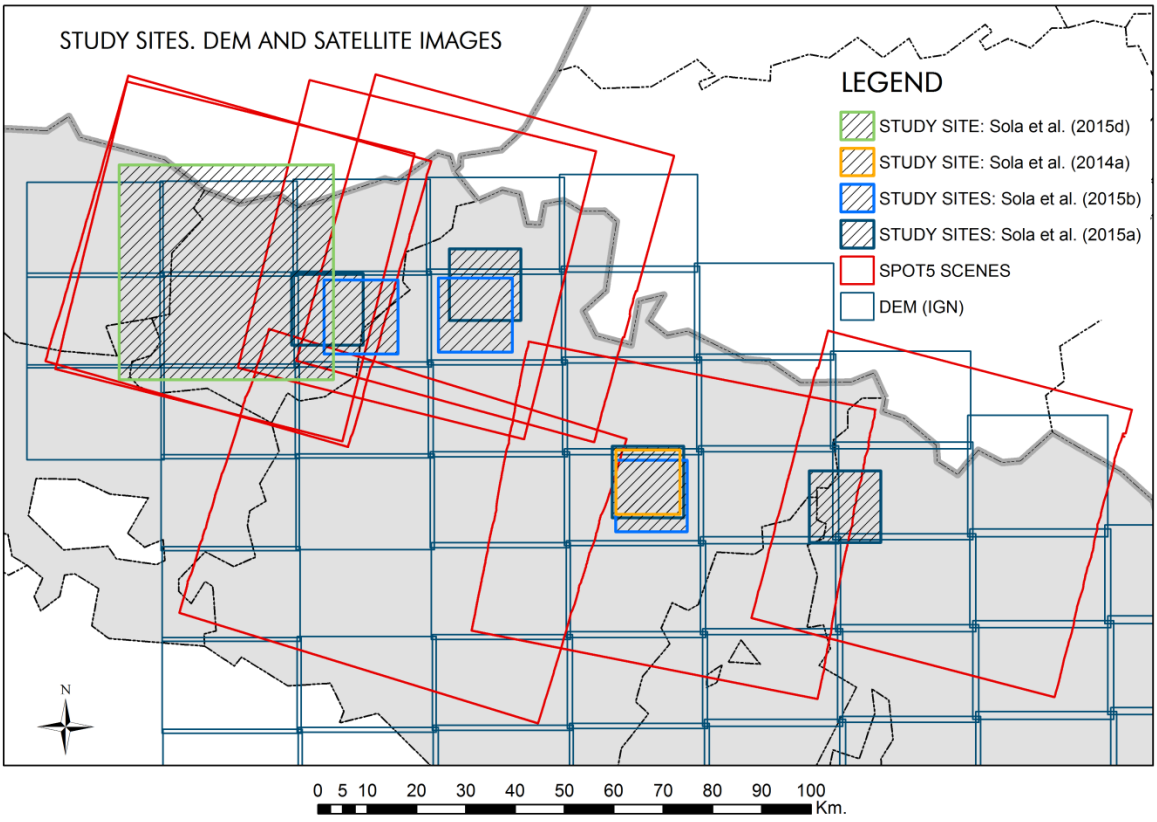

Fig. 2.1. Study sites, DEM and SPOT 5 scenes used in the thesis

Table 2.3 shows the predominant land cover, extension, and topographic factors of each case study. As already explained, most of the scenes or subscenes used in this thesis corresponded to mountainous regions, to assess the performance of TOC methods on areas where topographic effect is important, but also flat areas were considered. The mean terrain slope of the study sites ranged from 7° to 20°, with maximum slopes up to 80°, while altitudes varied from sea level to 1700 m. These figures are representatives of a rough relief. The statistics of $\cos\gamma_i$ (i.e., its mean value and SD) represent the illumination conditions of the study site. The lower the mean $\cos\gamma_i$ is, the stronger the topographic effect, while high SD($\cos\gamma_i$) is indicative of a wide range of illumination conditions. The case studies considered cover different combinations of these statistics in order to represent the different Sun-Terrain-Sensor geometries a TOC method has to confront.

Table 2.3. Land cover and topographic data of the study sites

Paper	Image	Size (km)	Land cover	$\cos\gamma_i$		Slope (°)	Height (m)		
				mean	SD	mean	min	max	mean
Sola et al. (2014a) (Chapter 3)	1	13 x 13	Agricultural/forest	0.493	0.197	16.2	436	1110	644
Sola et al. (2015a) (Chapter 4)	1	15 x 15	Forest/pastures	0.541	0.195	13.9	68	1130	473
	2	15 x 15	Agricultural/forest	0.790	0.133	8.8	435	1110	647
	3	15 x 15	Forest	0.860	0.099	14.0	609	1703	984
	4	15 x 15	Forest/pastures/urban	0.747	0.178	12.4	54	1070	379
Sola et al. (2014b) (Chapter 5)	1	15 x 15	Forest/pastures	0.584	0.240	13.8	68	1127	470
	2			0.811	0.146				
	3			0.743	0.183				
	4			0.324	0.290				
Sola et al. (2015b) (Chapter 6)	1	15 x 15	Agricultural/forest	0.533	0.175	7.9	426	1049	614
	2	15 x 15	Forest/pastures	0.557	0.240	12.8	104	1195	623
	3	15 x 15	Forest/pastures/urban	0.320	0.278	13.0	64	1341	448
Sola et al. (2015d) (Chapter 7)	1	44 x 44	Forest/pastures/urban	0.644	0.285	20.1	0	1369	354

Regarding to land cover distribution, these sites were mostly covered by arboreal land covers. Hill slopes were mainly covered by coniferous and broadleaf forests, but also shrubs, grasslands, bare soil and rocks or snow, whereas in flat areas agricultural crops and artificial

surfaces (i.e., urban areas, roads, etc.) were predominant. In some images large water bodies were present and these were used to detect undesirable radiometric changes eventually performed by TOC methods.

Three main climatic zones (Oceanic, Mediterranean and Semi-arid) can be distinguished in Spain, according to its geographical situation and orographic conditions, being the first one predominant of the study sites considered in this thesis. The oceanic climate (C_{fb} according to the Köppen climate classification) is located in the northern part of the country, especially in the regions of Basque Country, Asturias, Cantabria and Galicia. This climate is wet and characterized by relatively mild winters and warm summers. Apart from the three main climate zones, other sub-zones can be found, such as the alpine climate (group E in the Köppen climate classification) in the Pyrenees, which is the average climate for the regions above the tree line.

2.3. DEM requirements

The first requirement of a DEM for topographic correction mentioned by Baraldi et al. (2010) refers to it being precisely matched with the multispectral image. This issue was studied in detail by Sola et al. (2015c). Baraldi et al. stated that when TOC was applied, satellite image and DEM had to be orthorectified accurately to avoid unsatisfactory effects after the correction. Otherwise the quality of the correction decreased proportional to the co-registration error of the DEM, leading to large relative radiance errors exceeding 100% for critical geometries (ridges and valley lines). Thus the quality of the required DEM limited the final accuracy of the resulting image products in many cases. Sola et al. (2015c) performed a qualitative and quantitative evaluation of the effect of co-registration errors between DEM and satellite image on the quality of the topographic correction. For that purpose synthetic images over an area of the Pyrenees in the region of Navarre (Spain) were generated from an image of land covers' reflectance and a DEM of the area, so the former were perfectly co-registered with the DEM used in the topographic correction. The results of the topographic correction using this DEM were be compared with those obtained by correcting synthetic images with flawed DEMs where several displacements in X and Y axis were artificially introduced, so as to measure the decrease of quality of the correction produced by this displacement afterwards.

In the region of Navarre , a DEM with a spatial resolution of 5 m obtained through standard photogrammetric techniques was available, used in Sola et al. (2012, 2014a), while later the Spanish National Geographic Institute (IGN), provided a DEM, also with a spatial resolution of 5 meters, obtained from cubic convolution of LIDAR point cloud, with a density of 0.5 points/m^2. This DEM, generated in European Terrestrial Reference System 1989 (ETRS89), Universal Transverse Mercator projection, zone 30 North (UTM30N), was used in Sola et al. (2015a-d).

2.4. Methodology

In Chapter 3 a new procedure to assess the quality of topographic correction (TOC) algorithms applied to remote sensing imagery was proposed. This procedure was based on a model that simulated panchromatic synthetic scenes using state-of-the-art irradiance models. In particular, a pair of images was generated, considering the real topography of a certain area (Synthetic Real image, SR) and completely flat relief (Synthetic Horizontal image, SH). Subsequently, the performance of four different TOC algorithms was assessed comparing the corrected image obtained applying a TOC method to a SR image and the SH image of the same area. This comparison was quantified using the Structural Similarity index (SSIM).

In Chapter 4, this new procedure was extended to multispectral scenes in the visible, NIR and SWIR bands. Additionally, the model was validated by comparing synthetic scenes with four real SPOT 5 scenes acquired on different dates and different test areas along the Pyrenees mountain range (Spain).

Chapter 5 presented a multitemporal evaluation of TOC methods based on synthetically generated images in order to evaluate the influence of solar angles on the performance of TOC methods. For that purpose, four pairs of multispectral scenes (i.e., SR and SH) were simulated for a different study site considering four acquisition dates across the year and four different TOC algorithms were tested on these cases.

In Chapter 6 a multi-criteria analysis of ten widely used topographic correction methods was carried out in three different case studies. Three different locations in mountainous areas of Northern Spain were considered and also different acquisition dates and solar angles, in order to evaluate their performance for different land covers and for images taken under

varying illumination conditions. The performance of TOC methods was evaluated using seven different evaluation strategies: Visual assessment, radiometric stability, land covers' IQR reduction, correlation analysis, comparison of conifer forests radiometry between sunlit and shaded slopes, presence of outliers and the new methodology based on synthetic images, presented in Chapters 3 and 4.

Finally, Chapter 7 compared the performance of the best TOC in Chapter 6 (i.e., SCS+C) combined with six different stratification approaches, based on vegetation indices and land cover maps, with a non-stratified approach. For that purpose, a multi-criteria analysis was applied using six evaluation criteria. Furthermore, the influence of the stratification approach on the correction coefficient, c_λ, was evaluated.

CHAPTER 3

EVALUATION OF TOPOGRAPHIC CORRECTION ALGORITHMS: New methodology based on the use of synthetic images

Published in:

- Sola, I; González de Audícana, M.; Álvarez-Mozos, J.; Torres, J. L. (2014). Synthetic images for evaluating Topographic Correction Algorithms. *IEEE Transactions on Geoscience and Remote Sensing, 52,* 1799-1810.

Abstract — In the last years many Topographic Correction (TOC) methods have been proposed to correct the illumination differences between areas observed by optical remote sensors. Although the available number of TOC methods is high, the evaluation of their performance generally relies on the existence of precise land cover information, and a standardized and objective evaluation procedure has not been proposed yet. In this paper we propose an objective procedure to assess the accuracy of these TOC methods based on simulated scenes, i.e., synthetically generated images. These images represent the radiance an optical sensor would receive under specific geometric and temporal acquisition conditions and assuming a certain land cover type. A simplified method for creating synthetic images using state-of-the-art irradiance models has been proposed, both considering the real topography of a certain area (Synthetic Real image, SR) or considering the relief of this area as being completely flat (Synthetic Horizontal image, SH). The comparison between the corrected image obtained applying a TOC method to a SR image and the SH image of the same area, allows assessing the performance of each TOC algorithm. This comparison is quantitatively carried out using the Structural Similarity index (SSIM). The proposed TOC evaluation procedure has been *applied* to a specific *case study* in northern Spain in order to explain its implementation and demonstrate its potential. The procedure proposed in this paper could be also used to assess the behavior of TOC methods operating under different scenarios considering diverse topographic, geometrical and temporal acquisition configurations.

Keywords — Synthetic image, topographic correction, irradiance.

3.1. Introduction

The irradiance impinging on a certain point at the Earth surface depends, on the solar zenith and azimuth angles as well as on the slope and aspect of the terrain, which determine the solar incidence angle (γ_i) between the sun rays and the normal to the ground. Differences in the solar incidence angle (i.e., differences in the solar illumination) normally result in variations in the radiance detected by remote sensors between areas with similar land cover and biophysical-structural properties (Soenen et al. 2005). This effect can adversely affect the usefulness of RS data for different applications, such as Land-Use/Land cover mapping, vegetation cover monitoring, change detection or biophysical parameter estimation, especially in mountainous areas (Civco 1989; Lu et al. 2008; Meyer et al. 1993; Smith et al. 1980;

Teillet et al. 1982). The objective of Topographic Correction (TOC) methods is to compensate the differences in radiance between sunny and shaded areas caused by variations in the shape and aspect of terrain. In this paper, a new procedure to assess the performance of TOC algorithms using synthetic images is proposed. The paper is structured as follows. Section 3.2 reviews the basis of TOC methods and the evaluation procedures used normally. Section 3.3 describes the model used to create synthetic images and the quality index used to assess the topographic correction. Next, a case study is presented in Section 3.4, where the technique proposed has been applied and evaluated. Section 3.5 evaluates the performance of four selected TOC algorithms based on the procedure proposed and shows the results obtained. Finally, the main conclusions are drawn in Section 3.6.

3.2. Previous Works

3.2.1. Topographic correction algorithms

The topographic effect has a significant impact on the quantitative analysis of remotely sensed data (Lu et al. 2008). During the last two decades, several procedures were proposed to correct or attenuate it. Most of these procedures require the computation of the illumination conditions of the area to be corrected (Ghasemi et al. 2013; Hantson and Chuvieco 2011; Law and Nichol 2004; Lu et al. 2008; Soenen et al. 2005; Twele and Erasmi 2005). In those methods, the illumination conditions for each pixel are normally estimated using the cosine of the solar incidence angle, $cos\gamma_i$, which can be calculated from the solar zenith and azimuth angles and the slope and aspect, computed for each pixel using a Digital Elevation Model (DEM).

$$cos\gamma_i = cos\beta cos\theta_s + sin\beta sin\theta_s cos(\varphi_s - \varphi_n) \qquad (3.1)$$

where, β is the slope angle, φ_n the aspect angle, θ_s the solar zenith angle, and φ_s the solar azimuth angle. Both β and φ_n are computed from the DEM.

TOC methods can be grouped into two subcategories, Lambertian methods (LTOC), and non-Lambertian methods (NLTOC), depending on whether they assume reflectance as being independent or not of observation and incidence angles. The simplest and one of the most

widely used LTOC is the COS method, originally proposed by Smith et al. (1980) and later modified by Teillet (1982). Alternatively, Civco (1989) proposed an improved version considering average illumination conditions.

COS method assumes the incident radiation as being reflected in all directions equally. Besides, the method only models the direct portion of the irradiance, even if areas under low illumination conditions get a considerable proportion of diffuse irradiance. On these areas COS correction has shown a problem of overcorrection (Ghasemi et al. 2013; Hantson and Chuvieco 2011; Law and Nichol 2004; Meyer et al. 1993; Riaño et al. 2003; Twele et al. 2006).

To account for the shortcomings of these unrealistic assumptions, several semi-empirical non-Lambertian methods have been developed including band dependent parameters, i.e., MIN (Minnaert 1941; Smith et al. 1980; Teillet et al. 1982) and CC (Teillet et al. 1982). The former includes a constant modelling of the non-Lambertian behavior of each land cover for every band. The latter introduces, in order to emulate the effect of diffuse irradiance from the sky, a parameter c_λ which is the ratio between the slope and intercept of the linear regression equation between the radiance of each band and $\cos\gamma_i$. Similarly, and following the work of Teillet et al. (1982), Soenen et al. (2005) proposed the SCS+C correction, where the LTOC method proposed by Gu and Gillespie (1998) for forested areas, so called SCS, was modified to account for diffuse atmospheric irradiance by introducing the previously mentioned parameter c_λ.

Both SCS+C, MIN and CC methods are physically based, and consist of photometric functions modified using parameters estimated empirically. Nevertheless, purely empiric approaches have also been proposed (i.e., the SE method of Teillet et al. (1982)), which assumes a linear relationship between the radiance of each band and $\cos\gamma_i$, or the VECA, proposed by Gao and Zhang (2007), including an empirically estimated adjustment factor. Alternatively, many authors have proposed modifications in TOC methods to improve their performance, based on slope-smoothing (Kobayashi and Sanga-Ngoie 2009; Riaño et al. 2003), or on the use of different correction approaches for infrared and visible bands (Richter et al. 2009; Vincini et al. 2002).

The results obtained through the NLTOC methods described here have been reported to improve if stratifications were applied previous to the TOC in order to more precisely estimate the correction factors. The stratification may be based on the different non-Lambertian behavior (i.e., the different surface-roughness of the land covers on the image to be corrected) (Bishop and Colby 2002; Bishop et al. 2003; Hantson and Chuvieco 2011; Richter 1998; Tokola et al. 2001), the illumination conditions (Baraldi et al. 2010; Ekstrand 1996; Reese and Olsson 2011), the terrain slope (Ghasemi et al. 2013; Lu et al. 2008), the terrain orientation (Civco 1989; Reese and Olsson 2011) or a combination of any of these factors (Baraldi et al. 2010; Richter et al. 2009; Törmä and Härmä 2003).

3.2.2. Assessment of the quality of TOC methods

An essential point, necessary to evaluate objectively and accurately the different topographic correction methods, is the analysis of the quality of the corrected images. With this aim, traditionally an evaluation based on the visual assessment of the removal of the topographic effect in satellite imagery has been proposed (Civco 1989; Conese et al. 1993; Gu and Gillespie 1998; Itten and Meyer 1993). This approach gives a good first indication on the quality of the correction. However, it is indeed subjective and the assessment strongly depends on the skill of the observer.

A more objective assessment, and in fact one of the most widely used evaluation methods, is the quantification of the reduction of the dependence between $\cos\gamma_i$ and the radiance of each spectral band after the correction, measured through both the correlation coefficient or the slope of their linear regression, being $\cos\gamma_i$ the independent variable (Gao and Zhang 2009a). Such dependence tends to disappear in the TOC corrected images, being in these cases, both the correlation coefficient and the slope of the regression close to zero, showing that illumination dependence on reflectance values is successfully removed. This evaluation implicitly assumes land cover distribution (and hence reflectance) as being independent on terrain slope and aspect. Obviously, this assumption is not valid in areas where slope orientation determines the land cover. Therefore, in such areas a residual correlation between reflectance and $\cos\gamma_i$ is expected, even after a successful topographic correction (Hantson and Chuvieco 2011).

Civco (1989) proposed, as an evaluation approach, the analysis of the variations in the radiometry of the corrected scenes. Ideally the overall mean response of the original image should not change after TOC; otherwise the TOC method would have caused an under or overcorrection. Similarly, other authors (Lu et al. 2008; Riaño et al. 2003; Shepherd and Dymond 2003) proposed that the quality of topographic corrections could be best evaluated by measuring the reduction of the land cover class variability, measured through the standard deviation of the reflectance within each surface cover class. A perfect correction would result in more homogenous classes with a reduced variability. This assessment method is probably the most objective and quantitatively measurable criterion. However, the reduction of land cover class variability in topographically corrected imagery is restricted to cases where *a priori* knowledge of land cover distributions is available.

Many authors considered the improvement on classification accuracy after topographic correction as an adequate procedure to assess the goodness of the TOC (Conese et al. 1993; Teillet et al. 1982). A classification based on TOC corrected images should ideally yield a higher accuracy than one using uncorrected data. A similar approach is to evaluate the improvement in biophysical parameter retrievals (Ekstrand 1996; Tokola et al. 2001). However, classification and biophysical parameter estimation assessments carry their own uncertainties in both classification and retrieval algorithms and are unable to directly quantify the degree to which the topographic effect has been reduced.

Alternatively, Hantson and Chuvieco (2011) proposed to quantify the increase in temporal stability of a time series for individual pixels, which would represent the robustness of the TOC algorithms under different conditions over time. This option may not be adequate in all cases, being difficult to discern between the temporal variations of spectral response of land covers and an ineffective correction of the topographic effect, with the risk of excessively homogenizing the image.

3.3. Synthetic Images

We propose the use of synthetic imagery to quantitatively evaluate Topographic Correction algorithms. Synthetic images represent the radiance an optical sensor would receive under specific geometric and temporal acquisition conditions, considering a certain land cover

structure and assuming several simplifications. Synthetic images, based on the Lambertian reflectance law, can be generated considering the real topography of a specific area (Synthetic Real image, SR), or considering a perfectly flat surface (Synthetic Horizontal image, SH). The latter is, in fact, the image that should ideally be obtained after successfully removing the topographic effect from the Synthetic Real image. The comparison between this ideal SH image and topographically corrected SR images provides a means of objectively assessing the accuracy of the TOC method applied.

The approach proposed here allows simulating synthetic images considering different topographic, geometric and temporal configurations, as well as different land cover distributions. Therefore, the influence of acquisition conditions on the behavior of TOC methods can also be explored.

In short, the evaluation approach proposed here is based on the synthetic generation of the image a sensor would acquire for any given area, considering its topography completely flat. This image can be then used as a reference to compare against images corrected with different TOC, using quantitative indexes, in a rigorous, objective and consistent manner. In the next subsections the process proposed to generate synthetic images is explained in detail.

3.3.1. Synthetic image generation

During the last years, several complete and realistic physics-based scene simulators have been proposed for a great variety of tasks, i.e., the design of systems, the development of data processing algorithms or the understanding of the image formation process (Parente et al. 2010). Scenes simulators such as SENSOR, proposed by Börner et al. (2001), DIRSIG (2006), or the approach proposed by Guanter et al. (2009) allows computationally demanding but very realistic modelling of the at-sensor radiance. However, for our particular application a simplified simulation model which adequately represents the influence of topography on the image acquisition process is presented. Several simplifications can be adopted in order to facilitate the process of generating synthetic images. In this work, we assume a panchromatic sensor working in the 500-900 nm spectrum range, with a constant spectral response function for the whole wavelength range. The main parameters of the synthetic image generation model are summarized in Table 3.1.

Table 3.1. Summary of Scientific and Technical Notation

Symbol	Parameter	Units
γ_i	solar incidence angle	degree
β	pixel's slope angle	degree
θ_s	solar zenith angle	degree
φ_n	pixel's aspect angle	degree
φ_s	solar azimuth angle	degree
E_{ESNO}	extraterrestrial normal irradiance	W/m^2
m	relative optical air mass	--
a_{er}	optical thickness of a Rayleigh atmosphere	--
$T_{eL\ (2)}$	Linke's turbidity factor	--
ρ	land cover reflectance	--
T_u	upward atmospheric transmittance	--
d	Sun-to-Earth distance correction factor	--
θ_0	viewing angle of the satellite	degree
x_1, x_2, x_3	% of irradiance corresponding to 0.5-0.9 μm	---
$E_{e,s}$	direct horizontal irradiance	W/m^2
$E_{e,d}$	diffuse horizontal irradiance	W/m^2
$E_{e,g}$	global horizontal irradiance	W/m^2
$E_{\beta,s}$	direct tilted irradiance	W/m^2
$E_{\beta,r}$	ground-reflected irradiance	W/m^2
$E_{\beta,d}$	sky diffuse irradiance	W/m^2
$E_{\beta,g}$	global tilted irradiance	W/m^2
L_{sen}	at-sensor radiance	W/m^2.sr.
SH	synthetic image considering flat topography	W/m^2.sr.
SR	synthetic image considering its real relief	W/m^2.sr.
μ_x	mean radiance of reference image	W/m^2.sr.
μ_y	mean radiance of corrected image	W/m^2.sr.
σ_x	standard deviation of reference image	W/m^2.sr.
σ_y	standard deviation of corrected image	W/m^2.sr.
V_t	Terrain View Factor	--
V_d	Sky View Factor	--
AI	anisotropy index	--
Θ	binary factor to model cast shadows	--
ρ_{adj}	average reflectance	--
$E_{e,g\ adj}$	global average horizontal irradiance	W/m^2
L_e	direct radiance	W/m^2.sr.
L_p	path radiance	W/m^2.sr.
ρ'_a	atmospheric albedo	--

The process to simulate a synthetic image for a specific area (Fig. 3.1) can be summarized in two phases. First, the image representing the global irradiance on each point of the area of interest at a certain date and time is obtained. In a second phase the top-of-atmosphere radiance (TOARD) based on a surface reflectance map and a certain sensor configuration is generated. This is in fact, the final synthetic image.

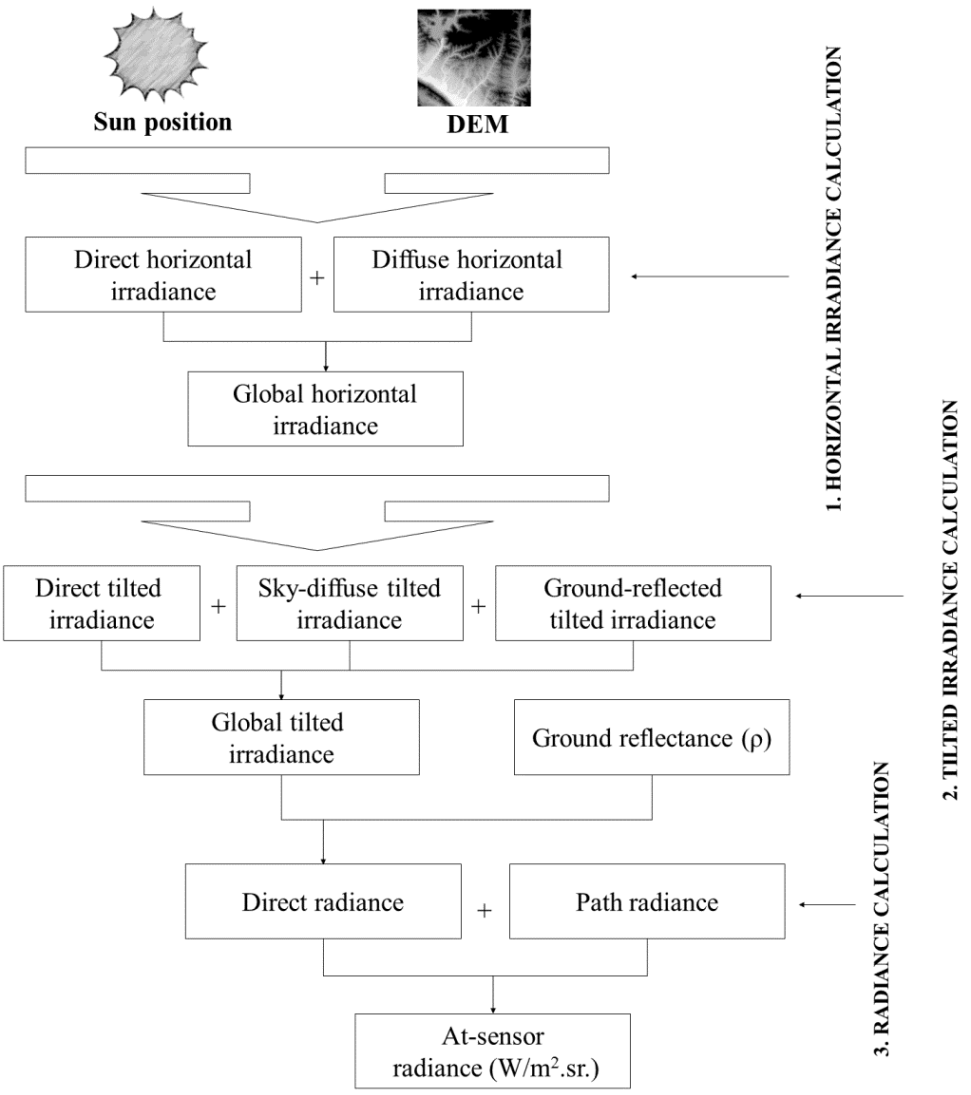

Fig. 3.1. Flowchart of synthetic scene generation procedure

To obtain the global irradiance at each point of the Earth surface it is necessary to initially estimate the Global Horizontal Irradiance ($E_{e,g}$) (i.e., the total amount of direct and diffuse radiation reaching the Earth surface), considering it horizontal, in cloudless conditions. Several models can be used to estimate $E_{e,g}$ and its diffuse and direct components (ASHRAE 1985; Hottel and Whiller 1958; Liu and Jordan 1960; Ma and Iqbal 1984). In this work the Cloud-free Global Radiation model (Page 1996) is used. This model was validated using 25 test sites spread across Europe within the SATEL-LIGHT project (Ineichen 1998). It showed a good correspondence between estimated and measured values under sunny or quasi sunny conditions.

$E_{e,g}$ is computed for a specific area, date and time as the sum of its direct and diffuse components. The direct component ($E_{e,s}$) is calculated using the equation of Page (1996) and the diffuse component ($E_{e,d}$) is calculated using the equation of Dumortier (1995):

$$E_{e,g} = E_{e,d} + E_{e,s} \qquad (3.2)$$

$$E_{e,s} = x_1 \, E_{ESNO} \, cos\theta_s \, exp\left(-0.8662 \, T_{eL(2)} \, a_{eR} \, m\right) \qquad (3.3)$$

$$E_{e,d} = x_2 \, E_{ESNO} \begin{bmatrix} 0.0065 + \left(-0.045 + 0.0646 \, T_{eL(2)}\right) cos\theta_s \\ -\left(-0.014 + 0.0327 \, T_{eL(2)}\right) cos^2\theta_s \end{bmatrix} \qquad (3.4)$$

where, x_1 and x_2 represent the fraction of irradiance corresponding to the simulated spectral range, calculated through the spectral radiation model SMARTS2 (Gueymard 1995), E_{ESNO} is the extraterrestrial normal irradiance, calculated as the product of the solar constant and the Sun-Earth correction factor, θ_s is the solar zenith angle obtained from the solar declination, pixel latitude and hour angle, m represents the relative optical air mass computed with the method of Kasten and Young (1989), a_{er} is the optical thickness of a Rayleigh atmosphere parameterized by Louche et al. (1986), and $T_{eL(2)}$ the Linke turbidity factor. This last parameter is time and site specific and the model of Dumortier *(1998)*, which describes the variations of turbidity over Western and Central Europe, has been used to estimate it.

Obviously, the topography of Earth surface areas is normally non-flat, being necessary to consider the specific geometrical or topographical characteristics of each area. To compute the Global Tilted Irradiance ($E_{\beta,g}$) it is necessary to take into account not only the Direct Tilted Irradiance or Sunlight ($E_{\beta,s}$), but also the Ground-Reflected Irradiance ($E_{\beta,r}$) as well as the Sky Diffuse Irradiance or Skylight ($E_{\beta,d}$):

$$E_{\beta,g} = E_{\beta,s} + E_{\beta,d} + E_{\beta,r} \qquad (3.5)$$

The first term, Direct Tilted Irradiance ($E_{\beta,s}$), is calculated applying the cosine law to Direct Horizontal Irradiance. The effect of surrounding topography on direct radiation is modelled by adding a binary factor to control cast shadows proposed by Richter (1998) (0 = shadow, 1 = sunlit pixel):

$$E_{\beta,s} = \Theta \frac{E_{e,s} \cos \gamma_i}{cos\ \theta_s} \qquad (3.6)$$

where, $E_{e,s}$ is the direct horizontal irradiance, calculated in (3.3), Θ is the cast shadow's binary factor, γ_i is the solar incidence angle and θ_s is the solar zenith angle.

The Sky Diffuse Irradiance on an tilted plane is calculated with Hay's Model (Hay and McKay 1985), also enhanced with the binary factor proposed by Richter. This term considers an isotropic and a circumsolar (anisotropic) component of diffuse irradiance:

$$E_{\beta,d} = E_{e,d} \left[\Theta \frac{AI \cos \gamma_i}{cos\ \theta_s} + (1 - \Theta\ AI) V_d \right] \qquad (3.7)$$

where, $E_{e,d}$ is the diffuse horizontal irradiance, calculated in (3.4), AI is Hay's anisotropy index, calculated from the ratio of direct irradiance on a surface normal to the sun's rays and the extraterrestrial normal irradiance, and V_d is the Sky View Factor.

The Sky View Factor is based on Dozier's horizon algorithm (Dozier et al. 1981; Zakšek et al. 2011) and accounts for the portion of overlying hemisphere visible to a grid point depending on the terrain neighborhood of each pixel. The algorithm computes the vertical elevation angle of the horizon in n directions to a specified radius. According to Dozier et al. (1981), $n = 60$ is sufficient for radiation models. Similarly, for estimating the effect of topography on the solar irradiation received by the surface, the radius can generally be limited to 10 km (Zakšek et al. 2011).

The third term in (3.5), Ground-Reflected Irradiance ($E_{\beta,r}$), depends on the Global Irradiance impinging on the adjacent slopes, the reflectance of the surrounding objects, and the portion of adjacent terrain seen from a certain location:

$$E_{\beta,r} = E_{e,g\ adj}\ \rho_{adj}\ V_t \qquad (3.8)$$

where, $E_{e,g\ adj}$ is the average Global Horizontal Irradiance reaching the adjacent slopes in a square box of 0.5 x 0.5 km, ρ_{adj} is the average terrain reflectance over a square box of the same size, and V_t is the Terrain View Factor, that is, the portion of adjacent terrain seen from a certain location. V_d and V_t are complementary.

$$V_d(x,y) = 1 - V_t(x,y) \qquad (3.9)$$

Finally, to generate the synthetic image, it is necessary to consider, in addition to $E_{\beta,g}$ and land covers' reflectance, the orbital and observational configuration of the sensor, i.e., sensor viewing angle, spatial resolution of the sensor and acquisition time. The at-sensor radiance (L_{sen}) values can be calculated using the following expression:

$$L_{sen} = L_p + \frac{\rho T_u E_{\beta,g}}{\pi} \qquad (3.10)$$

where, L_p is the path radiance (i.e., radiation scattered into the sensor's instantaneous field of view without having ground contact), ρ is the land cover reflectance value, T_u is the upward atmospheric transmittance, and $E_{\beta,g}$ is the Global Irradiance reaching each pixel. The path radiance is calculated by:

$$L_p = \frac{x_3 E_{ESNO} \cos\theta_s \rho'_a}{\pi} \qquad (3.11)$$

where, x_3 is a parameter representing the fraction of irradiance corresponding to the simulated spectral range, calculated through SMARTS2 spectral radiation model (Gueymard 1995), E_{ESNO} is the solar extra-terrestrial irradiance corrected by Sun-Earth distance, θ_s is the solar zenith angle and ρ'_a is the atmospheric albedo, calculated with Bird and Hulstrom's model (1981) using values of aerosol's optical depth (AOD) for the considered area and date.

The direct upward atmospheric transmittance value (T_u), depends, in turn, on the previously calculated optical thickness of the atmosphere, and the viewing angle of the satellite, and it is obtained through the following expression neglecting diffuse upward transmittance (Gilabert et al. 1994).

$$T_u = e^{0.8662\, a_{eR} T_{eL(2)} / \cos\theta_0} \qquad (3.12)$$

where, a_{eR} is the optical thickness of the atmosphere and θ_o the viewing angle of the satellite.

3.3.2. Real (SR) and Horizontal (SH) Synthetic Images

As already mentioned, a synthetic image represents the radiance an optical sensor would receive under specific geometric and temporal acquisition conditions, assuming a certain land cover structure. Following the procedure proposed in Section 3.3.1, it is possible to generate a synthetic image for a specific area considering its real relief or topography (Synthetic Real image, SR) or a synthetic image considering a completely flat topography (Synthetic Horizontal image, SH). The comparison between the corrected image obtained applying a TOC method to a SR image and the SH image of the same area is used to assess the performance of the TOC applied.

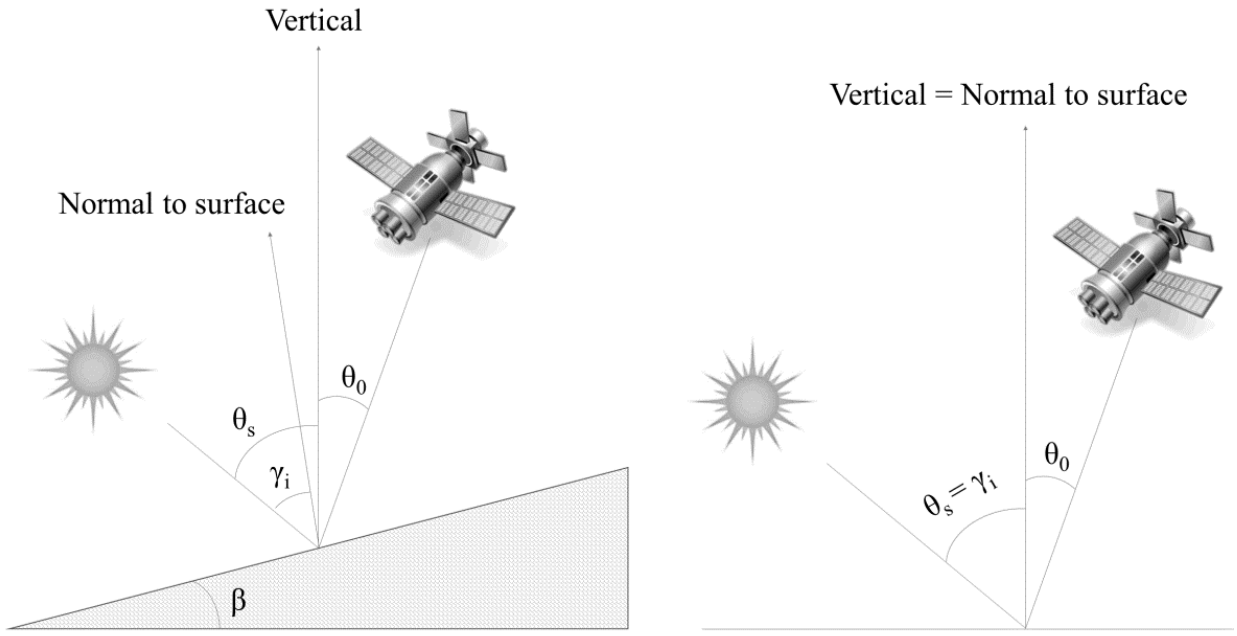

Fig. 3.2. Geometry on tilted and horizontal surfaces

The procedure to generate a Synthetic Horizontal Image (SH) for a specific area is exactly the same to that applied to obtain the image, but considering horizontal DEM. When horizontal surfaces are simulated, the topographic effect is nonexistent, but there is still an influence of height on the atmospheric parameters involved in horizontal irradiance calculation. Consequently, horizontal irradiances are equal in both SR and SH calculation but for the former, topography affects the tilted irradiance calculation, unlike in SH.

3.3.3. Structural Similarity Index (SSIM)

The synthetic image generated considering flat topography (SH) corresponds to the ideal TOC, when the topographic distortions disappear entirely. In order to measure the similarity between this mentioned ideal correction SH and the TOC corrected SR images, the Structural Similarity Index (SSIM) is used. The SSIM is a quantitative metric that gives relatively accurate similarity prediction (Rezazadeh and Coulombe 2009), which correlates well with perceptual image fidelity (Brunet et al. 2012). This index is an improved version of the Universal Quality Index (UQI) (Wang and Bovik 2002); proposed by Wang *et al.* (2004), and has gained widespread popularity because of its simple formulation and its applicability to different image processing tasks, e.g., image compression (Bo et al. 2011), pan-sharpening (Ehlers et al. 2010; Ling et al. 2007; Rodriguez-Galiano et al. 2012), image de-noising (Yuan et al. 2012; Yue and Jiang 2012), image restoration (Jeromin and Pattichis 2012; Soccorsi et al. 2010) or downscaling (Rodriguez-Galiano et al. 2012). The SSIM index, considers three different components of similarity: Luminance comparison, contrast comparison and structural similarity. Therefore, it provides a more complete similarity measure than individual statistics such as RMSE or the correlation coefficient (r).

$$SSIM_{(x,y)} = \left(l_{(x,y)}{}^{\alpha}\right)\left(c_{(x,y)}{}^{\varepsilon}\right)\left(s_{(x,y)}{}^{\omega}\right) \qquad (3.13)$$

where, $SSIM_{(x,y)}$ is the Structural Similarity index between two images x and y; $l_{(x,y)}$ is the luminance component, calculated as a function of the means μ_x and μ_y; $c_{(x,y)}$ is the contrast component, depending on the standard deviations σ_x and σ_y; $s_{(x,y)}$ is the structure component, based on the correlation coefficient r; $\alpha > 0$, $\varepsilon > 0$, $\omega > 0$ are parameters used to adjust the relative importance of the three components. $l_{(x,y)}$, $c_{(x,y)}$ and $s_{(x,y)}$ are calculated using the equations proposed in Wang et al. (2004). Coefficients α, ε and ω are set to 1 to simplify the expression, as the authors proposed. In this case, (3.13) reduces to:

$$SSIM_{(x,y)} = \frac{(2\mu_x\mu_y+C_1)(2\sigma_{xy}+C_2)}{(\mu_x{}^2+\mu_y{}^2+C_1)(\sigma_x{}^2+\sigma_y{}^2+C_2)} \qquad (3.14)$$

where, μ_i is the mean value of the image i, σ_i its standard deviation and σ_{xy} the covariance of x and y. c_1 and c_2 are two user-defined constants included to avoid unstable results when $\mu_x{}^2$

$+ \mu_y^2$ and $\sigma_x^2 + \sigma_y^2$ are very close to zero. In our case, c_1 and c_2 are set to 0.065 and 0.585 respectively, following recommendations by Wang and Bovik (2002). These values are somewhat arbitrary, but the performance of the SSIM index has been demonstrated fairly insensitive to variations of these values (Wang and Bovik 2002).

The SSIM index is normally used for comparing an ideal reference image (in our case SH), with a distorted or erroneous one (in our case TOC corrected SR). Its dynamic range is [-1, 1]. The best value 1 is obtained only when perfect similarity is achieved.

In practice, one usually requires a single overall quality measure of the entire image (Wang et al. 2004). We use a mean SSIM (MSSIM) index to evaluate the overall image quality. MSSIM can be used to quantitatively rank the performance of TOC methods. Besides, for image quality assessment, it is useful to apply the SSIM index locally rather than globally (Wang et al. 2005), computing the local statistics within an 11 x 11 circular-symmetric Gaussian weighting function which moves pixel-by-pixel over the image (Brunet et al. 2012). A combination of MSSIM index and SSIM maps will provide a useful tool to select the best TOC depending on the subsequent use of the corrected images.

3.4. Case Study

3.4.1. Study area and field data

As already pointed out, synthetic images can be generated considering different topographic, geometric and temporal configurations, as well as different land cover distributions Rough topography can be responsible for topography-related image distortions, while terrain slope and aspect can influence the natural spectral variability within any land cover type (Teillet et al. 1982). Therefore, this case study is carried out on a mountainous area (Pyrenees) of the North-Eastern side of Navarre, Spain, where the relief is rough and the valleys have a wide variety of aspects.

The study area considered has an extension of 155 km^2, with heights ranging between 430 m and 1110 m, and slopes from 0° to 81°. For this area a 5 m resolution DEM of the region of Navarre obtained through standard photogrammetric techniques is available. From this DEM, terrain aspect and slope are calculated over a 3 x 3 cell neighborhood, through an

averaging process from altitude differences within the grid in both "x" and "y" directions. The date, time and acquisition configuration parameters selected for this case study are those of a hypothetical scene acquired the 15th of February of 2009, at 10:45 UTC. A winter time acquisition has been selected for this case study in order to show strong alterations due to the topographic effect.

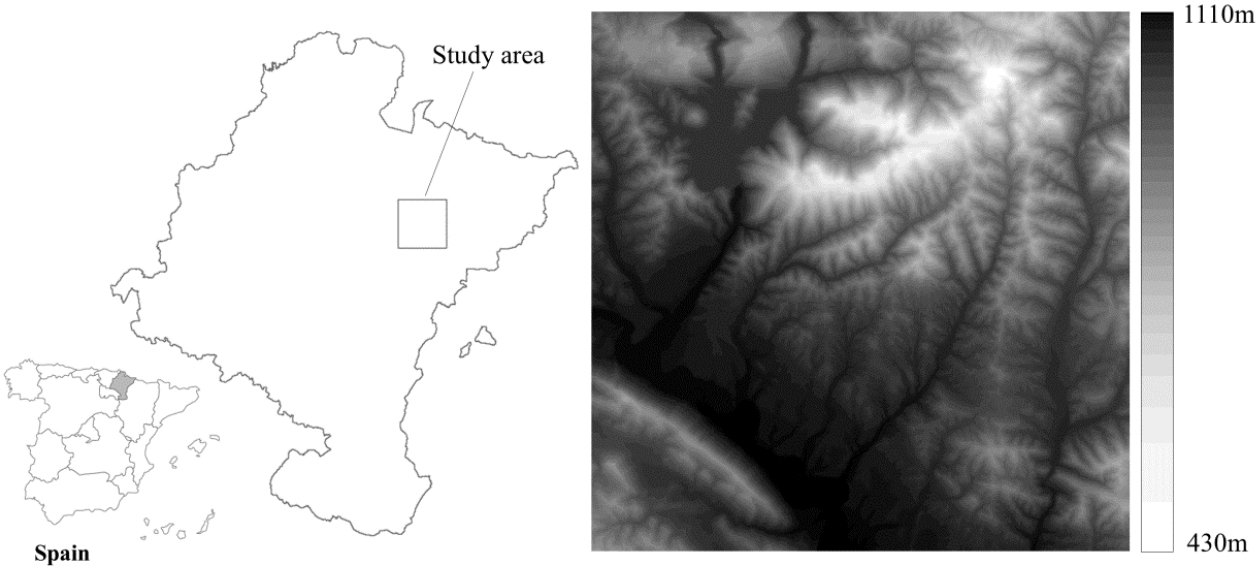

Fig. 3.3. Study area of 13 by 13 km in Northern Navarre and DEM available

Concerning the sensor configuration, we considered a panchromatic sensor with a spectral range between 500 and 900 nm, typical of panchromatic wide range sensors, with a spatial resolution of 5m and a nadiral viewing angle. In order to obtain a land cover reflectance image as realistic as possible, land-use cartography has been used as well as spectral information from twenty different land covers obtained from spectral libraries of ASTER and USGS for vegetation, rocks and soil (Baldridge et al. 2009; Clark et al. 2007). The study area is mainly covered by conifer forests (25%), deciduous and mixed forests (24%), herbaceous crops (21%), shrubs (14%) and grasslands and pasture lands (3%).

The parameterization of reflectance used here requires reference land cover information which might not be available in the general case. This type of parameterization was selected in our case in order to adequately validate the technique proposed. Other simpler parameterizations could be followed (e.g., considering constant reflectance throughout the scene) leading to more unrealistic, yet simple, synthetic images. Preliminary analyses suggest

that the influence of reflectance parameterization is only minor in the TOC evaluation procedure proposed here.

In the next subsection the Horizontal and Tilted Irradiance images and the SR and SH images generated are described. The computational time for the simulation of synthetic real and horizontal images in an area of 155 km^2 is about 2h 10 minutes, using an Intel Core 2 Quad CPU Q8400 2.66GHz, 3.49 Gb RAM, being the computation of the Sky View factor the most time-consuming task in the process.

3.4.2. Synthetic images obtained

The main parameters involved in the calculation of the horizontal irradiance, in (3.2), (3.3) and (3.4), both for SR and SH images, for our particular case study are shown in Table 3.2:

Table 3.2. Values of parameters required for the generation of global horizontal irradiance images (SR and SH)

	Synthetic Real (SR)		Synthetic Horizontal (SH)	
Parameters	$\mu \pm \sigma$	Range	$\mu \pm \sigma$	Range
h (m.)	646 ± 133	[435-1110]	646 ± 133	[435-1110]
θ_s (°)	59.4 ±0.1	[59.2-59.6]	59.4 ±0.1	[59.2-59.6]
Variables				
$E_{e,s}$(W/m^2)	201 ± 3.9	[194.7-214.6]	201 ± 3.9	[194.7-214.6]
$E_{e,d}$(W/m^2)	39 ± 1.3	[34.0-40.3]	39 ± 1.3	[34.0-40.3]
$E_{e,g}$(W/m^2)	239 ± 2.7	[235.0-248.5]	239 ± 2.7	[235.0-248.5]

The Global Horizontal Irradiance ($E_{e,g}$) is the sum of both direct and diffuse components, and its values range from 235.0 W/m^2 to 248.5 W/m^2, either for both SR and SH, being the variations of irradiance mainly caused by the effect of altitude on the different atmospheric parameters involved.

When flat terrain is considered slope is obviously zero, and therefore there is no ground-reflected irradiance. Next, the three components of Global Tilted Irradiance ($E_{\beta,g}$), shown in Fig. 3.5, are computed using direct, diffuse and global horizontal irradiances. In flat terrain (SH) the ground-reflected irradiance, $E_{\beta,r}$, is zero. As a result, $E_{\beta,g}$ is obviously the same as the Global Horizontal Irradiance, due to the flat terrain.

Table 3.3. Values of parameters required for the generation of Global Tilted Irradiance

Parameters	Synthetic Real (SR)		Synthetic Horizontal (SH)	
	$\mu \pm \sigma$	Range	$\mu \pm \sigma$	Range
β (º)	16.2 ± 10	[0-76]	0	[ ]
ρ	0.42 ± 0.13	[0.2-0.63]	0.42 ± 0.13	[0.2-0.63]
V_d	0.83 ± 0.08	[0.12-1]	1	[ ]
$\cos\gamma_i$	0.49 ± 0.2	[-0.71-1]	0.509	[ ]
Variables				
$E_{\beta,s}$ (W/m^2)	193.4 ± 78.7	[0-415.2]	200.6 ± 3.9	[194.7-214.6]
$E_{\beta,r}$ (W/m^2)	15.6 ± 6.8	[0-79.3]	0	[ ]
$E_{\beta,d}$ (W/m^2)	33.4 ± 3.8	[3.4-42.2]	200.6 ± 3.9	[34.0-40.3]
$E_{\beta,g}$ (W/m^2)	242 ± 80.2	[28.4-482.1]	239 ± 2.7	[235.0-248.5]

For the SR image, summing the three terms mentioned, in (3.5), a global tilted irradiance image with values ranging from 28.5 to 482.1 W/m^2 is obtained, with a mean value of 241.8 W/m^2 and a standard deviation of 80.2. In Fig. 3.4 some of the factors included in the synthetic image calculation are shown, such as the Sky View Factor (V_d), the binary factor controlling cast shadows (Θ), $\cos\gamma_i$ and the image of reflectances used.

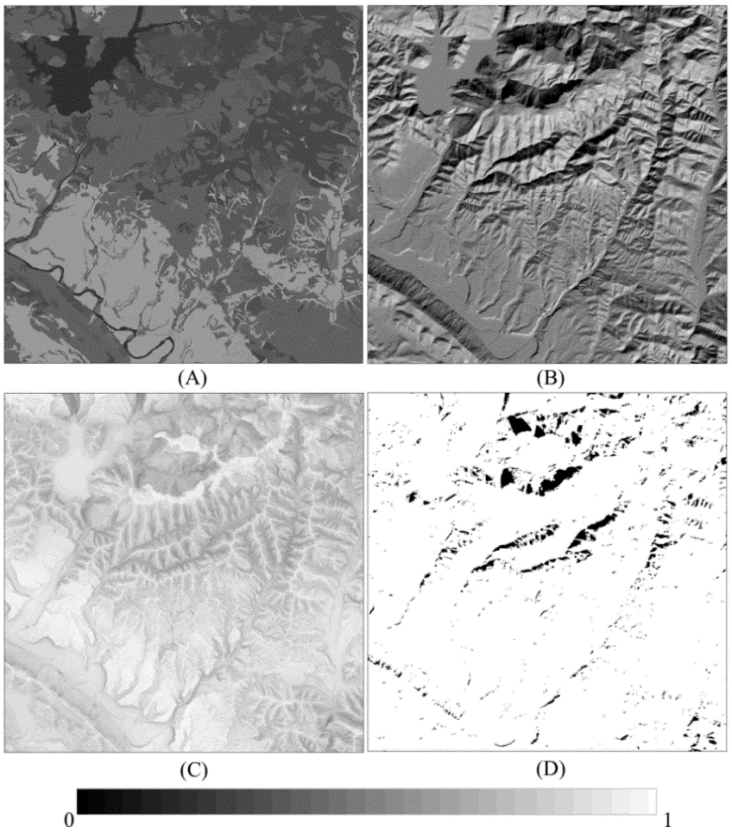

Fig. 3.4. Images of parameters used in the calculation of synthetic image when real relief is considered (SR) **(a)** Land cover's reflectance **(b)**, $\cos\gamma_i$ **(c)** Sky View Factor (V_d), and **(d)** Binary factor (Θ) controlling cast shadows

Obviously except for the reflectance image, the others have a constant value for the SH image, as they are terrain dependent. V_d is 1 across the whole image meaning a clear sky hemisphere for every pixel. In the absence of sloped surfaces, there is no need to control any shadow, therefore Θ is 1 as well. In addition, in flat terrain the solar incidence angle is equal to the solar zenith angle for every pixel.

Table 3.4. Values of synthetic images. Synthetic Real (SR) and Synthetic Horizontal (SH)

	Synthetic Real (SR)		Synthetic Horizontal (SH)	
Variables	$\mu \pm \sigma$	Range	$\mu \pm \sigma$	Range
L_e (W/m^2.sr.)	29.34 ± 13.06	[2.01-82.77]	28.62 ± 8.61	[13.47-43.76]
L_p (W/m^2.sr.)	7.77 ± 0.02	[7.72-7.81]	7.77 ± 0.02	[7.72-7.81]
Synthetic image (L_{sen}) (W/m^2.sr.)	37.12 ± 13.06	[9.78-90.50]	36.39 ± 8.62	[21.26-51.50]

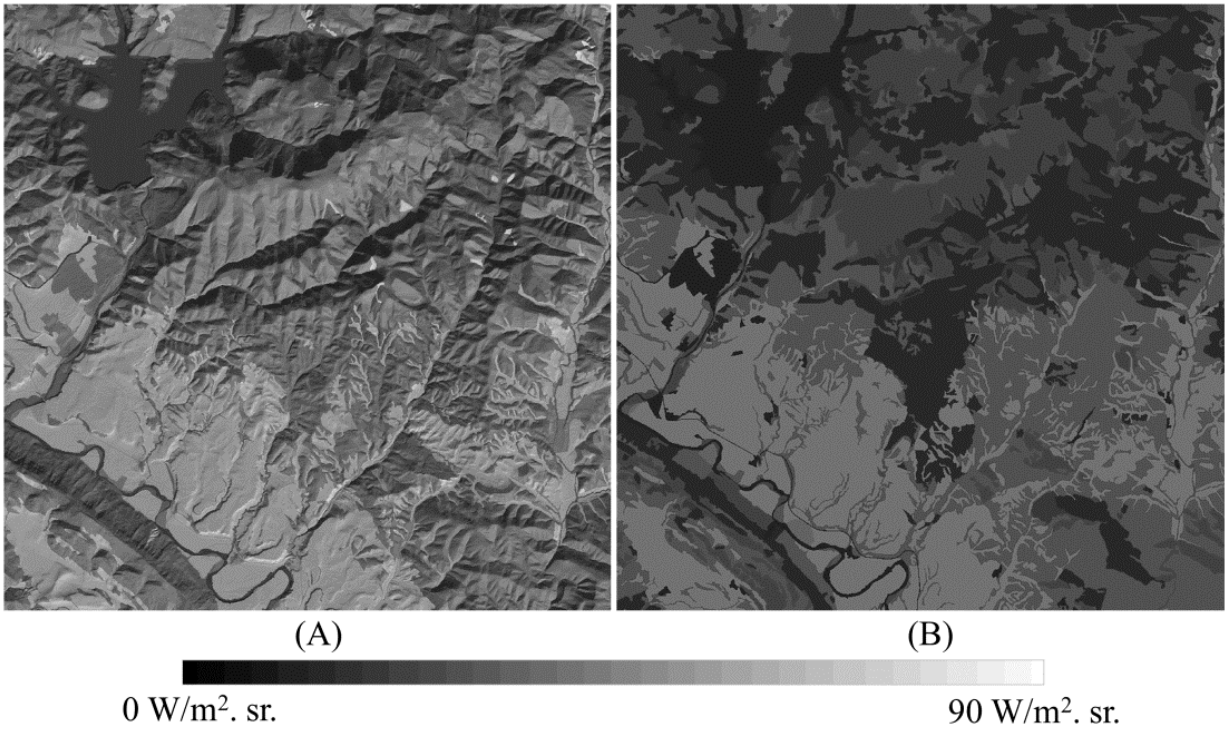

Fig. 3.5.(a) Synthetic image (SR), when real topography is considered **(b)** Synthetic Horizontal image (SH), when flat topography is considered

Finally, synthetic images are obtained using (3.8), considering the ground reflectance image and the previously mentioned sensor configuration parameters (Fig. 3.5). The SR image shows values of radiance between 9.8 and 90.5 W/m^2.sr., with a mean of 37.1 W/m^2.sr and a

standard deviation of 13.06 (Table 3.4). On the other hand, the SH image ranges from 21.3 to 51.5 W/m^2.sr., being the mean 36.4 W/m^2.sr. and a standard deviation of 8.6. The differences between SR and SH are only due to the topographic effect, which leads to variations in different radiance components (Table 3.4).

As seen in Table 3.4, the direct radiance (L_e) is the main component of the resultant synthetic scenes, and the influence of topography on it is obvious, since variance is clearly higher in the SR scene. This topographic effect should be corrected by TOC algorithms.

3.5. Results and discussion

The algorithms tested in this study are SE Method (Teillet et al. 1982), CC (Teillet et al. 1982), EMIN including slope (Smith et al. 1980), and COS method (Teillet et al. 1982). Their formulation is shown in Table 3.5, where A and B are, respectively, the intercept and the slope of the regression line between radiance and illumination (i.e., cosγ_i), and k_λ and c_λ are empiric constants calculated for each method as described by Teillet et al. (1982). These four TOC methods were selected for being probably some of the most frequently used in the literature. Besides, their differences will hopefully provide contrasting results for discussing the utility of the proposed evaluating method.

Table 3.5. Formulation of TOC method tested

TOC	Expression	Authors
COS	$L_{sen,corr,\lambda} = L_{sen,\lambda} \frac{\cos \vartheta_s}{\cos \gamma_i}$	Teillet et al. (1982)
CC	$L_{sen,corr,\lambda} = L_{sen,\lambda} \frac{\cos \vartheta_s + c_\lambda}{\cos \gamma_i + c_\lambda}$	Teillet et al. (1982)
EMIN	$L_{sen,corr,\lambda} = L_{sen,\lambda} \cos \beta \left(\frac{\cos \vartheta_s}{\cos \gamma_i \cos \beta} \right)^{k_\lambda}$	Smith et al. (1980)
SE	$L_{sen,corr,\lambda} = L_{sen,\lambda} - (A \cos \gamma_i + B) + \overline{L_{sen,\lambda}}$	Teillet et al. (1982)

In Fig. 3.6 the SR corrected images using the four TOC methods selected are shown, including a zoom area to see in detail some of the most problematic areas in the image. Areas where the solar incidence angle is close or even higher than 90° are normally not corrected because most TOC methods are unstable at these low cosγ_i values (Baraldi et al.

2010). However, the γ_i boundary might be different for each TOC due to differences in their approach and formulation. In this work, when COS method is applied, pixels with $\gamma_i > 85°$ are left uncorrected. This 85° angle boundary was proposed as a limit for excluding shadowed areas by Baraldi et al. (2010). When $\gamma_i \in [90°,180°]$, corrected radiance is negative, which has no physical meaning (Baraldi et al. 2010), and when $\gamma_i \in [85°,90°]$, the pixel information is low, and topographic correction with COS method produces strong overcorrection (Tokola et al. 2001). In our particular case, those pixels represent the 5% of the image. EMIN uses logarithms on its equation to compute k_λ constant. As a consequence, areas with $\cos\gamma_i < 0$ cannot be corrected with this method, leading to 1.6% of the pixels masked out in this case. In the case of the CC method, this boundary can be relaxed because its formulation already introduces a c_λ factor to reduce overcorrection. So, in order to avoid negative radiance values in the computations, a boundary depending on the c_λ factor obtained for each particular case is proposed. In our case, pixels with $\cos\gamma_i \leq {}^{-c_\lambda}/_{2}$ are masked out for CC method, those pixels represent the 0.2% of the pixels. Finally, SE method does not have any limitations with this regard and no areas of the image need to be masked out before the correction, so it can be applied to 100% of the image.

Those uncorrected pixels (areas in black in Fig. 3.6), form areas with low radiance values, equal to those of the original SR image, and contrast with the surrounding pixels, which might still be over-corrected with some methods. In particular, overcorrection is still noticed when the COS method is used, leading to bright zones surrounding dark uncorrected areas (Fig. 3.6a). Some overcorrection is also present in EMIN corrected image (Fig. 3.6d), although much less than in COS method. Finally, the CC method and particularly the SE give better results in these problematic areas with almost negligible overcorrection effects. It must be remarked that due to the particular extreme conditions of our simulated images, regarding acquisition date and time, these problems of overcorrection are particularly severe.

At a first sight it is quite easy to appreciate differences between the TOC corrected images obtained with each method (Fig. 3.6). On the one hand, visually, the CC and SE methods appear as the most successful in reducing the topographic effect in the original SR image (Figs. 3.6b and c). The former's performance seems slightly better, although the latter has the advantage of correcting every pixel in the image, with no signal of overcorrection.

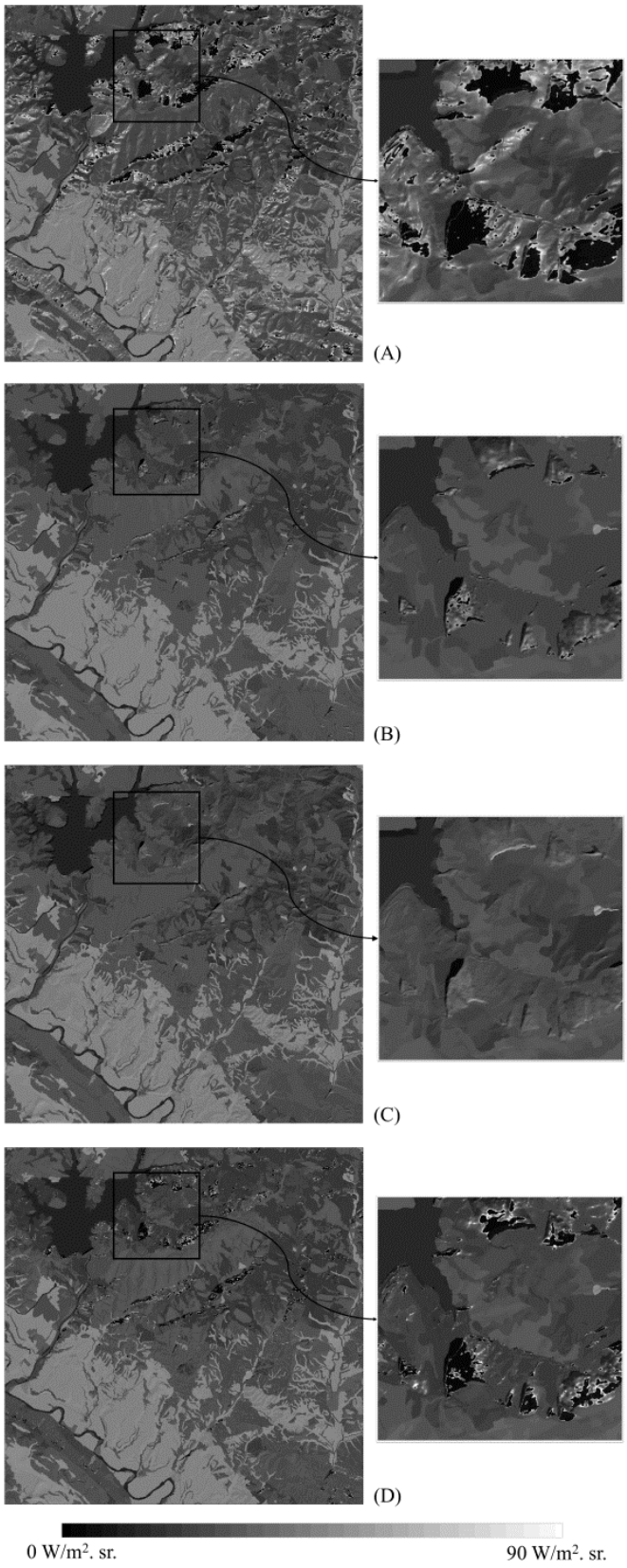

Fig. 3.6. TOC corrected images using the 4 different TOC algorithms selected (a) COS (b) CC (c) SE (d) EMIN

On the other hand, COS method does not achieve a proper correction of the shadowed areas, as mentioned above. Finally, EMIN method seems to successfully correct the effect of topography in general (Fig. 3.6d), but overcorrection is observed in some pixels.

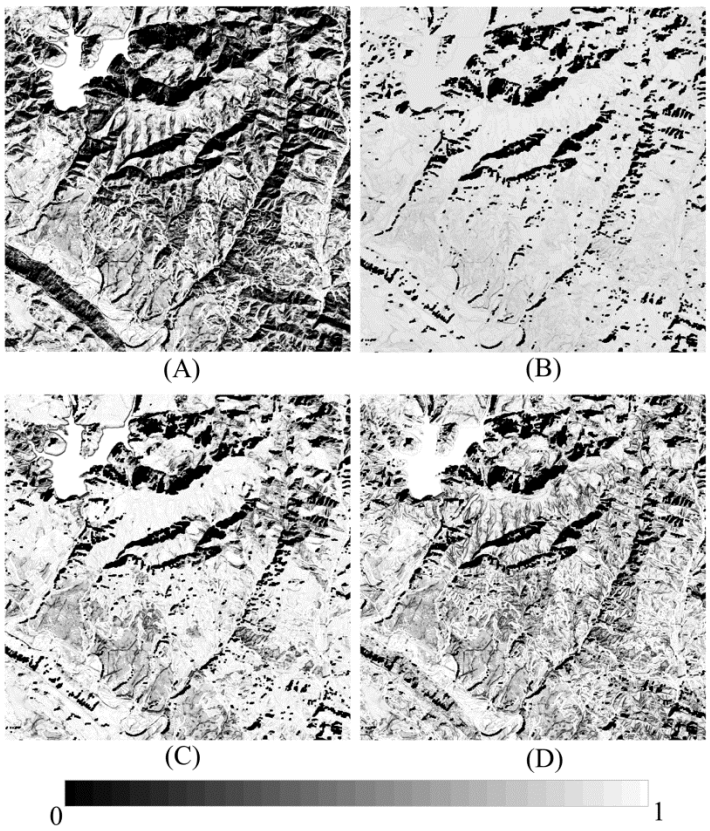

Fig. 3.7. SSIM index maps computed using a moving window of 11 x 11 pixels for the four methods selected. **(a)** COS (**b**) CC (**c**) SE and (**d**) EMIN

Apart from the visual assessment, a quantitative evaluation is performed using the SSIM index (Wang et al. 2004) to accurately determine the quality of the corrected images. A SSIM index map of the area is generated for each TOC method (Fig. 3.7)

The SSIM maps generated for each TOC-corrected image show the performance of the correction pixel by pixel. It is easy to appreciate the poorer correction of COS method, while CC method performs better than other TOC-s, but still has problems to successfully correct pixels where $\cos\gamma_i$ is close to zero or even negative. So, although CC method corrects most of the pixels in the image, leading to visually appealing results, the corrected radiances obtained for areas of low $\cos\gamma_i$ are still quite different from what they should, and give low SSIM values.

These areas with low SSIM values are also obtained in the SE correction and, to a much larger extent, in EMIN correction. Flat areas (e.g., lower left of the image) and south facing slopes are normally adequately corrected with most methods. Areas with moderate slopes are corrected better with SE method, and especially with the CC method.

In practice, one usually requires a single overall quality measure of the entire image (Wang et al. 2004). We use a mean SSIM (MSSIM) index to evaluate the overall image quality.

The MSSIM indexes obtained comparing the SH image and the TOC corrected SR images, are shown in Table 3.6. For comparison, along with the MSSIM its three components; luminance $l_{(x,y)}$, contrast $c_{(x,y)}$ and structure $s_{(x,y)}$, are shown in Table 3.6, as well as other statistical indexes to compare each image pair, such as the coefficient of correlation (r), the RMSE, and normalized standard deviation difference ($\Delta\hat{\sigma}$). The latter represents the normalized difference in standard deviation (i.e., $(\sigma_x-\sigma_y)/(\sigma_x+\sigma_y)$), with 0 representing two images with the same standard deviation.

According to MSSIM the original SR image (no TOC) shows a similarity of 0.466 with the ideal SH image. This value is improved with all the four TOC methods tested. On the one hand, COS method ranks last, only slightly improving the original image. On the other hand, CC methods perform best with a MSSIM value higher than 0.88 in the corrected scene. EMIN and the SE methods give intermediate MSSIM values.

The quantitative evaluation and ranking of TOC methods can be analyzed in more detail looking at the values of the three SSIM components. For example, CC and SE are the best methods according to the luminance, contrast and structure comparison, result confirmed by the values of RMSE, r and $\Delta\hat{\sigma}$, where these methods ranked 1st and 2nd for all of them. On the contrary, COS method ranks last for the six criteria considered.

Table 3.6. MSSIM values and other similarity measures obtained for the TOC methods tested

STATISTICAL INDEXES	TOC METHODS				
	SR	*COS*	*CC*	*SE*	*EMIN*
MSSIM	0.466	0.584	0.889	0.820	0.783
$\mathbf{l_{(x,y)}}$	0.966	0.979	0.998	0.997	0.995
$\mathbf{c_{(x,y)}}$	0.544	0.637	0.906	0.850	0.811
$\mathbf{s_{(x,y)}}$	0.884	0.878	0.969	0.959	0.938
RMSE	8.556	9.795	2.824	2.622	8.549
$\Delta\hat{\sigma}$	-0.205	-0.185	-0.034	-0.030	-0.179
r	0.765	0.654	0.962	0.961	0.728

The three components of SSIM are conceptually related to the RMSE, $\Delta\hat{\sigma}$ and r, respectively, but they do not represent exactly the same magnitudes (i.e., their equations are related but not the same). Therefore the rankings of TOC methods obtained with $l_{(x,y)}$, $c_{(x,y)}$ and $s_{(x,y)}$ on the one hand and RMSE, $\Delta\hat{\sigma}$ and r on the other might not be exactly the same.

Finally, in order to compare the TOC evaluation procedure proposed here with other assessment approaches used traditionally, the reduction of the standard deviation of land cover classes has been computed and compared with the MSSIM results (Fig. 3.8).

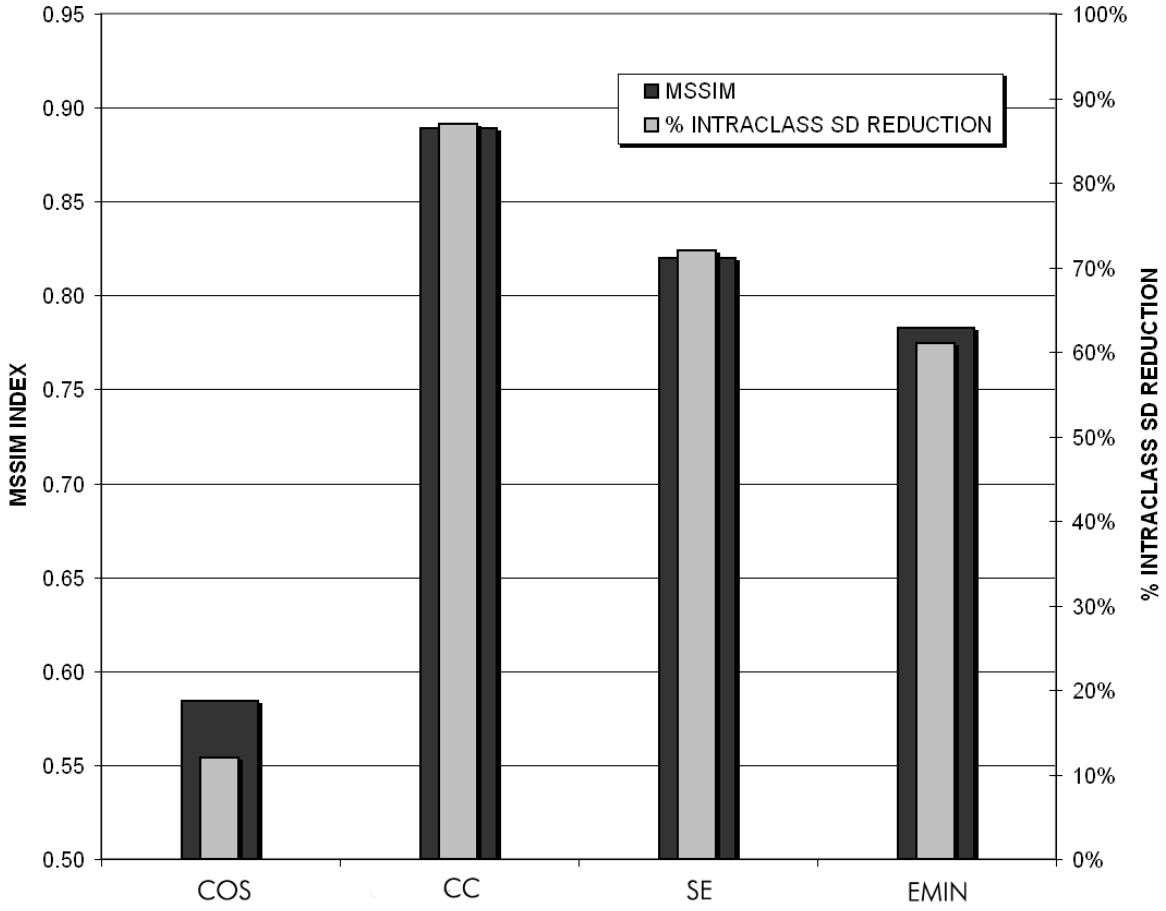

Fig. 3.8. MSSIM index compared with percentage of reduction of intraclass standard deviation

As already explained in Section 3.2.2, a traditional indirect procedure to assess the goodness of topographic corrections is via the reduction of the standard deviation within each land cover class. Successful TOC algorithms will result in more homogeneous land covers, allowing a better accuracy in subsequent classifications. In Fig. 3.8 the average reduction of the standard deviation of classes (in %) is shown for the four TOC methods tested, along with

their MSSIM value. The correspondence between both criteria is clear, with the CC method ranking first, followed by the SE, the EMIN and the COS method. These results confirm the validity of the MSSIM based TOC evaluation procedure proposed here.

Finally, comparing the results of the TOC evaluation performed here with those of the literature, we can find an overall agreement. The simplistic hypothesis of COS method, considering only direct irradiance, was also found inappropriate in previous studies (Law and Nichol 2004; Twele et al. 2006; Gao and Zhang 2009a). COS method has frequently shown a problem of over-correction, particularly when the algorithm has been applied for correcting steep, naturally vegetated slopes (Twele and Erasmi 2005), this is only partially avoided by introducing a limit incident angle, above which no correction is done.

Similarly to Meyer et al. (1993) and Twele and Erasmi (2005) we observed that only small differences exists between CC, SE and EMIN. Between those methods, in contrast to our results, Twele and Erasmi (2005) observed the best correction of EMIN in natural tropical forests, slightly better than the other non-Lambertian approaches, i.e., SE and CC. In that study, TOC performance was measured using the reduction in coefficient of variation and linear regression analysis between corrected data and $\cos\gamma_i$ as a criterion.

Alternatively, Riaño et al. (2003) observed that most TOC methods produced an overcorrection where $\cos\gamma_i$ is low, even if they worked with a summer scene, which had good illumination conditions. EMIN method did not give acceptable results in their studies, modifying the mean of the original scene. Besides, CC showed better results than EMIN method according to the reduction of intra-class variation, which is consistent with our work (Fig. 3.8).

When the image is taken under unfavorable illumination conditions, Hantson and Chuvieco (2011) observed the SE method gave the best results for bare soil pixels, and to a lesser extent the CC, These two methods gave the best results for pine forest pixels as well. The performance of TOC methods was evaluated via the reduction of standard deviation of pixel values within the same land cover in different slopes and aspects (Kobayashi and Sanga-Ngoie 2009).

In general, other studies concluded that SE and CC methods gave the most adequate results, retaining the spectral characteristics of the data, homogenizing land covers and

improving overall classification accuracy (Hantson and Chuvieco 2011; McDonald et al. 2002; Riaño et al. 2003; Gao and Zhang 2009b). In this work, CC method resulted in the best TOC for the study area and the acquisition conditions considered. This result was confirmed both by the MSSIM index and the reduction of intraclass deviation. It must be remarked that the scene acquisition date and time considered here are representative of winter scenes, where sun illumination is lowest. Analogous to Hantson and Chuvieco (2011), we observed that when the image is taken at a low sun elevation angle, no TOC method is able to correct entirely the topographic effect.

3.6. Conclusions

This paper presents an objective and universal procedure to evaluate the quality of TOC methods applied to RS imagery. The approach proposed is based on the use of synthetic images, which can be generated for a certain area and acquisition conditions considering both real topography (Synthetic Real image, SR) or a completely flat topography (Synthetic Horizontal image, SH). The latter is not affected by illumination differences caused by topography and, therefore, can be considered a reference against which to compare TOC corrected SR scenes. The comparison of TOC corrected SR scenes and the reference SH is carried out using a widely accepted quality metrics, i.e., the SSIM index (Wang et al. 2004). This index quantitatively evaluates several aspects of image similarity and can be used to build a ranking of best performing TOC methods for each specific case.

The approach presents several advantages compared to traditional evaluation techniques. Firstly, the approach is objective because the results of each TOC method are quantitatively evaluated and ranked using the SSIM index. Secondly, the approach does not necessarily require ancillary information on land cover distribution to perform the TOC quality assessment. Finally, synthetic images representing different settings and scene acquisition conditions can be generated to select the best performing TOC for each particular situation (e.g., solar angles, spatial resolution, etc.). Accordingly, the influence of each configuration parameter on the performance of the TOC methods can be evaluated. Obviously, this approach assumes that a TOC showing a good performance for synthetic imagery also performs correctly for real imagery with similar acquisition configuration.

The case study analyzed here, considering a winter panchromatic scene, showed similar results using the approach proposed and the assessment of the reduction of the intra-class standard deviation (a traditional TOC evaluation procedure). In particular, CC method ranked first, followed by SE and EMIN methods. COS method achieved the poorest correction. The SSIM can be applied locally to detect the areas where TOC methods perform the worst. In this case, areas with low illumination conditions showed the worst results with all methods. The combination of SSIM maps and Mean SSIM index provides a useful tool to decide the best TOC according to the future use of the corrected scene.

Further research is needed to apply the proposed technique over a range of sensor (e.g., spatial resolution, band frequency, etc.) and acquisition (e.g., acquisition date and time) configurations, to derive guidelines on which TOC method performs best under each situation. Therefore, the technique proposed, can be used to perform a detailed analysis of the accuracy of existing TOC methods.

CHAPTER 4

MODEL VALIDATION: Validation of a Simplified Model to Generate Multispectral Synthetic Images

Published in:

- Sola, I.; González-Audícana, M.; Álvarez-Mozos, J. (2015). Validation of a Simplified Model to Generate Multispectral Synthetic Images. *Remote Sensing, 7*, 2942-2951.

Abstract — Sola et al. (2014a) proposed a new procedure to assess the quality of topographic correction (TOC) algorithms applied to Remote Sensing imagery. This procedure was based on a model that simulated synthetic scenes, representing the radiance an optical sensor would receive from an area under some specific conditions. TOC algorithms were then applied to synthetic scenes and the resulting corrected scenes were compared with a horizontal synthetic scene free of topographic effect. This comparison enabled an objective and quantitative evaluation of TOC algorithms. This approach showed promising results but had some shortcomings that are addressed in this letter. First, the model, originally built to simulate only broadband panchromatic scenes, is extended to multispectral scenes in the visible, NIR and SWIR bands. Next, the model is validated by comparing synthetic scenes with four real SPOT 5 scenes acquired on different dates and different test areas along the Pyrenees mountain range (Spain). The results obtained show a successful simulation of all the spectral bands. Therefore, the model is deemed accurate enough for its purpose of evaluating TOC algorithms.

Keywords — topographic correction; synthetic images, model validation.

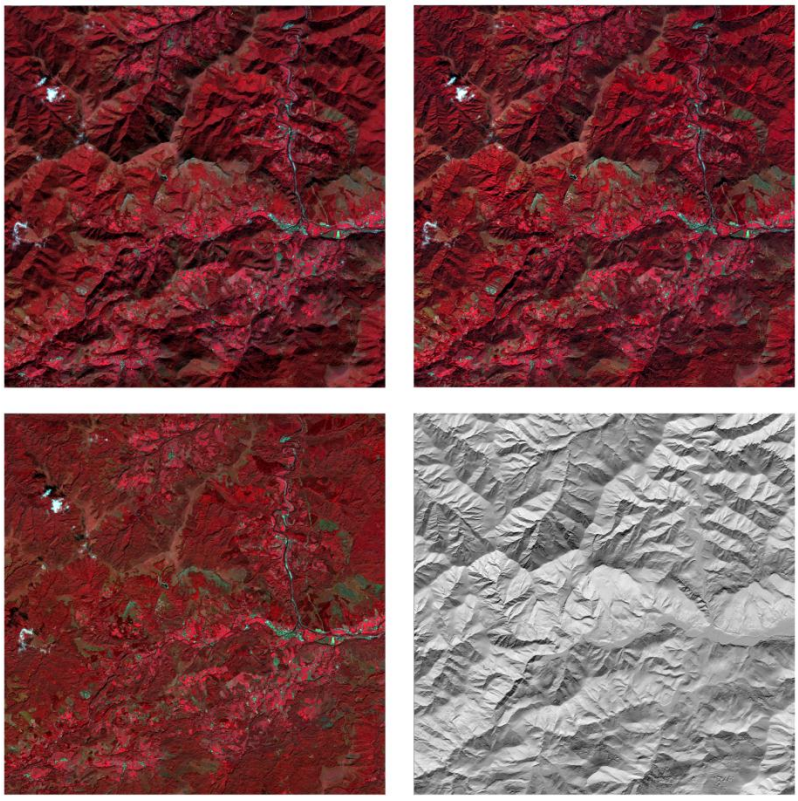

Graphical abstract

4.1. Introduction

The use of remotely sensed data from mountainous regions generally requires additional pre-processing, including topographic correction (TOC). Specifically, variations in the solar incidence angle (γ_i) affect land cover discrimination, since the radiance observed for a given land cover varies depending on whether it is located on shadowed or non-shadowed areas (Soenen et al. 2005). This effect, normally referred to as the topographic effect, can adversely affect the usefulness of RS data for different applications, such as Land-Use/Land cover mapping, vegetation cover monitoring, change detection or biophysical parameter estimation (Civco 1989; Lu et al. 2008; Meyer et al. 1993; Smith et al. 1980; Teillet et al. 1982). The objective of topographic correction algorithms is to compensate the differences in radiance between sunny and shaded areas caused by variations in the slope and aspect of terrain.

A number of TOC algorithms were proposed in the past (e.g., Minnaert 1941; Richter 1998; Soenen et al. 2005; Teillet et al. 1982), but their evaluation is not as simple as it might seem. In this sense, several strategies to evaluate TOC algorithms have been developed: Visual assessment of the removal of the topographic effect in satellite imagery (Civco 1989; Conese et al. 1993; Gu and Gillespie 1998; Itten and Meyer 1993), quantification of the reduction of the dependence between $\cos\gamma_i$ and the radiance of each spectral band after the correction (Gao and Zhang 2009a), analysis of the variations in the radiometry of the corrected scenes (1989), measurement of the reduction of land cover class variability (Lu et al. 2008; Riaño 2003; Shepherd and Dymond 2003), and improvement on classification accuracy after topographic correction (Conese et al. 1993; Teillet et al. 1982). However, these procedures were not purely objective (Baraldi et al. 2010; Hantson and Chuvieco 2011; Sola et al. 2014a). Therefore, Sola et al. (2014a) proposed a new methodology to quantitatively evaluate topographic correction algorithms based on synthetic imagery. In short, the approach proposed by Sola et al. (2014a) was based on the generation of a pair of synthetic images a sensor would acquire for any given area, considering, on the one hand, its real topography and, on the other hand, a completely flat surface. Then, the latter could be used as a reference to compare against the TOC corrected synthetic scenes, using quantitative indexes, in a rigorous and consistent manner.

The approach proposed in Sola et al. (2014a) presents several advantages compared to traditional evaluation techniques, such as being objective, simple and not requiring ancillary information on land cover distribution to perform the TOC quality assessment. However, the model proposed for generating synthetic images was developed to simulate only broadband panchromatic scenes. This could imply an important limitation for applying this methodology to evaluate TOC algorithms over a range of sensor (e.g., spatial resolution, band frequency, etc.) and acquisition (e.g., solar geometry and acquisition time) configurations. In addition, the whole approach was based on the assumption of model validity, and this needs to be verified.

For that purpose, in this work the model to generate synthetic images is extended to multispectral scenes (i.e., visible and infrared bands) to adapt the approach for a range of sensors. The model is then validated, since this is something necessary on any modelling attempt, by comparing simulated multispectral scenes with real SPOT 5 imagery acquired in four different study areas and four different dates.

4.2. Study Area

Four different study areas of 15 x 15 km were selected, all of them located in northern Spain, in regions of rough relief in different parts of the Pyrenees. The dominant land covers in these areas were deciduous and mixed forest, pastures and agricultural crops, with a sparse presence of bare soil and urban areas. For this work a Digital Elevation Model (DEM) of 5 m resolution was used, obtained from LIDAR data acquired by the Spanish National Geographic Institute (IGN).

Table 4.1. Details of the study areas used for the simulation

AREA	CENTER LAT/LONG	SENSOR ZENITH	DATE	TIME	SUN ELEVATION	SUN AZIMUTH
1	43°08'35"N / 1°42'54"W	12.6	15/10/2009	11:13	37.66	167.58
2	42°46'40"N / 1°19'09"W	-24.3	15/08/2009	10:45	56.44	140.70
3	42°43'28"N / 0°49'55"W	14.5	19/08/2009	11:08	57.97	152.54
4	43°06'06"N / 2°06'33"W	15.0	30/08/2008	11:11	53.53	155.01

As seen in Table 4.1, different dates and solar geometry were selected to validate the model over different acquisition configurations. Furthermore, these corresponded to real

SPOT 5 acquisitions. The effect of the topography was expected to be more severe in area 1 due to its lower solar elevation angle.

4.3. Methods

4.3.1. Extension of the model to multispectral images

The model to generate synthetic images was described in detail in Sola et al. (2014a). In this work the model was adapted to simulate multispectral SPOT 5-like scenes with four bands, i.e., green, red, NIR and SWIR bands. As already explained, a synthetic image represents the radiance the sensor would receive under certain conditions and within a spectral range. This spectral radiance ($L_{sen,\lambda}$) is obtained as follows (Moran et al. 1992):

$$L_{sen,\lambda} = L_{p,\lambda} + \frac{\rho_\lambda T_{u,\lambda} E_{\beta,g,\lambda}}{\pi} \qquad (4.1)$$

where, $L_{p,\lambda}$ is the path radiance of the corresponding spectral band, ρ_λ is land cover spectral reflectance value, $T_{u,\lambda}$ is the upward atmospheric transmittance, and $E_{\beta,g,\lambda}$ is the global irradiance reaching each pixel. In Sola et al. (2014a), $L_{p,\lambda}$ was calculated with Bird and Hulstrom's model (1981), and LU/LC cartography and spectral libraries were used to obtain ρ_λ. However, in this work $L_{p,\lambda}$ and ρ_λ of each spectral band were obtained from real imagery to avoid introducing further uncertainties, since the focus is placed on validating the model, and in particular the simulation of the effect introduced by topography.

The global irradiance of each band ($E_{\beta,g,\lambda}$) was obtained through the physical model of Sandmeier and Itten (1997) as the sum of its three terms, i.e., direct, diffuse and reflected irradiance:

$$E_{\beta,g,\lambda} = \Theta \frac{E_{e,s,\lambda} \cos\gamma_i}{\cos\theta_s} + E_{e,d,\lambda}\left[\Theta \frac{AI \cos\gamma_i}{\cos\theta_s} + (1 - \Theta\ AI)V_d\right] + E_{e,g,\lambda\ adj}\ \rho_{\lambda,adj} V_t \qquad (3.2)$$

where, Θ is the cast shadow's binary factor, $E_{e,s,\lambda}$ is the direct horizontal irradiance for each spectral band, γ_i is the solar incidence angle, θ_s is the solar zenith angle, $E_{e,d,\lambda}$ is the diffuse horizontal irradiance, AI is Hay's anisotropy index (Hay and McKay 1985), V_d is the Sky View Factor (Zakšek et al. 2011), $E_{e,g,\lambda\ adj}$ is the average Global Horizontal Irradiance reaching the

adjacent slopes, $\rho_{\lambda,adj}$ is the average terrain reflectance for each spectral band, and V_t is the Terrain View Factor, that is, the portion of adjacent terrain seen from a certain location. The calculation of all these terms is explained in detail in Sola et al. (2014a).

To extend the original model to multispectral simulation some changes were introduced. First, both $L_{p,\lambda}$ and ρ_λ were obtained for each spectral band. Besides, the direct and diffuse horizontal spectral irradiances were calculated for the considered bands, i.e., green, red, NIR and SWIR. For that purpose, the fraction of direct and diffuse irradiance corresponding to each spectral band was calculated through SMARTS2 spectral radiation model (2006), considering mid-latitude summer/winter atmospheres, rural aerosol model and Thuillier solar spectrum. Finally, the obtained radiance values were converted from band-integrated values ($W \cdot m^{-2} \cdot sr^{-1}$) to band-averaged values ($W \cdot m^{-2} \cdot sr^{-1} \cdot \mu m^{-1}$) dividing by the effective bandwidth of each band, obtained from the spectral response functions of the HRG2 sensor of SPOT 5.

4.3.2. SPOT 5 imagery

Four SPOT 5 scenes were used for the validation. These were acquired under the same temporal and geometric conditions as the simulated scenes (Table 4.1). The sensor zenith angle ranges from -24° to 15°, (a negative incidence angle means the tilt direction is right of the flight direction), although these variations do not significantly affect the resulting synthetic scenes. The SPOT 5 scenes, at a spatial resolution of 10 m, were orthorectified and converted from digital numbers (DN) to top of atmosphere radiance ($W \cdot m^{-2} \cdot sr^{-1} \cdot \mu m^{-1}$) by using the gain and offset provided in the metadata for each spectral band.

4.3.3. Validation

To validate the model, simulated scenes were compared with real SPOT 5 scenes band per band. Three widely used statistical indexes were used to quantitatively evaluate the accuracy of the model: determination coefficient (r^2) that measures the correlation between real and simulated spectral bands; mean structural similarity index (MSSIM) that measures their structural similarity (Wang et al. 2004); and RMSE their root mean squared error. Also scatterplots and histograms of both simulated and observed radiances were plotted to evaluate the quality of the simulation.

4.4. Results and Discussion

Four different synthetic scenes were generated (Fig. 4.1, and supplementary results) and compared to their corresponding SPOT 5 images. Only results of area 1 were shown in this letter, while the rest were included as supplementary data.

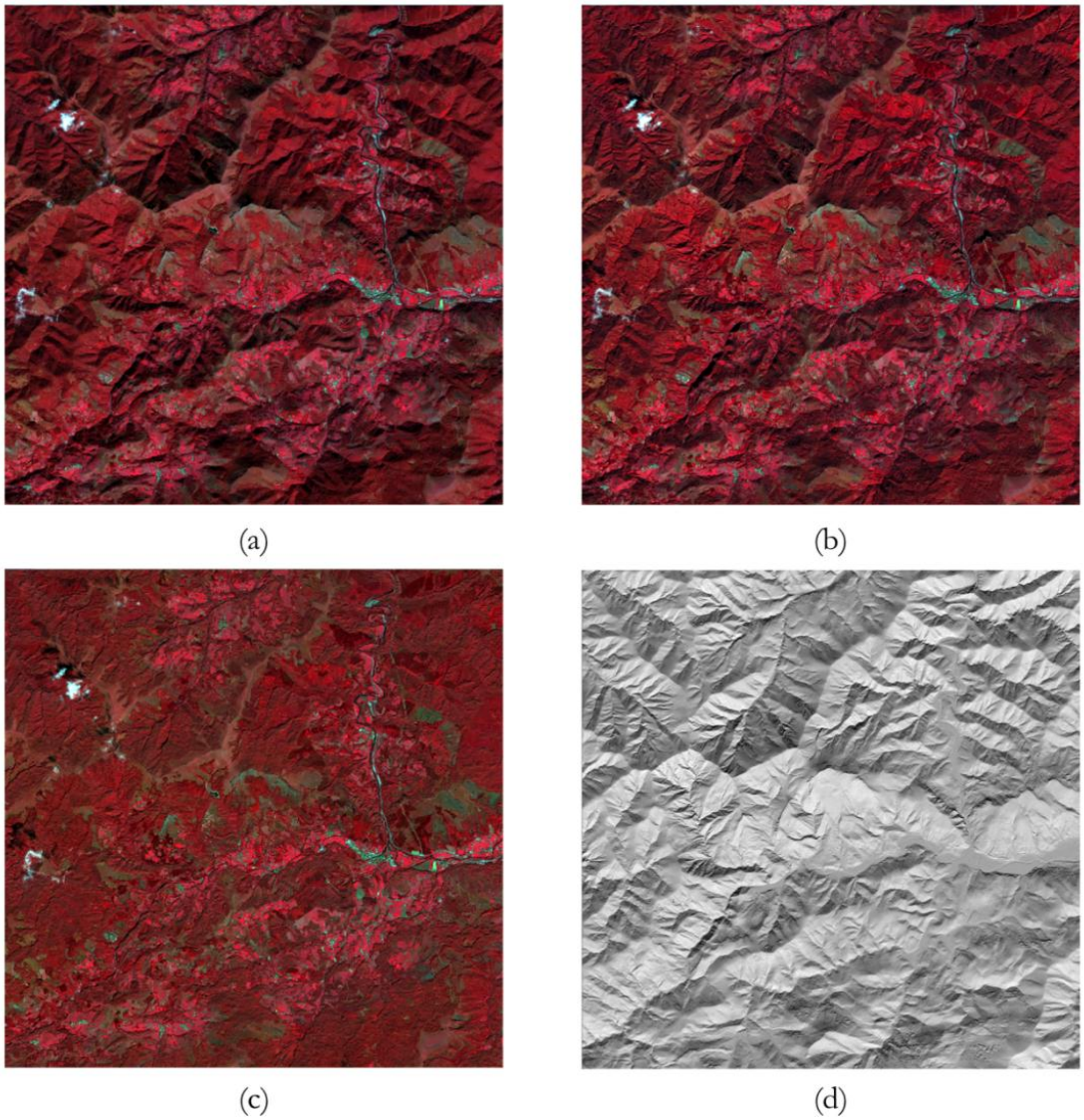

Fig. 4.1. Area 1 **(a)** RGB false color composite of the real scene **(b)** RGB false color composite of the simulated scene **(c)** RGB false color composite of terrain reflectance **(d)** Cosine of solar incidence angle

Fig. 4.1c showed the false color composite of ground reflectance used in the simulated scene. In Fig. 4.1d the illumination (i.e. cosine of the solar incidence angle) was displayed. Both were used in the model to generate synthetic images. Visually, the simulated false color

composites were very close to their corresponding real scenes (Figs. 4.1a and 4.1b and supplementary results), but the former showed more spatial detail introduced by the 5 m DEM, while the real scenes looked slightly smoother. In this work the DEM was resampled to 10 m, without smoothing it.

Although this issue is considered to be minor for the purpose of this letter, further research is needed on the effect of spatial resolution and DEM smoothing on TOC performance, as discussed by several authors in the last years (Riaño et al. 2003; Richter and Schläpfer 2002; Zhang et al. 2015).

The shadowed areas introduced by the topography were well modeled, especially in areas 1 and 4. A more detailed analysis using scatterplots and histogram comparison confirmed this observation, with scatterplots following closely the 1:1 line and histograms of very similar shapes for the observed and simulated scenes.

Some limitations were observed though. In some areas, mainly area 2 and area 3, infrared bands, and in particular SWIR, seemed to introduce some more topographic effect than observed in real scenes, slightly underestimating low values of radiance and overestimating high radiances, i.e., slopes facing the sun. This effect had an influence in the results of statistical indexes, with lower values of MSSIM for the 4th band. This could be due to a higher influence of the direct irradiance term on the global irradiance impinging the surface for these bands, since this term is strongly influenced by $\cos\gamma_i$, incrementing the variance in at-sensor radiances. However, this effect was not consistent in all the test sites, and thus in most cases the topographic effect seemed to be well modelled.

In area 1, pixels with low radiance were slightly overestimated in all bands, so the false color composite in shadowed areas looked slightly darker in the real scene (Fig. 4.1b) than in the simulated one (Fig. 4.1b). This was also clearly visible in scatterplots (Fig. 4.2) with values above the 1:1 line for low radiances and also in histograms, with simulated radiances slightly skewed to the right, but this effect was not apparent in areas 2, 3 and 4 (supplementary results).

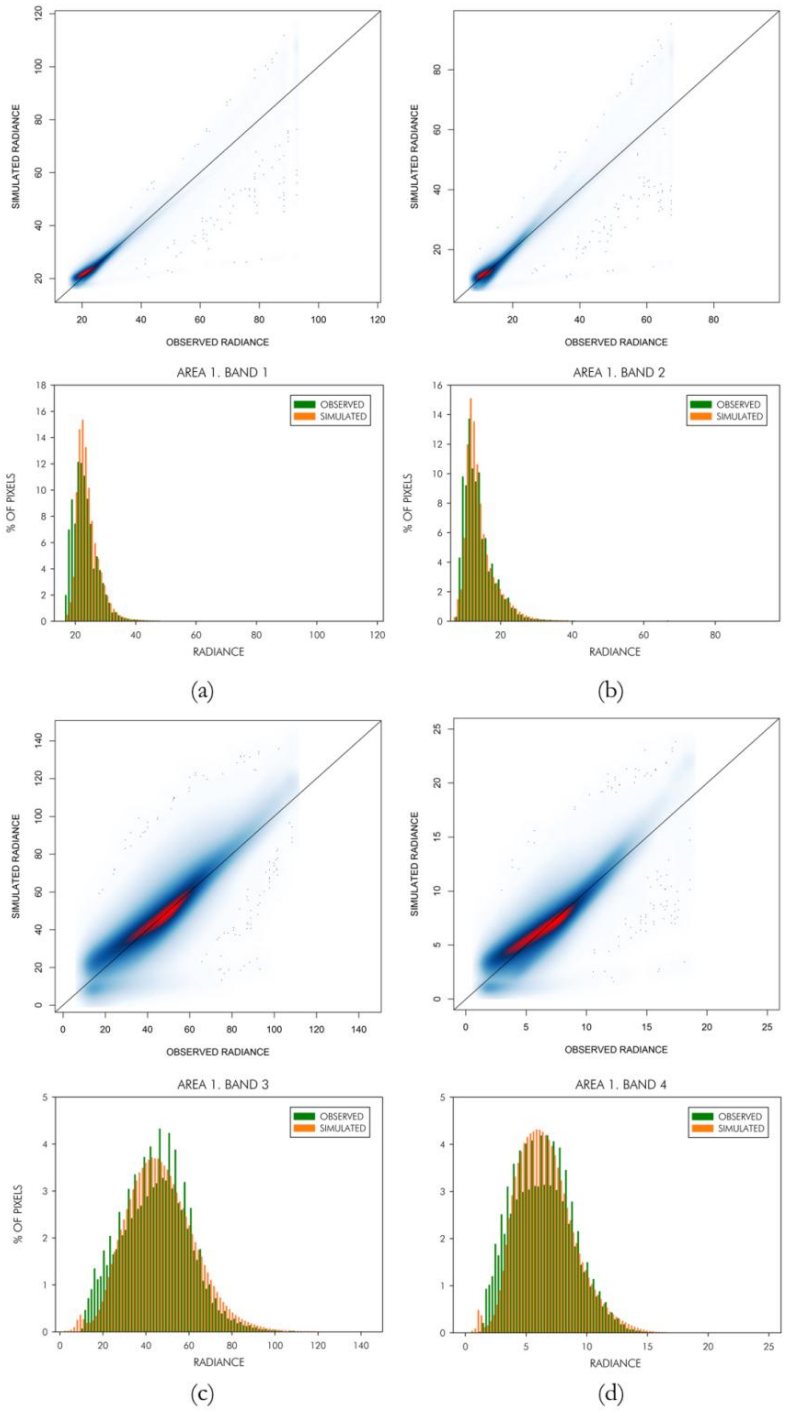

Fig. 4.2. Results for area 1. Scatterplots and histograms of observed and simulated radiance (in units of $W \cdot m^{-2} \cdot sr^{-1} \cdot \mu m^{-1}$) of **(a)** Band 1 **(b)** Band 2 **(c)** Band 3 **(d)** Band 4

In area 2 histogram shapes were well reproduced, showing a bimodal distribution due to the presence of agricultural crops on the one hand and forest areas on the other hand.

Scatterplots showed a good coincidence between simulated and observed radiances. However, in band 3 and 4 the variance of the radiance was higher in the simulated scene. This effect was visible in Fig. 4.S2d, where the small peak at the lowest region of the histogram corresponding to a reservoir was underestimated, while the high radiances corresponding to agricultural crops in the left bottom corner of the area were overestimated.

Also, in area 3 and 4 high radiances of band 1 and 2 were underestimated, probably corresponding to urban areas, with more complex reflective behavior and mainly located in the valleys, so therefore not affected by topography. Anyhow, those were only a few pixels and they do not affect the quality of the simulation, as can be assessed both visually, and statistically (Table 4.2).

It was noticeable the presence of a clear high bound in the observed radiances in the scatterplots, which was not present in the synthetic images. This was caused by the format of the original imagery, stored at 8 bits. When the DN were transformed to radiance an upper limit was set, but this was not occurring in the synthetic images, where areas of high ground-reflectance in slopes facing the sun ended in higher values of at-sensor radiance. Also histograms of observed radiances seemed to be serrated, which is a typical effect when a smaller integer color space is expanded to a larger one.

Table 4.2. Statistical indexes to measure similarity between real and simulated scenes.

AREA	B1			B2			B3			B4		
	r^2	RMSE	MSSIM	r^2	RMSE	MSSIM	r^2	RMSE	MSSIM	r^2	RMSE	MSSIM
1	0.92	1.38 (6.1%)	0.848	0.92	1.38 (10.6%)	0.802	0.87	5.93 (11.5%)	0.787	0.86	0.95 (14.1%)	0.633
2	0.96	2.85 (5.1%)	0.840	0.95	4.07 (9.1%)	0.806	0.86	4.10 (6.2%)	0.807	0.93	1.41(9.9%)	0.681
3	0.92	2.51 (5.3%)	0.876	0.90	2.25 (9.9%)	0.803	0.97	2.15 (3.9%)	0.966	0.87	1.14 (14.3%)	0.701
4	0.99	1.09 (3.2%)	0.977	0.99	1.19 (5.8%)	0.966	0.98	3.75 (5.8%)	0.961	0.97	0.65 (7.5%)	0.911

As seen in Table 4.2, all the three indexes showed good results for the first three spectral bands, but a poorer performance of band 4, in particular in areas 1 and 3. Anyway, in all the cases the statistics were in line with results of other simulation models (Borner et al. 2001; Datcu and Holecz 1993). The coefficient of determination (r^2) kept above 0.85, and MSSIM above 0.60. The RMSE between observed and simulated spectral radiances ranged from 1 to 6 $W \cdot m^{-2} \cdot sr^{-1} \cdot \mu m^{-1}$ (3 to 14% of the mean value), very close to the results obtained by Verhoef

and Bach (2012) for similar spectral bands. Among the study areas, all of them performed good but the 1st seemed to perform slightly worse than others according to the statistical indexes, probably due to the more severe illumination conditions derived from the lower solar elevation angle.

4.5. Conclusions

The aim of this letter was to extend the synthetic image simulation model proposed in (Sola et al. 2014a) to the multispectral case and to validate this model using real SPOT 5 imagery. The results obtained using four test sites with different acquisition conditions illustrate a good behavior of the model. The comparison between simulated and real SPOT 5 scenes yielded r^2 values above 0.90 for visible bands, and above 0.86 for the NIR and SWIR. Similarly, using MSSIM values could be ranked in order of accuracy as follows: green (>0.84), red (>0.80), NIR (>0.78) and SWIR (>0.63). These results were consistent for the four different test areas, although there were differences between them, with study area 1 achieving the lowest accuracies. This could be partly explained by the lower solar elevation angle of this area. All in all, relative RMSE values were normally below 10% of the observed radiance, which is considered accurate enough for the purpose this model was designed for. Thus, the TOC evaluation approach proposed in Sola et al. (2014a) could be subsequently used with multispectral data for evaluating TOC algorithms on different areas and acquisition conditions.

Acknowledgements

The authors gratefully acknowledge the financial support provided by the Public University of Navarre (UPNA). The authors would also like to thank the Spanish National Geographic Institute (IGN) for providing the test data. Part of the research presented in this paper is funded by the Spanish Ministry of Economy and Competitiveness in the frame of the ESP2013-48458-C4-2-P project.

Author Contributions

Ion Sola, María González de Audícana and Jesús Álvarez-Mozos provided the overall conception of this research, designs the methodologies and experiments, and wrote the majority of the manuscript; Ion Sola carried out the implementation of proposed algorithms, conducted the experiments and performed the data analyses.

4.6. Supplementary Results

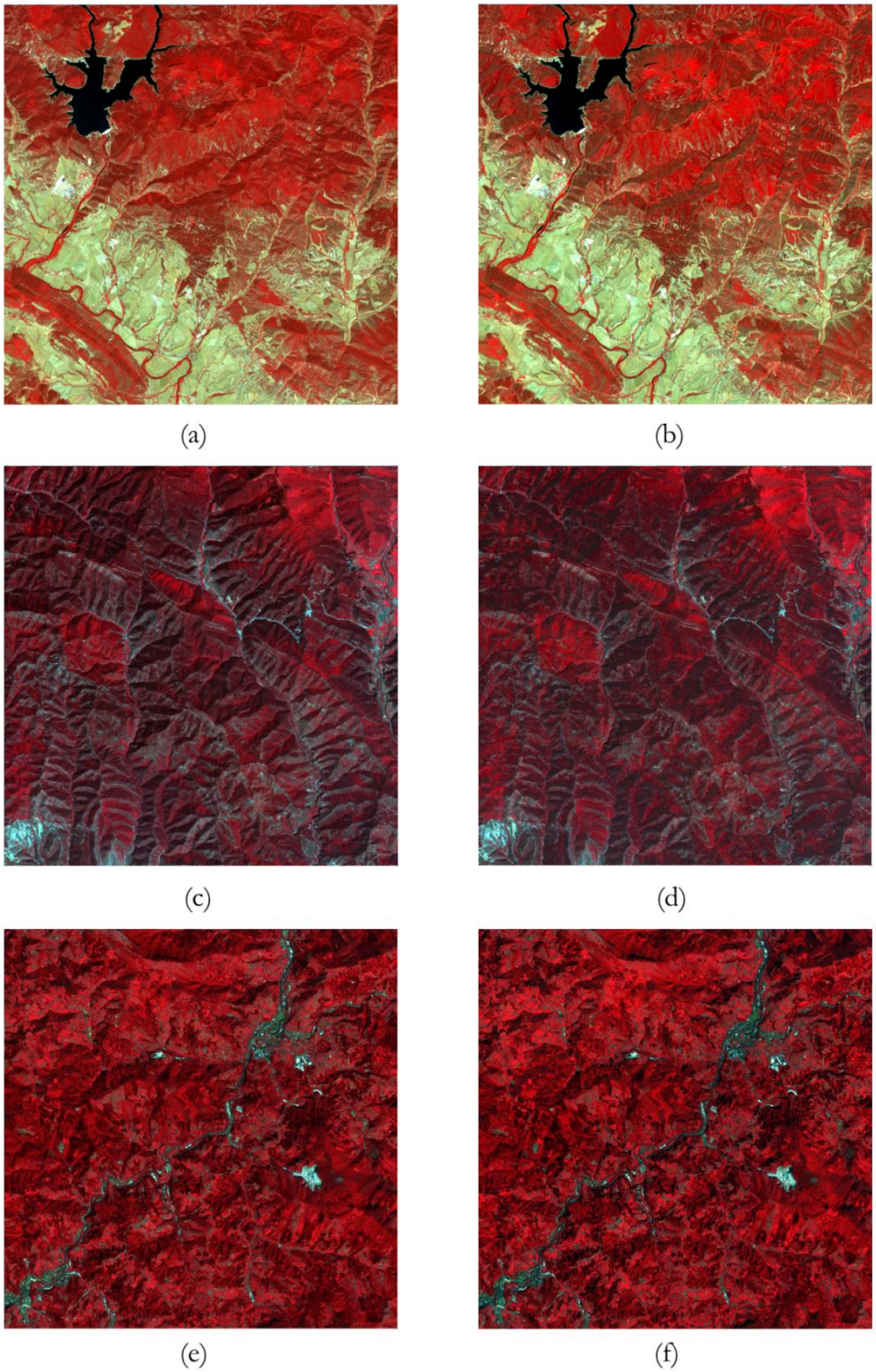

Fig. 4.S1. RGB false color composition of real and simulated scenes of **(a)** Area 2. Real **(b)** Area 2. Simulated **(c)** Area 3. Real **(d)** Area 3. Simulated **(e)** Area 4. Real **(f)** Area 4. Simulated

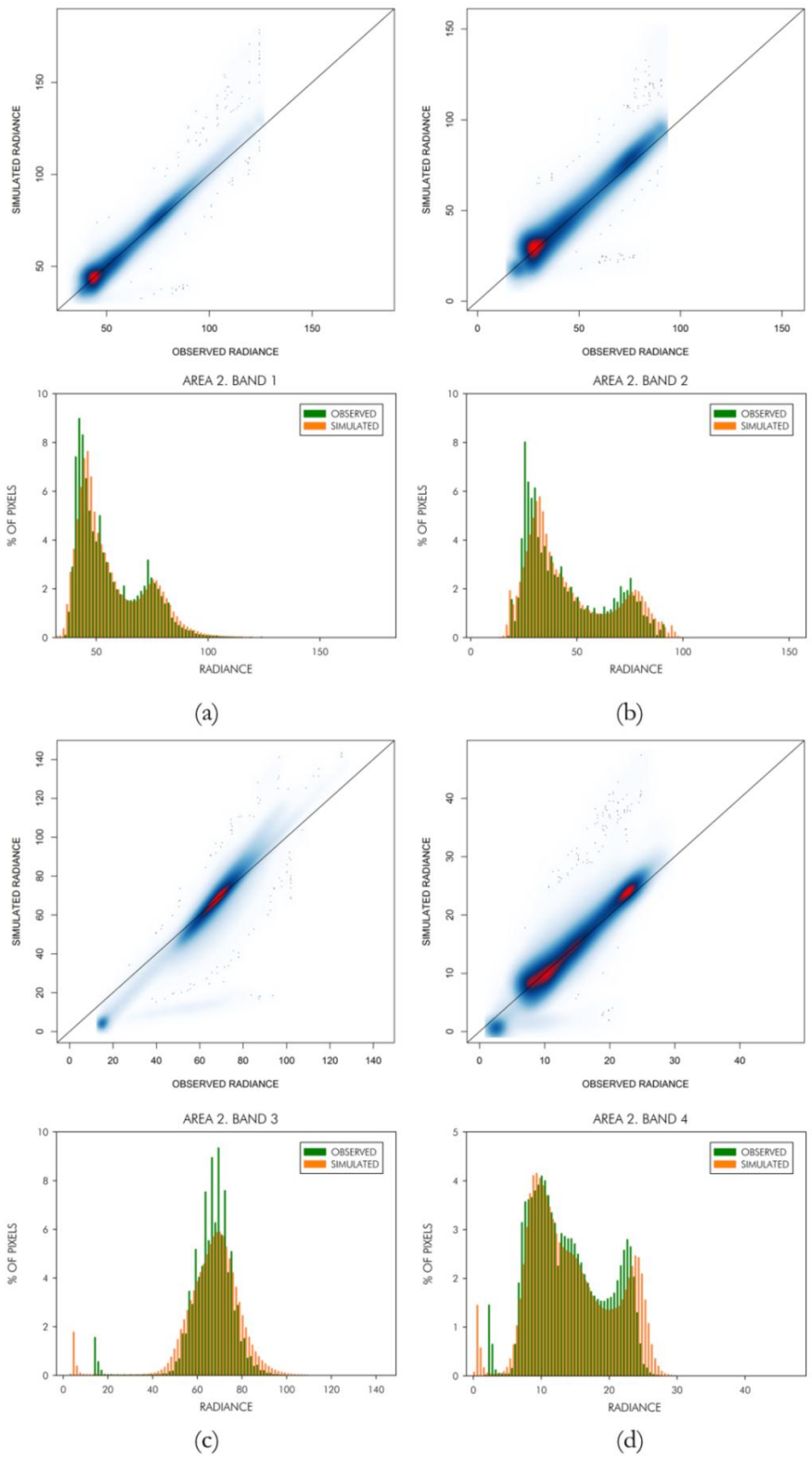

Fig. 4.S2 Results for area 2 . Scatterplots and histograms of observed and simulated radiance (in units of $W \cdot m^{-2} \cdot sr^{-1} \cdot \mu m^{-1}$) of **(a)** Band 1 **(b)** Band 2 **(c)** Band 3 **(d)** Band 4

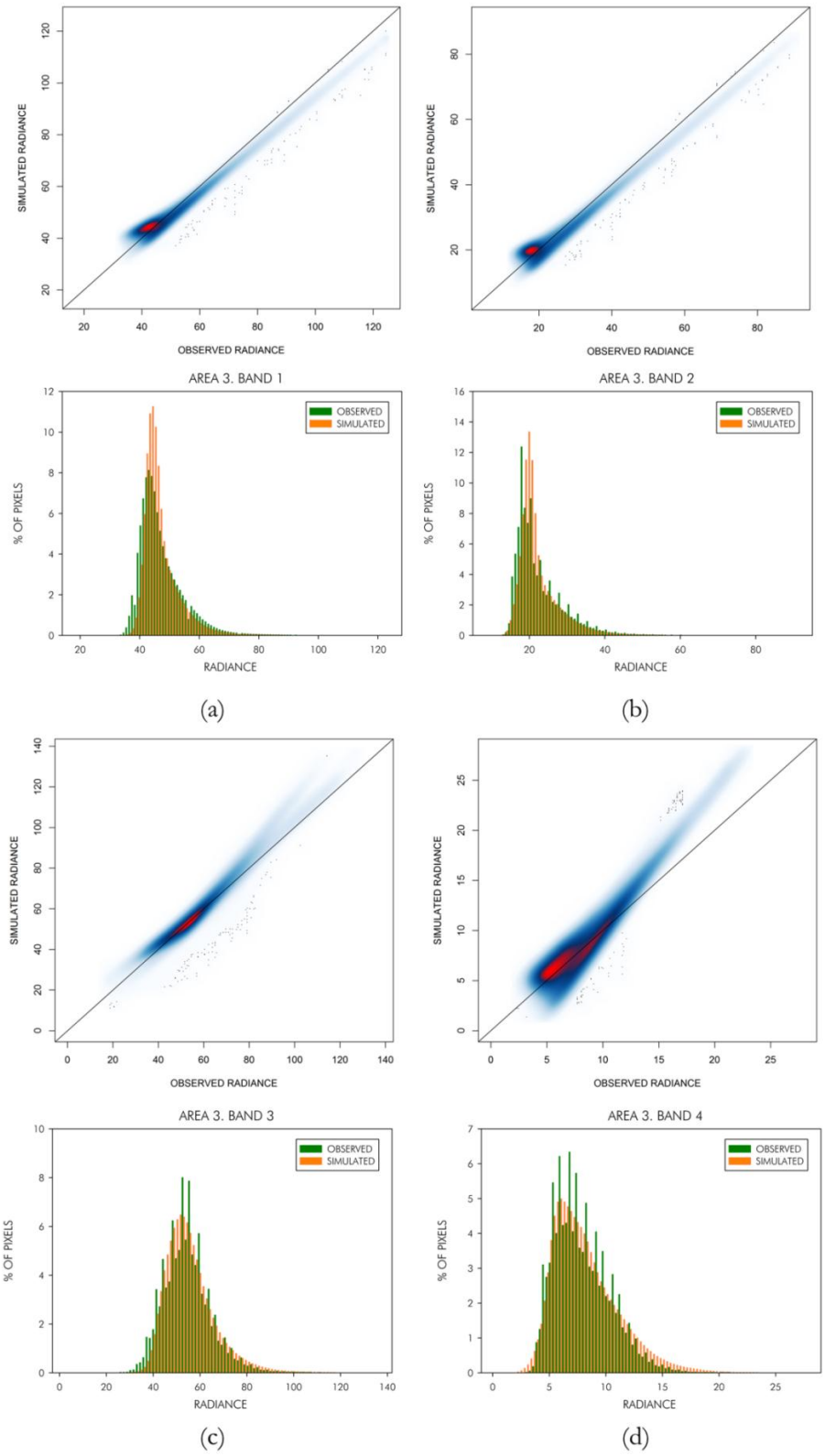

Fig. 4.S3 Results for area 3 . Scatterplots and histograms of observed and simulated radiance (in units of $W \cdot m^{-2} \cdot sr^{-1} \cdot \mu m^{-1}$) of **(a)** Band 1 **(b)** Band 2 **(c)** Band 3 **(d)** Band 4

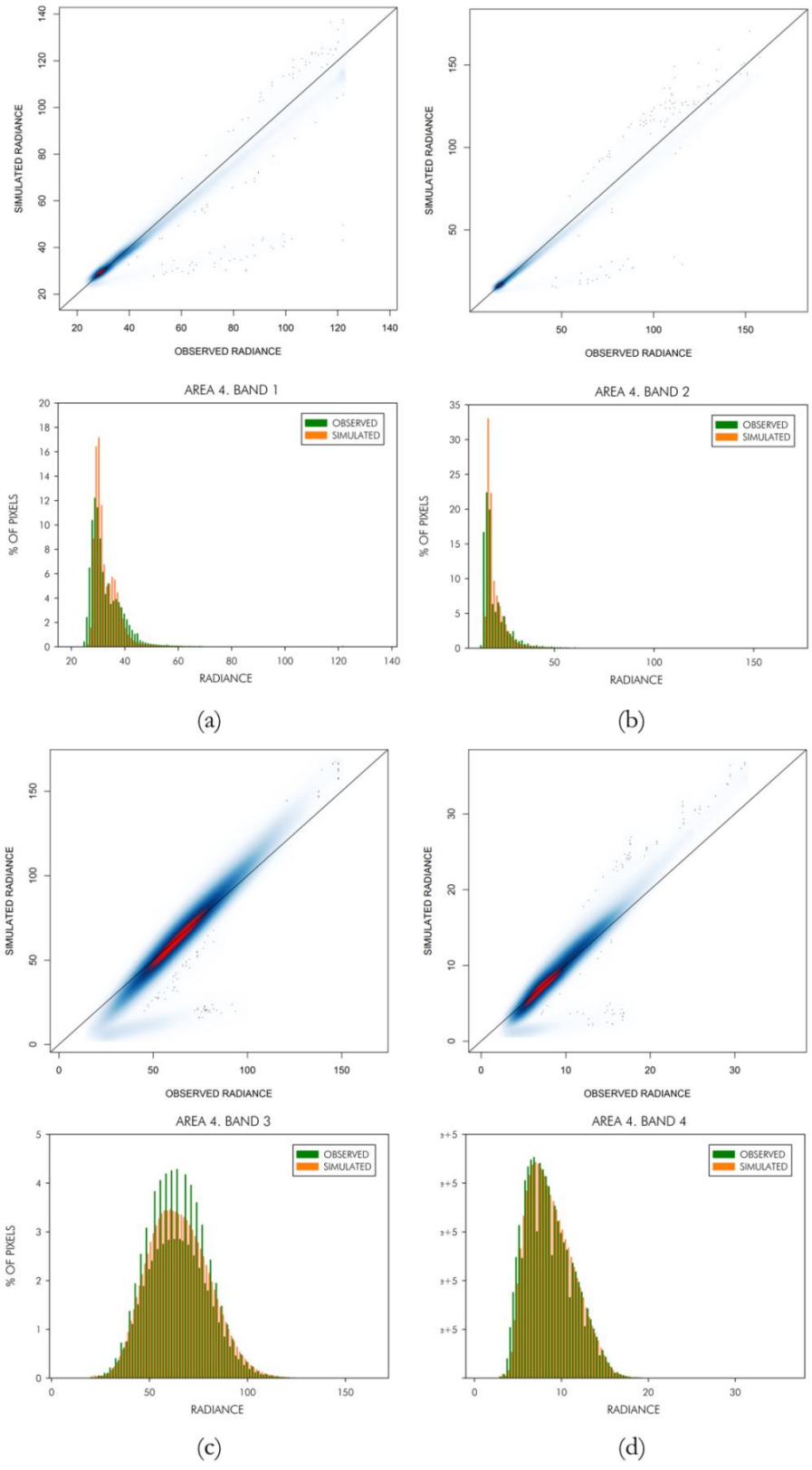

Fig. 4.S4 Results for area 4. Scatterplots and histograms of observed and simulated radiance (in units of $W \cdot m^{-2} \cdot sr^{-1} \cdot \mu m^{-1}$) of (a) Band 1 (b) Band 2 (c) Band 3 (d) Band 4

CHAPTER 5

MULTITEMPORAL ANALYSIS OF TOPOGRAPHIC CORRECTION ALGORITHMS

Adapted from:

- Sola, I.; González-Audícana, M.; Álvarez-Mozos, J.; Torres, J. L. (2014). Evaluación multitemporal de métodos de corrección topográfica mediante el uso de imágenes sintéticas multiespectrales. *Revista Teledetección, 41*, 71-78.

Abstract — This chapter presents a multitemporal evaluation of TOC methods based on synthetically generated multispectral images in order to evaluate the influence of solar angles on the performance of TOC methods. For that purpose, four different dates across the year were considered. For each of them two synthetic images were generated, one considering the real topography of a specific area and another one considering the relief of this area as being completely flat, following the procedure described in Sola et al. (2014a; 2015a). The comparison between the corrected image obtained applying a TOC method to the former image and the later image of the same area, considered the ideal correction, allowed assessing the performance of each TOC algorithm. This performance was quantitatively measured through the Structural Similarity Index (SSIM) on four selected semi-empirical TOC methods, assessing their behavior over the year. All of them showed the same trend, with a clear decrease of quality in scenes simulated for lower solar elevation angles. Among them, C-Correction ranked first, giving satisfying results in all the simulated dates, while other algorithms showed a good performance in summer but gave worse results in winter.

Keywords — Synthetic image, topographic correction, multitemporal evaluation, SSIM, TOC, DEM

5.1. Introduction

The relative inaccessibility of mountainous regions areas favors RS techniques as a monitoring tool (Lambin and Geist 2008). Nevertheless the use of RS data in topographically complex terrain is affected by the radiometric distortions introduced by the relief. These distortions depend on the solar incidence angle (γ_i), that is, the angle between the normal to the ground surface and the solar zenith direction, which in turn varies depending on the solar geometry at the acquisition time.

The usefulness of RS data for different applications, such as land cover/use mapping, forest change detection or vegetation cover monitoring (Tokola et al. 2001; Zhan et al. 2002; Vicente-Serrano et al. 2008; Masek et al. 2008) is hampered by these variations in the radiance detected by remote sensors due to differences in illumination (i.e., $\cos\gamma_i$). Consequently, topographic correction (TOC) becomes a necessary preprocessing step to improve interpretation of satellite imagery.

Different TOC methods have been developed in the last decades in order to eliminate or at least reduce this effect, so called topographic effect, but the selection of a suitable method to topographically correct satellite images in areas with rugged terrain is still an unresolved problem (Ediriweera et al. 2013).

To date, three primary categories of TOC methods have been developed: 1) purely empirical methods, such as spectral band ratioing (Colby 1991; Ono et al. 2007), 2) semi-empirical methods, based on the computation of the solar incidence angle. These methods require a DEM of enough spatial resolution (Gao and Zhang 2009a), and can be divided in two subcategories: Lambertian (LTOC) and Non-Lambertian (NLTOC) methods. The former are based on the very simple but unrealistic assumption that surface reflectance is isotropic, whereas the latter introduce band-dependent empirical correction parameters and assume non-Lambertian behavior, and 3) physically based TOC methods, which employ radiative transfer codes to obtain a deterministic description for the correction of topographic effects. These methods are considerably more sophisticated but they are more complex to implement in a pre-processing chain and have requirements hardly available.

Several semi-empirical NLTOC methods have been developed accomplishing a great balance between ease of implementation and good performance. These techniques generally include band dependent parameters in order to model the non-Lambertian behavior of each land cover for every band. For instance, Teillet et al. (1982) proposed the CC correction, introducing a parameter c_λ (i.e., the ratio between the slope and intercept of the linear regression equation between the radiance of each band and $\cos\gamma_i$) to the COS method to emulate the effect of diffuse irradiance from the sky and avoid overcorrection problems. Similarly, Soenen et al. (2005) introduced this same parameter to SCS correction (Gu and Gillespie 1998), originally proposed to correct the topographic effect on forest images, and designated it as SCS+C correction. Alternatively, other semi-empirical approaches have also been proposed, such as the MIN correction method (Smith et al. 1980; Teillet et al. 1982), based on the derivation for each band of a Minnaert k_λ coefficient characterizing surface anisotropic properties, or the SE method of Teillet et al. (1982), which assumes a linear relationship between the radiance of each band and the cosine of the solar incidence angle.

A key factor of topographic correction is the analysis of the quality of the corrected images.

For this purpose, several procedures to assess the goodness of TOC algorithms are found in the literature. The visual analysis of the removal of the topographic effect in satellite imagery gives a good first indication on the quality of the correction. A successful TOC led to a loss of the three-dimensional impression, but this criterion is subjective, thus rigorous quantitative assessments are required in order to evaluate the performance of each TOC method. Some of the widely used evaluation criteria are: 1) The quantification of the reduction of the dependence between $\cos\gamma_i$ and the radiance/reflectance of each spectral band after the correction (Gao and Zhang 2009a), 2) The analysis of the variations in the radiometry of the corrected scenes (Civco 1989), 3) The reduction of the land cover class variability (Lu et al. 2008; Riaño et al. 2003; Shepherd and Dymond 2003), 4) The improvement on classification accuracy after topographic correction (Conese et al. 1993; Teillet et al. 1982), 5) The improvement in biophysical parameter retrievals (Ekstrand 1996; Tokola et al. 2001), or 6) The increase in temporal stability of a time series for individual pixels (Hantson and Chuvieco 2011).

These evaluation procedures have their own limitations, such as the need for *a priori* knowledge on structural landscape characteristics (Baraldi et al. 2010). This information is normally not available. In fact, this is the type of information pursued from the images to be corrected. Due to this, different evaluation studies published in the recent years did not agree on which TOC method performs the best in every situation. To overcome these limitations a new procedure based on the use of synthetically generated images has been proposed (Sola et al. 2014a). These images, generated under specific geometric and temporal acquisition conditions and considering a certain land cover structure, allow evaluating the performance of different TOC methods. The aim of this paper is to analyze the behavior of four semi-empirical selected TOC methods on different acquisition dates. With this purpose, a set of four different temporal configurations have been selected to simulate synthetic scenes acquired along the year, following a previous multitemporal study of TOC methods (Sola et al. 2012).

For each considered date a pair of synthetic images is generated. On the one hand, the Synthetic Real (SR) image is simulated accounting for the real topography of the study area obtained from a high-resolution DEM. On the other hand, a perfectly flat surface is assumed

in order to simulate the Synthetic Horizontal image (SH). The latter is, in fact, the ideal situation in the absence of topographic effect, and consequently the aim of TOC methods. The new evaluation methodology proposed by Sola et al. (2014a) is subsequently based on the comparison between the topographically corrected SR image and the SH image. This comparison is conducted through the Structural Similarity (SSIM) Index (Wang et al. 2004), and provides a means for quantitatively assess the goodness of TOC algorithms.

Most of the evaluations of TOC methods presented in the literature were applied under specific and generally favorable conditions, i.e., just for a certain platform and usually in summer months. Nevertheless, few studies assessed the behavior of these methods on a variety of dates and illumination conditions. Hantson and Chuvieco (2011) evaluated different TOC methods on 15 images taken under different illumination conditions, whereas Vicente-Serrano et al. (2008) conducted multitemporal evaluation of the performance of TOC methods, combined with atmospheric correction, for time series of Landsat images, but in both cases these images were affected by confounding factors, that is, not only by different illumination conditions but also different atmospheric conditions and differences in spectral signatures due to phenological changes. In this work though, four different temporal configurations, are considered to generate the synthetic images, being these configurations representative of different illumination conditions. Therefore, the influence of date, that is, solar geometry on the behavior of TOC methods can be explored, while other factors such as land cover reflectance or atmospheric effect remain constant.

5.2. Synthetic image generation

The process to simulate a synthetic image for a specific area, explained by Sola et al. (2014a), was adapted to simulate multispectral SPOT 5-like scenes with four bands, i.e., green, red, NIR and SWIR bands in (Sola et al. 2015a). This process can be summarized in two phases, carried out for each spectral band (see Fig. 5.1). On the first phase, the image representing the global irradiance at each point of the area of interest at a certain date and time is obtained. On the second phase, the top-of-atmosphere radiance (TOARD) a sensor would receive is generated, considering a certain sensor configuration. This is in fact, the final synthetic image.

Firstly, it is necessary to estimate the Global Horizontal Irradiance of each spectral band ($E_{e,g,\lambda}$). This term has two different components, direct and diffuse radiation, that can be estimated through different models (Ma and Iqbal 1984; ASHRAE 1985; Bird and Riordan 1986), considering sunny or quasi sunny conditions and horizontal surface. In this work the Cloud-free Global Radiation model, validated within the SATEL-LIGHT project (Dumortier 1995, 1998; Kasten 1996; Page 1996; Ineichen 1998) was selected, as it exhibited a good correspondence between estimated and measured values under cloudless conditions. Subsequently, the fraction of direct and diffuse irradiance corresponding to each spectral band was obtained through SMARTS2 model (2006).

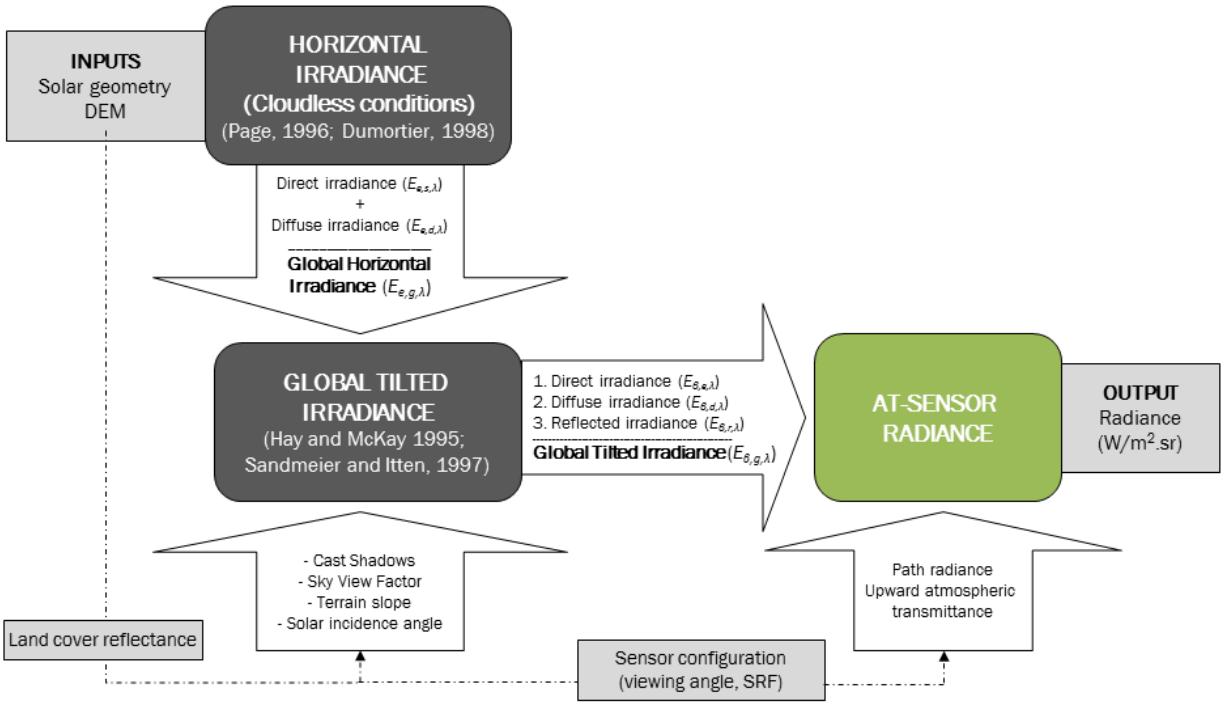

Fig. 5.1. Process to simulate synthetic images

Later on, the Global Tilted Irradiance ($E_{\beta,g,\lambda}$) of λ band was estimated, accounting for the topographical characteristics of the study area. With this aim, its three components had to be calculated, i.e., Direct Tilted Irradiance or Sunlight ($E_{\beta,s,\lambda}$), Ground-Reflected Irradiance ($E_{\beta,r,\lambda}$) and Sky Diffuse Irradiance or Skylight ($E_{\beta,d,\lambda}$). The first term was calculated applying the cosine law to Direct Horizontal Irradiance. Additionally, a binary factor was added for the purpose of controlling cast shadows originated by adjacent slopes (Richter et al. 1998). $E_{\beta,d,\lambda}$ was

calculated with Hay and McKay's Model (1985), also including the binary factor proposed by Richter. Finally, Ground-Reflected Irradiance ($E_{\beta,r,\lambda}$), was obtained following Sandmeier and Itten (1997).

On the second phase, the at-sensor radiance values were calculated as follows, considering the previously obtained Global Tilted Irradiance as well as land covers' reflectance for each spectral band, the sensor viewing angle, Spectral Response Function (SRF) and spatial resolution of the sensor and acquisition date and time:

$$L_{sen,\lambda} = L_{p,\lambda} + \frac{\rho_\lambda T_{u,\lambda} E_{\beta,g,\lambda}}{\pi} \qquad (5.1)$$

where, $L_{p,\lambda}$ is the atmospheric path radiance calculated with Bird and Hulstrom's model (1981), ρ_λ is the land cover's reflectance value, $T_{u,\lambda}$ is the upward atmospheric transmittance, obtained following the expression of Gilabert et al. (1994), and $E_{\beta,g,\lambda}$ is the Global Irradiance of λ band. Land cover's reflectance is a key factor in the generation of synthetic multispectral scenes. On the one hand, they can be simulated from spectral libraries (Sola et al. 2012; 2014a). On the other hand, they can be obtained from a satellite image, converted from DN to reflectance, and atmospherically and topographically corrected (Sola et al. 2015a).

This same process was applied to SH image, but excluding the calculation of global irradiance on tilted surfaces in order to simulate the radiance a sensor would acquire if the topography was completely horizontal. As explained previously, this image is used as a reference to evaluate the quality of each correction applied to the generated SR images.

5.3. TOC algorithms

Four established semi-empirical TOC methods were evaluated to assess the impact of acquisition time and date, and in turn solar geometry, on the performance of topographic corrections (see Table 5.1). One of the selected TOC was COS method, which is the simplest and one of the most widely used Lambertian TOC (LTOC), originally proposed by Smith et al. (1980) and later modified by Teillet et al. (1982). The method assumes that the lower the illumination, the higher is the corrected radiance. Furthermore, the solar zenith angle is used to take into account non-verticality of sun rays. Several authors have reported problems of

overcorrection applying this algorithm, mainly in poorly illuminated slopes (Twele et al. 2006; Füreder 2010).

Also SCS+C correction (Soenen et al. 2005) and CC method (Teillet et al. 1982) were tested here, which are semi-empirical non-Lambertian methods (NLTOC) including a band dependent parameter, c_λ. This parameter was introduced by Teillet el al. (1982) to avoid the overcorrection produced by COS method, whereas Soenen et al. (2005), in an analogous procedure introduced this parameter to the SCS method, based on the Sun-Canopy-Sensor geometry and originally designed for forests. Finally the SE method, a semi-empiric method also proposed by Teillet et al. (1982), was evaluated. This algorithm is a regression-based approach which assumes a linear correlation between the radiance of each band and the illumination, i.e. $\cos\gamma_i$.

Table 5.1. Equations of the TOC methods tested

TOC METHOD	*EQUATION*
COS	$L_{sen,corr,\lambda} = L_{sen,\lambda}\frac{\cos\theta_s}{\cos\gamma_i}$
CC	$L_{sen,corr,\lambda} = L_{sen,\lambda}\frac{\cos\theta_s + c_\lambda}{\cos\gamma_i + c_\lambda}$
SE	$L_{sen,corr,\lambda} = L_{sen,\lambda} - (A + B\cos\gamma_i) + \overline{L_{sen,\lambda}}$
SCS+C	$L_{sen,corr,\lambda} = L_{sen,\lambda}\frac{\cos\theta_s + c_\lambda}{\cos\gamma_i\cos\beta + c_\lambda}$

where, $L_{sen,corr,\lambda}$ and $L_{sen,\lambda}$ are, respectively TOC-corrected and non-corrected at-sensor radiance, θ_s is the solar zenith angle, γ_i is the solar incidence angle, β is the terrain slope, *A* and *B* are, respectively, the intercept and the slope of the regression line between radiance and illumination (i.e., $\cos\gamma_i$), and c_λ is the empiric constant calculated for CC and SCS+C methods as described by Teillet et al. (1982).

5.4. TOC evaluation

The objective of this work is to conduct a multitemporal evaluation of TOC methods. With this aim, the procedure described in Fig. 5.2 is followed.

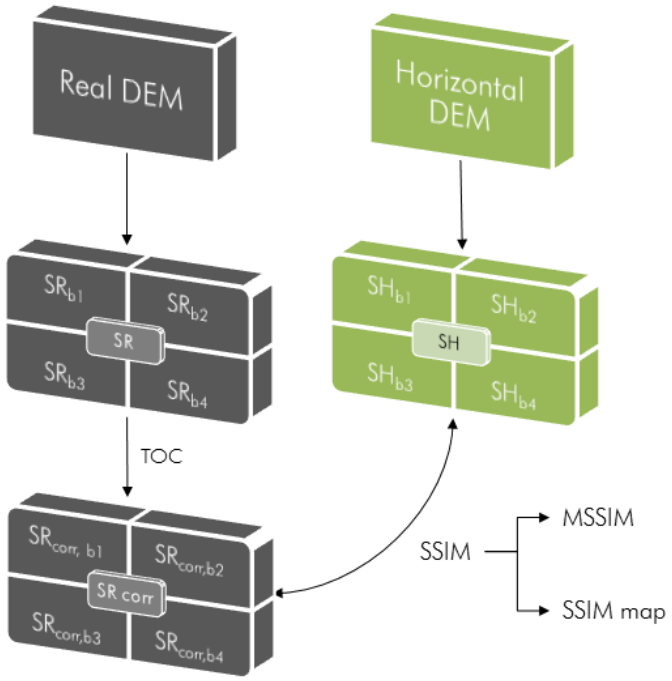

Fig. 5.2. Scheme of the methodology to evaluate TOC algorithms based on synthetic images

As explained above, the Synthetic Horizontal (SH) image corresponds to the ideal situation where topography has no influence on the radiance detected by remote sensors. Thus, the TOC corrected SR images are compared with this ideal image to assess the degree of similarity to the perfect correction. Consequently, this comparison allows us to quantitatively measure the goodness of topographic correction. For that purpose, the Structural SIMilarity Index (SSIM) is used. The SSIM is an universal and objective image quality index proposed by Wang et al. (2004) to measure the similarity between two images though its three components (luminance comparison, contrast distortion and structural similarity), and it ranges from -1 to 1, being the value of 1 only reachable in case of two identical sets of data.

$$SSIM = \frac{(2\mu_x\mu_y+c_1)(2\sigma_{xy}+c_2)}{(\mu_x{}^2+\mu_y{}^2+c_1)(\sigma_x{}^2+\sigma_y{}^2+c_2)} \qquad (5.2)$$

where, x refers to the reference image, y to the TOC corrected image, μ_i is the mean value of the image, and σ_i the standard deviation. c_1 and c_2 are two user-defined constants included to avoid unstable results when $\mu_x{}^2 + \mu_y{}^2$ and $\sigma_x{}^2 + \sigma_y{}^2$ are very close to zero. These constants are obtained from $c_1=(k_1.L)^2$ and $c_2=(k_2.L)^2$, where L is the dynamic range of the image, set to

255. In this paper values of $k_1 = 0.01$ and $k_2 = 0.03$ have been used following recommendations by Wang et al. (2004).

In practice, a quantitative evaluation usually requires a single overall quality measure of the entire image (Wang et al. 2004), so a mean SSIM (MSSIM) index is used to evaluate the overall image quality of TOC. Nevertheless, SSIM maps, computing the local statistics within an 11 x 11 circular-symmetric Gaussian weighting function, are also interesting and useful to detect problematic areas where TOC methods failed. The SSIM maps generated for each TOC corrected image show the performance of the correction pixel by pixel.

5.5. Case study

This study has been carried out for four different dates over the year, from March to December, over a mountainous area (Pyrenees) of the North-Eastern side of Navarre, Spain (see Fig. 5.3) covering an extension of 15 x 15 km, where broad-leaved forests are predominant.

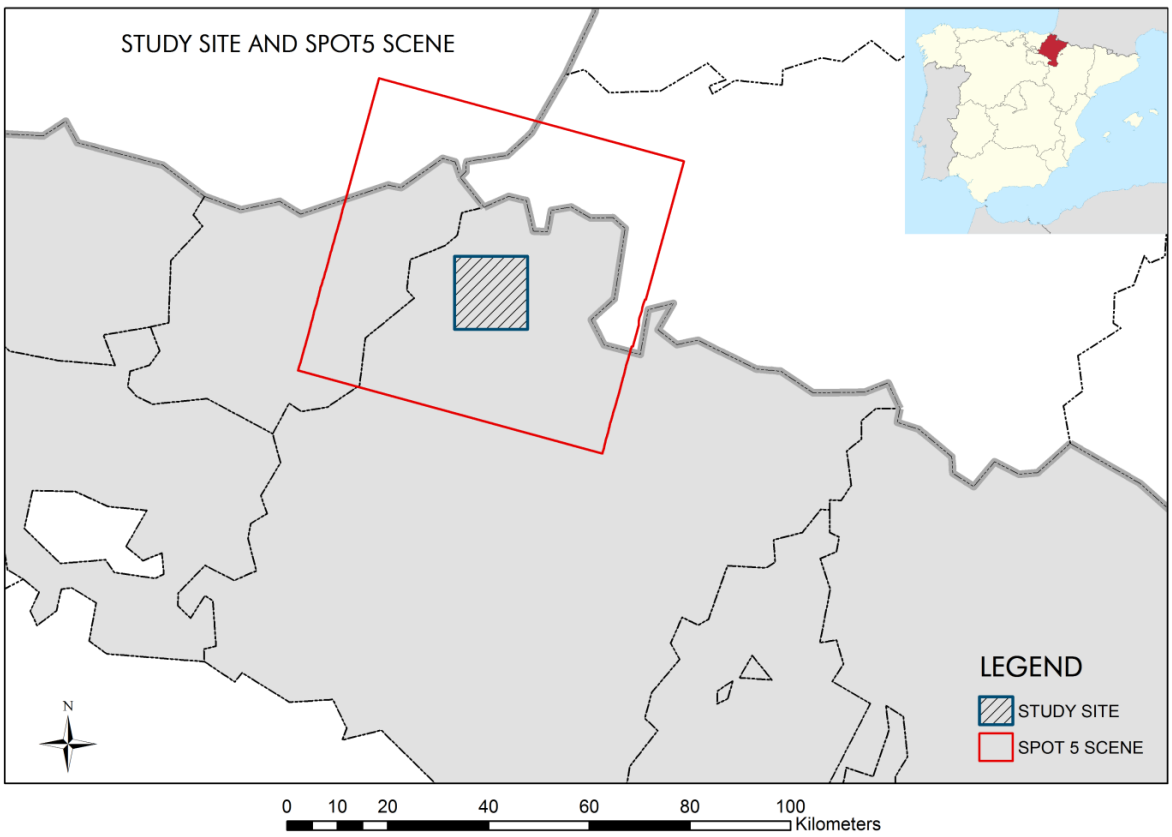

Fig 5.3. Study site, located on North-Eastern side of Navarre.

In order to analyze different illumination conditions synthetic images corresponding to four different dates were generated (see Table 5.2), with solar elevation angles ranging from 21 to 64°. For each scene, four spectral bands were simulated, corresponding to the wavelength of green (500-590 nm), red (610-680 nm), near infrared (780-890 nm) and short wave infrared (1580-1750 nm), considering both the real relief of the area (SR image) and an horizontal topography (SH scene).

Table 5.2. Date, time and solar angles considered

Parameters	*1*	*2*	*3*	*4*
Date	March 15th	June 15th	August 15th	December 15th
Time (UTC)	10:45	10:45	10:45	10:45
Solar azimuth (°)	150.0	133.0	141.1	161.5
Solar elevation (°)	40.8	64.3	55.8	21.7

As inputs, a DEM with a spatial resolution of 5 m obtained through standard photogrammetric techniques, and ground reflectance obtained from a real SPOT 5 multispectral scene were used. The latter was converted from at-sensor radiance to ground reflectance through atmospheric and topographic correction by the methods of Dark Object Subtraction (DOS) of Chavez (1988) and CC of Teillet et al. (1982), respectively, due to their simplicity and good performance. In order to simulate synthetic images on different acquisition dates, the corresponding solar geometry of each case was considered, but the land covers' reflectance was assumed to be constant for the four cases. This is an unrealistic assumption, as the vegetation variability and phenological changes were neglected, but it was beneficial for the purpose of this study, i.e. assessing the behavior of TOC methods on different illumination conditions, as the radiance variations between images were only due to irradiance differences, that is, solar geometry configurations, across the year. Finally, clear sky conditions and a sensor zenith angle of 12° were considered, typical value in the geometry of acquisition of this platform.

In Fig 5.4 synthetic multispectral images corresponding to March, June, August and December are shown. As seen in the RGB composition, SH images (on the bottom) represented the at-sensor radiance detected for a completely flat surface. On the contrary, the SR images (on the top) introduced a clear topographic effect, increasing in winter dates and becoming dramatic in the scene of December. On these dates the solar elevation angle

was lower (see Table 5.2) and consequently the topographic effect was more severe. In this particular conditions, large shadowed areas appeared (see Fig. 5.4d), corresponding to slopes were no direct irradiance reaches the ground.

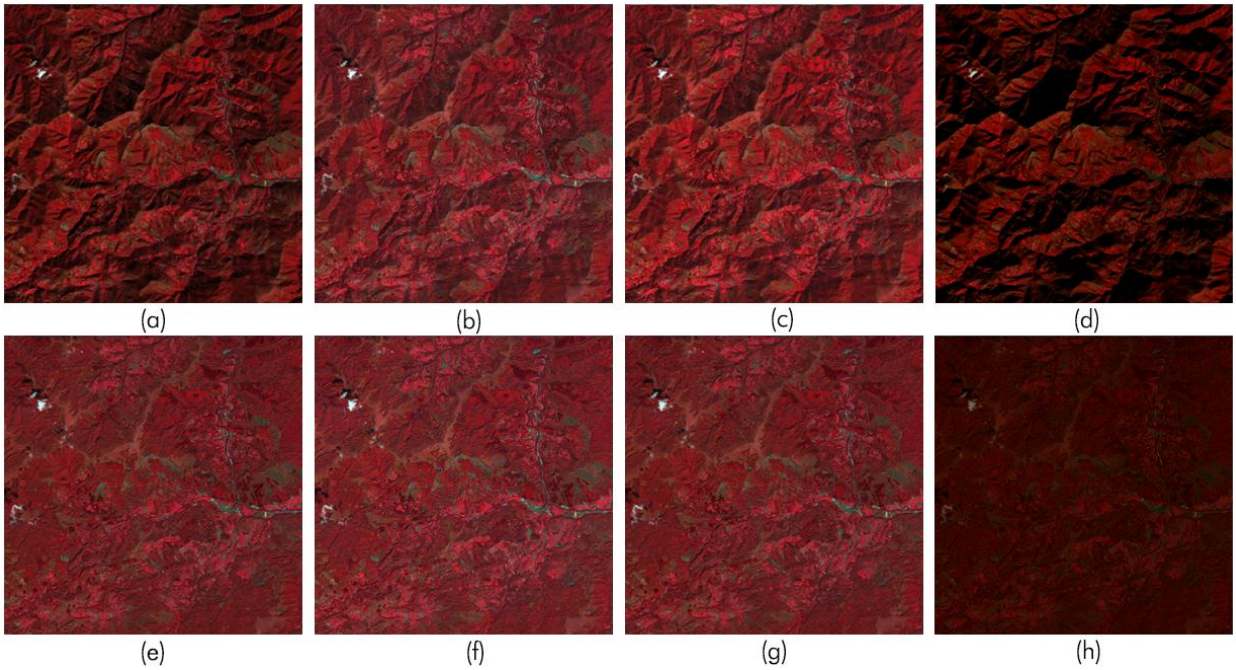

Fig. 5.4. Synthetic Real (SR) images of **(a)** March **(b)** June **(c)** August **(d)** December. Synthetic Horizontal (SH) images of **(e)** March **(f)** June **(g)** August **(h)** December.

Fig 5.4 also showed an evident decrease of the mean radiance detected by the sensor on winter scenes, clearly observed in the lower intensity of RGB composition on these cases. On the contrary, the image of June exhibited the highest brightness and the lower variance in radiance values among the four cases, and also the highest similarity between SR and SH, signal of a gentler topographic effect.

5.6. Results and Discussion

The resulting mean SSIM indexes (MSSIM) and SSIM maps for each spectral band and for the four considered dates were used to analyze the multitemporal performance of TOC algorithms under different solar geometries. In Fig. 5.5 the RGB composite of the corrected images of March, June, August and December are shown. On top the images corrected by CC method are shown, while on the bottom the corrected images by SE method are displayed. Similar to Fig. 5.4, the images of March and December exhibited a lower intensity

due to the decrease of irradiance impinging the surface on these dates.

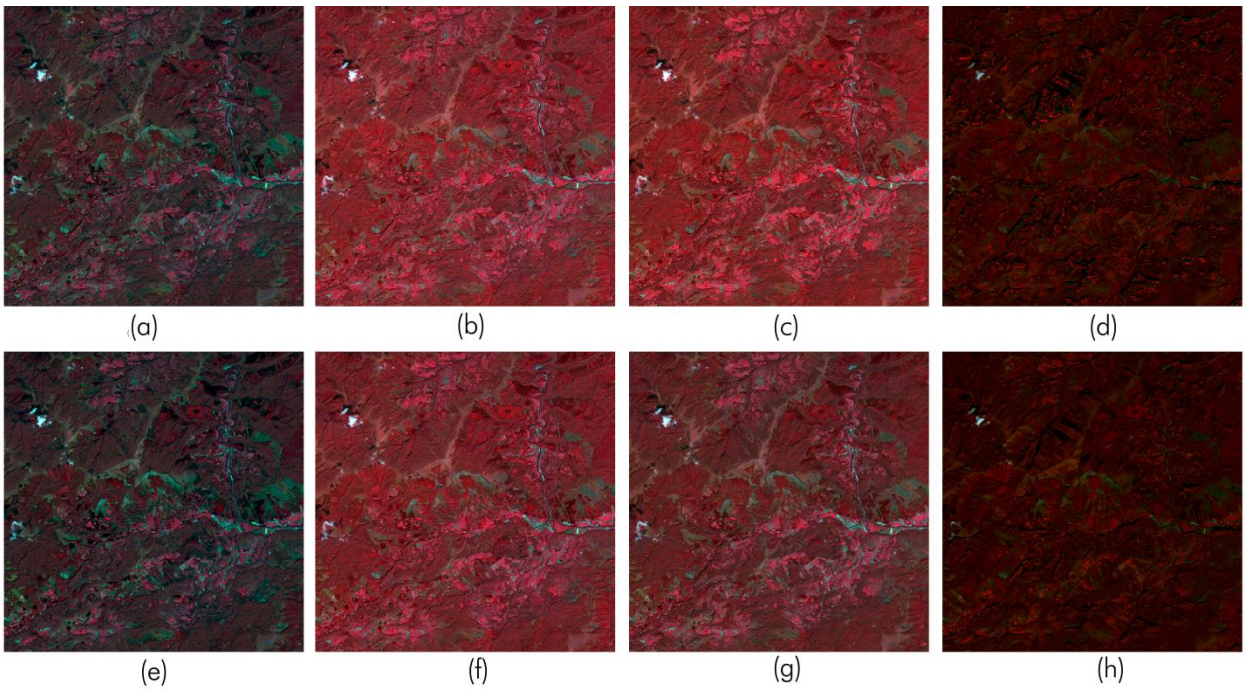

Fig. 5.5. Corrected synthetic images through CC for **(a)** March **(b)** June **(c)** August and **(d)** December, and through SE for **(e)** March **(f)** June **(g)** August and **(h)** December

Additionally, Fig 5.5. showed minor differences between TOC methods, but their performance varied significantly from date to date. In June and August both methods removed the three-dimensional effect of topography almost completely, with slightly higher intensity of the RGB composition for CC method. On the contrary, in the image of December both methods failed to correct some problematic areas. While SE method exhibited shadowed slopes, CC tended to introduce some artifacts on these areas, also noticeable in the image o March to a lesser extent.

When an area with rough relief was observed, including shaded slopes where TOC methods have problems usually, differences between methods were clearer, especially in the images of March and December. In Figs. 5.6d and 5.6h the poor correction of shaded slopes produced by CC method was again noticeable. Similarly, some problems were observed in Figs. 5.6a and 5.6e in areas where no direct irradiance is impinging on the surface. These problems seemed to be slightly better solved by the SE method.

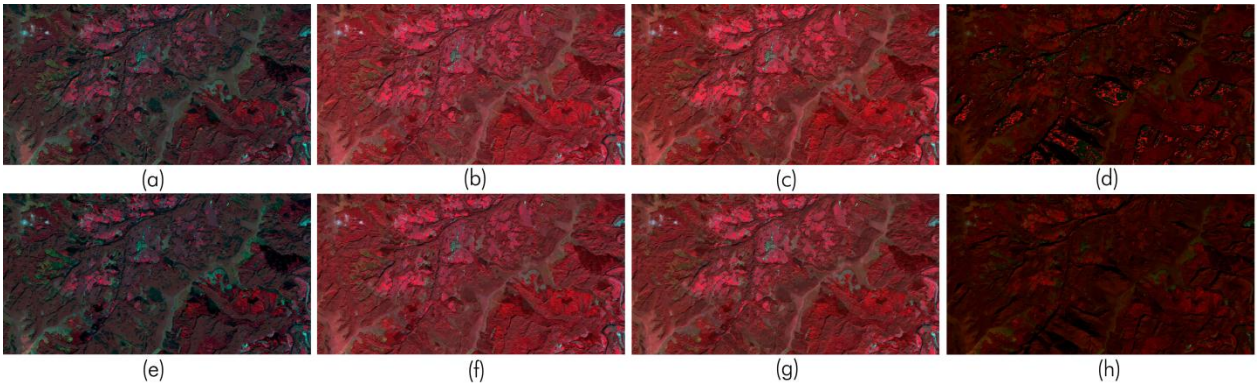

Fig. 5.6. Detail zone of corrected image through CC for **(a)** March (**b)** June (**c)** August and **(d)** December, and through SE for **(e)** March **(f)** June **(g)** August and **(h)** December

Fig. 5.7 shows SSIM maps of these corrections, in this case only for band 3 (NIR). Darker areas mean low values of SSIM due to poor topographic correction. These areas correspond to shaded slopes in the original image, more frequent in winter scenes and poorly corrected by CC and SE methods. In contrast, the images of June and August showed high values of SSIM and therefore a good correction represented by a near-white SSIM map, with values close to the ideal situation (i.e., SSIM = 1) in most of the pixels (Figs. 5.7b, 5.7c & 5.7f), especially when CC was used. Finally, the better performance of SE method on shaded slopes of winter scenes was demonstrated by Fig. 5.7h and 5.7e, in line with the results of Fig. 5.6.

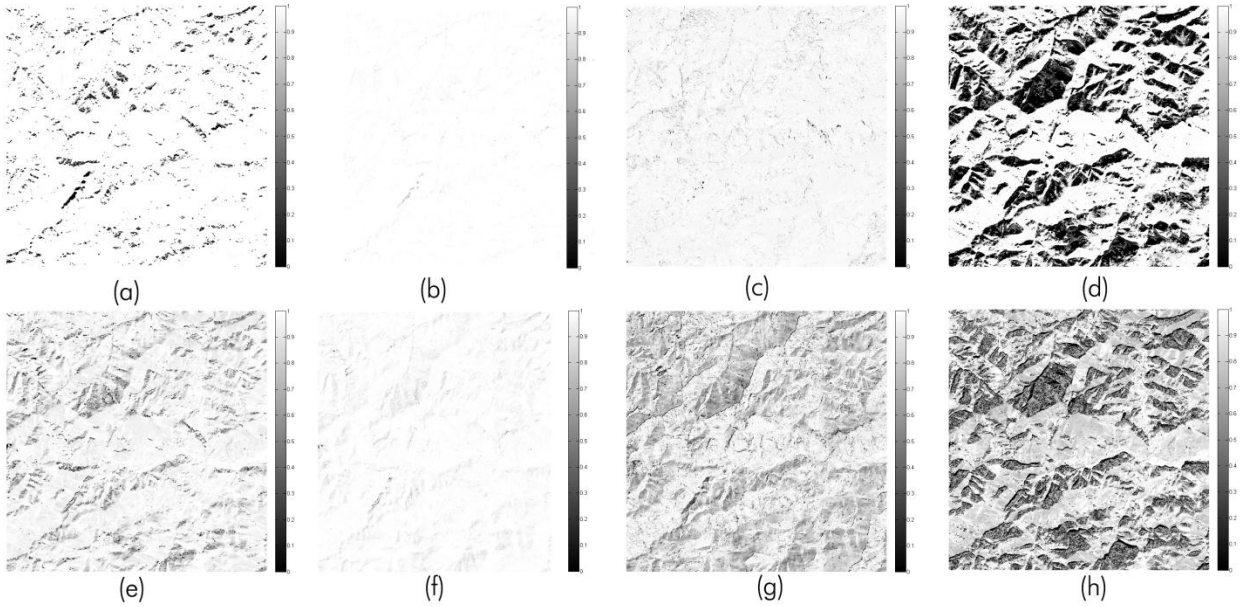

Fig. 5.7. SSIM map of band 3 for synthetic image corrected through CC for **(a)** March **(b)** June **(c)** August and **(d)** December, and through SE for **(e)** March **(f)** June **(g)** August and **(h)** December

In Fig. 5.8 the performance of each method is showed through the MSSIM of each band and image. As explained before, a MSSIM close to 1 means a good correction, so it is clearly observed an improvement after TOC is applied, mainly for CC, SCS+C and SE methods. MSSIM was higher in both non-corrected and corrected images for summer images (i.e., June and August) due to the lower effect of topography in these months.

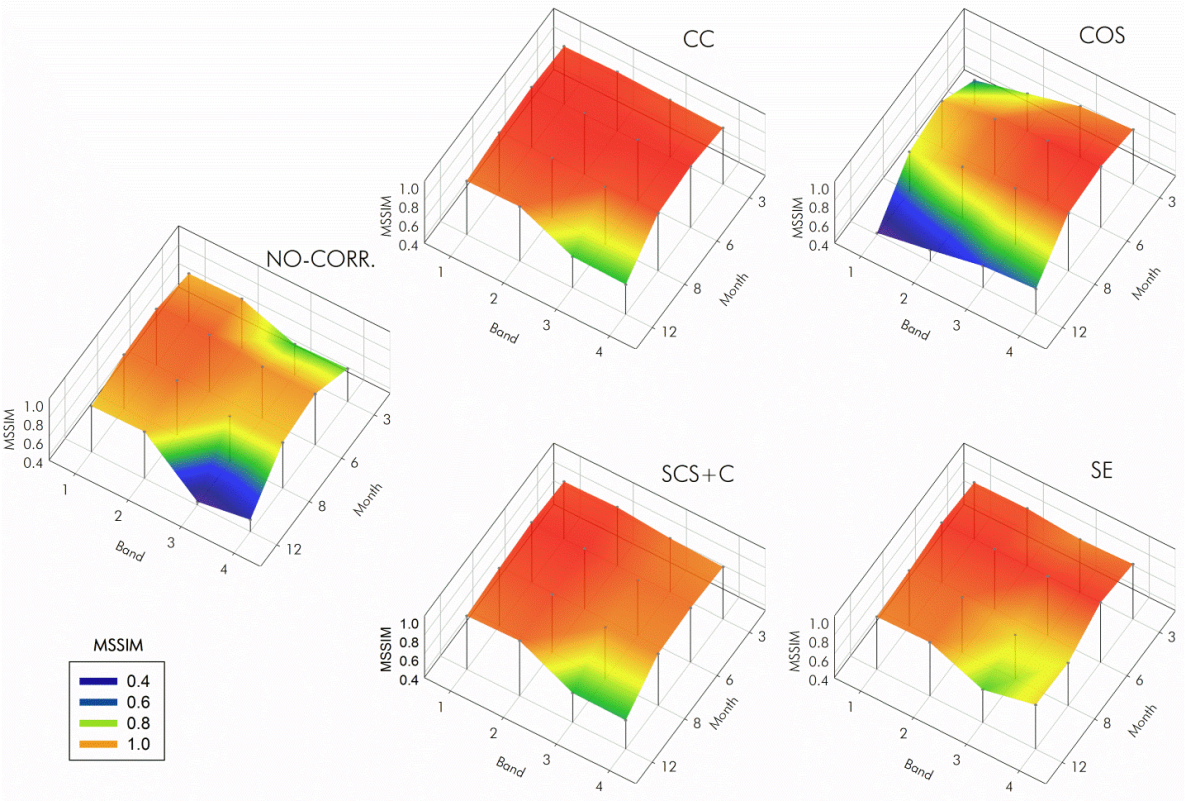

Fig. 5.8. MSSIM values of each TOC for the 4 spectral bands and 4 dates considered. In Y axis months are displayed, from 3 (March) to 12 (December).

In line with previous studies (Ghasemi et al. 2013), Fig. 5.8 showed an unsatisfactory performance of COS method, especially in visible bands, i.e., band 1 and band 2. Differences between the other 3 methods were minor, with slightly better performance of CC.

In extreme conditions, associated to slopes facing away from the sun, it is difficult to apply a good topographic correction, as the spectral information to restore is scarce, since no direct irradiance arrives to the surface. Nevertheless, the general performance of TOC methods was satisfactory, excluding COS method, whose limitations have been widely reported in the literature.

Table 5.3. Average MSSIM values of the four spectral bands for each date and TOC

Image	*March*	*June*	*August*	*December*
SR (NO-CORR.)	0.654	0.842	0.706	0.528
COS	0.678	0.824	0.739	0.452
CC	0.971	0.993	0.962	0.747
SE	0.934	0.983	0.943	0.771
SCS+C	0.919	0.931	0.910	0.741

In Table 5.3 average MSSIM indexes of the four spectral bands for each TOC and date are shown. In line with the results seen in Fig. 5.8, CC ranked first in images of March, June and August. On the contrary, SE ranked the best in December even if no TOC achieves a complete topographic correction with MSSIM below 0.8, due to the extreme illumination conditions.

5.7. Conclusions

We can conclude here that there is a strong influence of the acquisition date on the performance of TOC methods, due to different illumination conditions. So, TOC methods do not perform the same over the year. In summer months topographic effects are softer, so the differences between corrected and not corrected images are minor, since there is less to correct. On the contrary, more severe topographic effects in winter dates results in larger increase of MSSIM value if compared with the non corrected image, due to the greater topographic effect on this date.

When synthetic images were simulated under favorable illumination conditions (i.e., images of June and August), CC method ranked first, but minor differences were observed between the best performing algorithms. On the contrary, on the scene of December SE slightly outperformed other methods. Our results are in line with results obtained by other authors (Hantson and Chuvieco 2011; Goslee 2012), indicating the worse performance of COS method.

These findings suggest that there is no TOC algorithm that successfully corrects the topographic effect when solar elevation angle decreased below 30°, especially in infrared bands, i.e., NIR and SWIR. Similarly, as other authors suggested (Richter et al. 2009), there is no TOC method performing the best under every conditions, and differences are minor

among the best methods. Still, more research is required, including more study sites, more TOC methods and more acquisition dates.

Finally, this paper shows how synthetic images could be used to evaluate in detail TOC algorithm performance, in particular their behavior during the year. The scene simulator and the SSIM index application have been proved effective in order to assess the goodness of topographic corrections under specific conditions. The method proposed offers a means of generating synthetic scenes acquired under a variety of settings and acquisition configurations (i.e., solar angles, spatial resolution, etc.). Accordingly, the influence of each configuration parameter on the performance of the TOC methods can be evaluated. Obviously, this approach assumes that a TOC showing a good performance for synthetic imagery also performs correctly for real imagery with similar acquisition configuration. In the future, the validation of the model to simulate multispectral synthetic images with real imagery is strongly encouraged, in order to confirm the usefulness of this new evaluation methodology. This approach could be used to analyse the influence of land cover spatial variability on the performance of TOC algorithms and also the influence of sensor configuration.

CHAPTER 6

MULTI-CRITERIA: Multi-criteria evaluation of topographic correction methods

Published in:

- Sola, I.; González-Audícana, M.; Álvarez-Mozos, J. (2015). Multi-criteria evaluation of topographic correction methods. *Remote Sensing of Environment*. Impact factor: 6.393. Manuscript ID: RSE-D-15-00879R1

Abstract — In the last decades several topographic correction methods (TOC) have been proposed, but there is not an agreement on which method is the best. Furthermore, there is not any simple and objective evaluation procedure to measure the quality of the correction and different assessment criteria have been used in the past. Consequently a multi-criteria analysis of widely used topographic correction methods is required, evaluating their performance over different sensor, terrain and temporal configurations. In this work ten TOC methods were assessed using seven different evaluation strategies. The analysis was carried out in three different case studies, considering three locations in mountainous areas of northern Spain and also different acquisition dates and solar angles, in order to evaluate their performance for different land covers and for images taken under varying illumination conditions. The results obtained showed SCS+C, CC, and SE method performed the best, although differences were minor when favorable illumination conditions were considered. Regarding the seven evaluation strategies tested, interquartile range reduction of land covers and the use of synthetic images gave very similar results whereas there were great contrasts among other criteria.

Keywords — topographic correction; evaluation; comparison; multi-criteria.

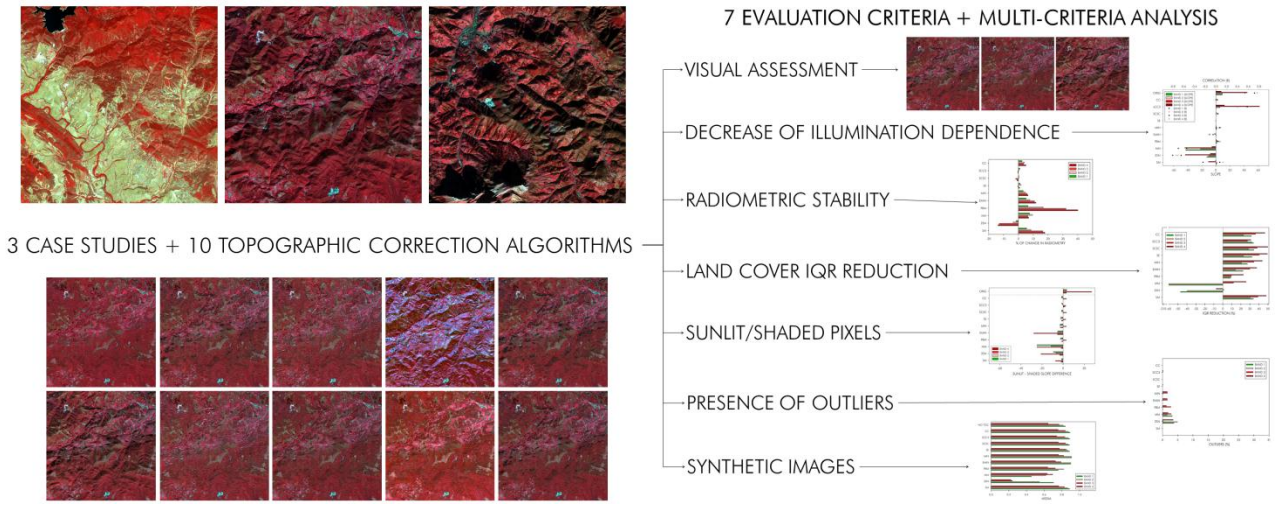

Graphical abstract

6.1. Introduction

The availability of RS data has exponentially grown in the last years and their applications in different fields, such as LU/LC mapping, vegetation cover monitoring and change detection, retrieval of land cover biophysical parameters, agriculture, or risk assessment, have increased accordingly.

In order to retrieve accurate information from RS scenes it is necessary to perform some pre-processing operations, where distortions (inherent to any image acquisition process) are corrected. The radiance recorded by an optical satellite sensor is affected by several factors, including sensor and system induced errors, atmosphere, topography and solar illumination angles, that need to be resolved by correction methods (Balthazar et al. 2012; Reese and Olsson 2011; Veraverbeke et al. 2010).

In non-flat areas, illumination correction, also known as topographic correction, is an important step in pre-processing high-resolution RS data (Tan et al., 2013), since it directly influences the solar irradiance impinging on the Earth surface and, consequently, the radiance detected by sensors. Such radiance can vary significantly depending, not only on the reflectance of land cover, but also on the slope and aspect of the areas where they are located (Riaño et al. 2003).

The objective of topographic correction is thus to compensate the differences in solar irradiance between areas with differing slope and aspect and, ultimately, to obtain the radiance values the sensor would have obtained in case of a perfectly flat surface.

Numerous TOC methods have been developed to correct topographic effects on the radiance measured by satellites. In those TOC algorithms, the illumination conditions for each pixel are estimated using the cosine of the solar incidence angle, $\cos\gamma_i$, which can be calculated based on the solar geometry (i.e., sun position) and slope and aspect of these pixels (Eq. 6.1).

$$cos\gamma_i = cos\beta cos\theta_s + sin\beta sin\theta_s cos(\varphi_s - \varphi_n) \qquad (6.1)$$

where, β is the slope angle, φ_n the aspect angle, θ_s the solar zenith angle, and φ_s the solar azimuth angle. Both β and φ_n are pixel-based values computed from the DEM.

According to Balthazar et al. (2012), TOC methods can be grouped into three subcategories: Empirical methods, semi-empirical methods, and physically based methods. The first group consists of simple empirical methods, such as band ratioing, that do not require additional ancillary data (Civco 1989; Ekstrand 1996). These procedures are based on the assumption that radiance values vary, due to topography, proportionally in all bands. They are easily implemented, but their output does not have a physical meaning (Blesius and Weirich 2005). The second category groups semi-empirical approaches that need a DEM to model the solar irradiance differences between slopes of the area to be corrected (Ghasemi et al. 2013; Hantson and Chuvieco 2011; Law and Nichol 2004; Lu et al. 2008; Soenen et al. 2005; Twele and Erasmi 2005).

Finally, the last category of topographic correction methods are the physically based TOCs, that model the full path of radiance through the atmosphere to the target object and backwards (Gu and Gillespie 1998; Sandmeier and Itten 1997; Soenen et al. 2005; Kane et al. 2008; Kobayashi and Sanga-Ngoie 2008; Soenen et al. 2009; Zhang and Gao 2011).

In order to examine the precision and accuracy of the parameters required by each TOC algorithm, Reese and Olsson (2011) recommended different sampling strategies for their determination. Similarly, some authors demonstrated that TOC methods in combination with a pre-classification stratification approach provided parameters that better resulted in correcting the topographic effect (Bishop and Colby 2002; Bishop et al. 2003; Szantoi and Simonetti 2013). This pre-classification stratification approach was used to split the different land cover types into strata that were corrected individually with the selected topographic correction method to achieve better reduction of the topographic effect. This enabled a more precise estimation of the correction factors for each stratum.

A number of TOC algorithms were proposed in the past, but there is not an agreement on their performance, as authors suggested different accuracy assessments (Civco 1989; Lu et al. 2008; Richter et al. 2009; Hantson and Chuvieco 2011). Most of these evaluation criteria are summarized in Table 6.1, including their pros and cons.

The visual evaluation of the removal of the topographic effect is generally the first indicator on the quality of the correction (Szantoi and Simonetti 2013; Tan et al. 2013; Shepherd et al.

2014). Nevertheless, it is imperative to evaluate quantitatively the results to select the best TOC method (Balthazar et al. 2012).

The decrease in the dependence between $\cos\gamma_i$ and the radiance/reflectance of each spectral band after TOC is also one of the most widely used procedures to quantitatively assess the effect of topographic corrections, measured through the correlation coefficient (Gao et al. 2014), the slope of their linear regression (Vanonckelen et al. 2014) or both (Gao et al. 2014; Goslee 2012; Szantoi and Simonetti 2013; Gao and Zhang 2009a). The lower the dependence between the incidence angle and the radiance/reflectance, the better the effect of topographic correction. Obviously, this is not valid in areas where slope and aspect are considered to be key factors influencing land covers, and consequently its reflectance behavior. In these areas, a residual correlation between radiance and $\cos\gamma_i$ should be expected, even after a successful topographic correction (Hantson and Chuvieco 2011).

Table 6.1. TOC evaluation techniques used in the literature

Evaluation technique	References	Pros	Cons
Visual	Zhang et al. 2015; Singh et al. 2015; Shepherd et al. 2014	Direct indicator. No ancillary data required	Subjective
Correlation $\cos\gamma_i$ - L_{sen}	Gao et al. 2014; Vanonckelen et al. 2014; Moreira and Valeriano 2014	Easy to compute, quantitative, no ancillary data required	Residual correlation if slope orientation determines land cover
Spectral stability of land cover	Ghasemi et al. 2013; Goslee 2012; Moreira and Valeriano 2014	Detects possible biases introduced by the correction	Measure of stability, not a proper TOC evaluation technique
Reduction of land cover variability	Gao et al. 2014; Moreira and Valeriano 2014; Fan et al. 2014	Objective. Analysis on different land cover	Need of reliable information on land cover
Classification accuracy	Hoshikawa and Umezaki 2014; Vanonckelen et al. 2013; Füreder 2010	Assesses the effects of correction on thematic products derived from RS. Quantitative. Analysis on different land covers	Depends on the quality of ground truth data, classification algorithm, etc.
Difference North-facing/South-facing pixels of same land cover	Civco 1989; Fan et al. 2014; Vicente-Serrano et al. 2008; Notarnicola et al. 2014	Good correction, under-correction or over-correction detected	Only selected land cover is assessed
Presence of outliers	Balthazar et al. 2012	Quantifies the percentage of pixels each TOC could correct	Not a proper TOC evaluation technique
Similarity to SH (synthetic images)	Sola et al. 2014a	Comparison between TOC corrected image and ideal situation	Need to generate a pair of synthetic images

Ideally, the spectral stability of land covers should be maintained before and after TOC, otherwise the TOC method would have introduced a bias. An ideal topographic correction should not change the spectral characteristics (i.e., mean radiance value) of land cover substantially (Riaño et al. 2003; Richter et al. 2009). This evaluation procedure has been used image-wide (Ghasemi et al. 2013; Goslee 2012; Gao and Zhang 2009a), or stratified by land cover classes (Goslee 2012; Moreira and Valeriano 2014). However, it cannot be consider a criterion to assess the performance of the correction, but just a measure of stability (Baraldi et al. 2010).

The quantification of the reduction of the land cover class variability is another criterion to evaluate the performance of TOC algorithms (Fan et al. 2014; Gao et al. 2014; Moreira and Valeriano 2014), measured through the SD or the CV of the reflectance within each surface cover class. Land cover homogeneity should theoretically increase after correction, since the intra-class radiometric variations caused by the topographic effect are to be minimized. This criterion is probably the most objective and quantitatively measurable evaluation technique. However, the reduction of land cover class variability in TOC corrected imagery is restricted to cases where a priori knowledge of land cover distributions is available. Therefore, broad land cover classes based on vegetation index thresholds (i.e., vegetation/no vegetation (Szantoi and Simonetti 2013) or forest/pastures (Goslee 2012; Lu et al. 2008)) or samples of representative land covers (Gao et al. 2014) have been selected to evaluate the reduction of the intra-class variability.

Alternatively, land cover classification accuracy improvement has been considered a good measure of the effects of pre-processing (i.e., atmospheric and/or topographic correction) of satellite imagery (Hoshikawa and Umezaki 2014; Moreira and Valeriano 2014; Vanonckelen et al. 2013). A classification based on TOC corrected images should ideally yield a higher accuracy than one using uncorrected data, but there is not an agreement in the degree of improvement provided by TOC algorithms. A similar approach is to evaluate the improvement in biophysical parameter retrievals (Ekstrand 1996; Tokola et al. 2001) or in change detection accuracy (Tan et al. 2013; Vanonckelen et al. 2015). However, these assessments entail their own uncertainties in both classification, change detection and retrieval algorithms

and are thus unable to directly quantify the degree to which the topographic effect has been reduced (Hoshikawa and Umezaki 2014; Sola et al. 2014a).

Furthermore, some authors evaluated TOC methods by extracting different samples in a certain land cover class (i.e., forest), for the North-facing and South-facing slopes (Notarnicola et al. 2014; Vicente-Serrano et al. 2008). On these samples the values of radiance before and after the topographic correction were compared. An ideal TOC should make North and South samples more similar. Nevertheless, this criterion assumes equal forest characteristics (i.e., structure, density, seral stage, etc.) between North-facing and South-facing slopes, which might not be always the case. Other authors used the terms sunlit/shaded slopes (Fan et al. 2014; Riaño et al. 2003; Vicente-Serrano et al. 2008). This strategy has been applied to other land covers too, such as pastures (Goslee 2012). Schulmann et al. (2015) applied a similar procedure but substituted the mean difference by the RMSD.

There is an issue that has not been thoroughly analyzed in the literature: The presence of statistical outliers after topographic correction. Balthazar et al. (2012) considered reflectance values for under- or overcorrected pixels as statistical outliers. Consequently, it was tested whether a given TOC generated radiance values that were far beyond the expected range of values.

Finally, in order to evaluate topographic correction algorithms in a throughout and objective manner, the use of simulated scenarios based on synthetic images was proposed by Sola et al. (2014a). These images represent the radiance an optical sensor would receive under specific geometric and temporal acquisition conditions and assuming a certain land cover type and can be generated to select the best performing TOC for each particular situation (e.g., solar angles, spatial resolution, etc.). In particular, a comparative analysis of the images obtained after correcting a Real Synthetic image (SR) with different algorithms and their respective Synthetic Horizontal image (SH) used as a reference provided a sound, objective and clear method for the quantitative assessment of those algorithms.

To summarize, many TOC algorithms have been proposed, but most of them have not been fully evaluated, since most studies only considered a limited set of illumination conditions and only one or two evaluation criteria. Therefore, the objective of this paper is to perform a multi-

criteria analysis of different topographic correction methods, providing a guideline of use of TOC methods under different conditions, including advantages and shortcomings of each TOC algorithm.

6.2. Material and methods

6.2.1. Study area

Three different case studies are analyzed corresponding to three different sites in the Pyrenees mountain range, Spain (see Fig. 6.1), where the relief is rough and valleys are oriented in a wide variety of directions. Regarding to land coverage, on the one hand, in zone 1 more than 30% of the area is covered by shrubs, while almost another 30% is covered by agricultural crops located on the southwest quadrant of the image. Coniferous, broadleaf and mixed forest together provide 33% of the area, while other classes, such as urban areas or reservoir and rivers have less coverage. On the other hand, zones 2 and 3 are mainly covered by different type of forests and pastures.

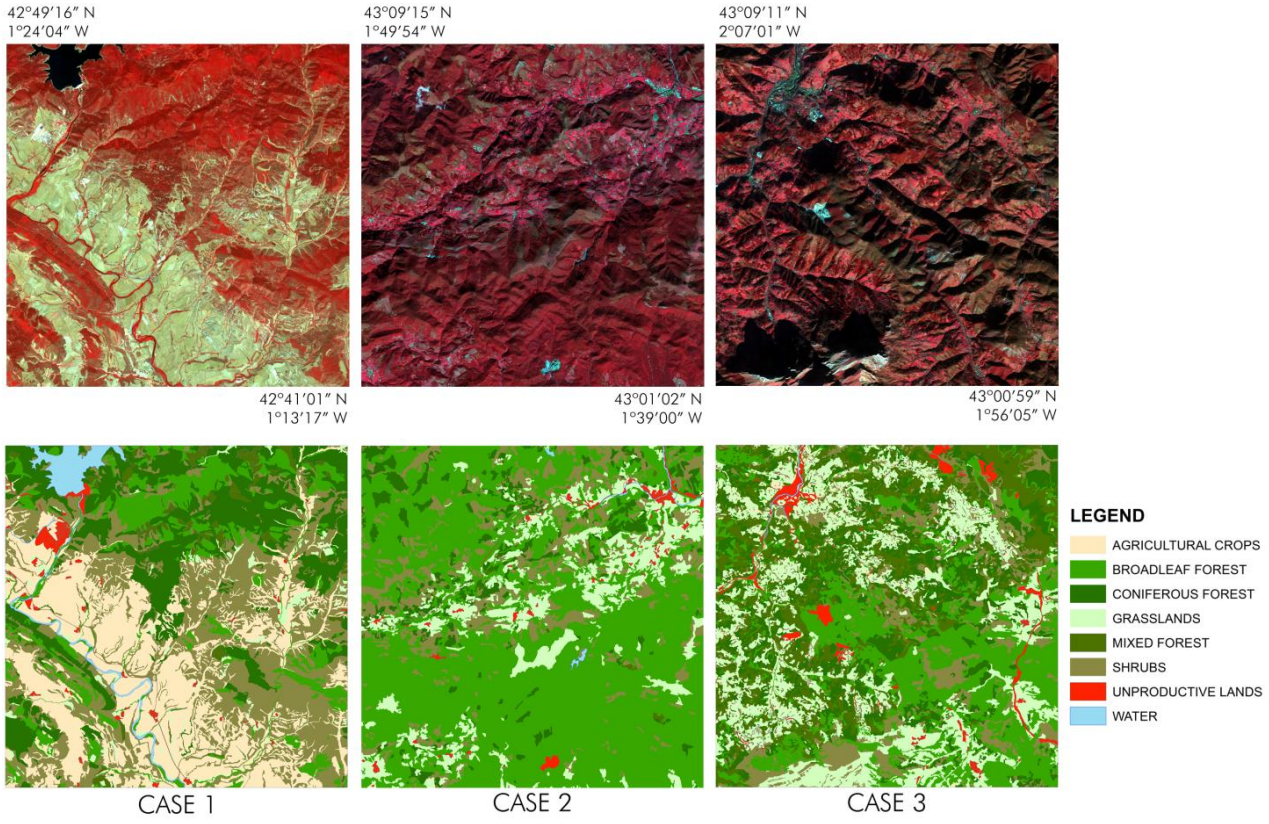

Fig. 6.1. The three study areas, located in northern Spain

The mean altitude of zone 1 is 614 m, ranging from 426 to 1049 m, and the maximum and mean slopes are 63.1° and 7.9°, respectively. Zone 2 has a mean altitude of 623 m, with a minimum and a maximum of 104 m and 1195 m. Mean slope is 12.8° and maximum slope is 68°. Finally, zone 3 ranges from 64 m to 1341 m, with a mean altitude of 448 m. In this zone the mean slope is 13.0° and the maximum rises to 80.0°. These figures show a gentler topography for study area 1 comparing with the others.

6.2.2. Data acquisition and Processing

The three areas correspond to subscenes of SPOT 5 images acquired under different temporal configurations in 2006 and 2009. The three of them have an extension of 15 x 15 km and a spatial resolution of 10 m. SPOT 5 multispectral scenes are composed by four spectral bands, i.e., green: 0.50 – 0.59 μm, red: 0.61 – 0.68 μm, NIR (near infrared): 0.78 – 0.89 μm and SWIR (short-wave infrared): 1.58 – 1.75 μm. The SPOT 5 scenes were orthorectified and converted from digital DN to top of atmosphere radiance ($W \cdot m^{-2} \cdot sr^{-1} \cdot \mu m^{-1}$) by using the gain and offset values provided in the metadata file for each spectral band.

Table 6.2. Configuration of SPOT 5 scenes for the different case studies

Case study	SPOT 5 grid reference	Sun elevation	Sun azimuth	Acquisition date	Acquisition time
1	37264	56.44	140.70	15/08/2009	10:45
2	36263	37.66	167.58	15/10/2009	11:13
3	35263	21.91	165.15	26/12/2006	11:07

Table 6.3. Percentage of area of each land cover for the three test sites (Z1, Z2, Z3)

Area coverage (%)	Z1	Z2	Z3
Broadleaf forest	12.2	65.3	24.1
Coniferous forest	18.9	6.6	17.8
Mixed forest	2.7	0.2	19.2
Shrubs	30.5	12.9	11.9
Grasslands	2.2	13.3	22.9
Agricultural crops	29.6	0.1	1.1
Urban area	1.4	1.2	3.0
Water	2.4	0.2	0.1

The land-use/land cover (LU/LC) information was obtained from specific cartography of the regions of Navarre (GN 2012) and Gipuzkoa (GV 2007). Using these maps, the land covers of the three study areas were reclassified in eight broad classes. The percentage of surface covered by each land cover class is shown in Table 6.3.

All the topographic parameters needed to apply each method were retrieved from the original DEM, at 5m resolution, and then resampled to 10m to match the spatial resolution of SPOT 5 images. This DEM, provided by the Spanish National Geographic Institute (IGN), was obtained from cubic convolution of LIDAR point cloud, with a density of 0.5 points m^{-2}.

6.2.3. Selected topographic correction algorithms

After a thorough revision of the literature, ten topographic correction algorithms (Table 6.4) were selected to be evaluated in this work, based on their popularity, i.e., times used, and performance reported by other authors. Some methods have been widely used but most authors claimed they had limitations, such as the Lambertian methods of COS and SCS, and thus were not considered in this study. On the contrary, some others performed well but were only tested in one case study, and thus more research might be necessary to fully demonstrate their performance. The latter algorithms were discarded too.

Regarding to their implementation and use, some of these methods are straightforward but in some others the authors encourage the users to adjust or tune the correction parameters in order to obtain adequate results for their specific dataset. In this work, after analyzing different values, a smooth factor of 3 was selected in sCC3 to calculate the smoothed β, as it provided the best results. Furthermore, following the suggestions of Lu et al. (2008) in PBM a second degree polynomic equation was used as the best fit to the regression between Minnaert k_λ and β, while in MM correction the "strong" correction option was selected and the lower bound g was set to 0.1 after some tests. Finally, in 2SN and SM the sunny and shady slopes were automatically masked from the image of $\cos\gamma_i$, as the results were more reliable than using areas selected manually or based on slope and aspect.

Table 6.4. Expressions of TOC algorithms analyzed

TOC	Expression	Authors
C-Correction (CC)	$L_{sen,corr,\lambda} = L_{sen,\lambda}\frac{\cos\vartheta_s + c_\lambda}{\cos\gamma_i + c_\lambda}$	Teillet et al. (1982)
Smoothed C-Correction (sCC3)	$L_{sen,corr,\lambda} = L_{sen,\lambda}\frac{\cos\vartheta_s + c_\lambda}{\cos\gamma'_i + c_\lambda}$	Riaño et al. (2003)
SCS+C (SCS+C)	$L_{sen,corr,\lambda} = L_{sen,\lambda}\frac{\cos\beta\cos\vartheta_s + c_\lambda}{\cos\gamma_i + c_\lambda}$	Soenen et al. (2005)
Statistic-Empirical (SE)	$L_{sen,corr,\lambda} = L_{sen,\lambda} - (A\cos\gamma_i + B) + \overline{L_{sen,\lambda}}$	Teillet et al. (1982)
Minnaert (MIN)	$L_{sen,corr,\lambda} = L_{sen,\lambda}\left(\frac{\cos\vartheta_s}{\cos\gamma_i}\right)^{k_\lambda}$	Minnaert (1941)
Enhanced Minnaert (EMIN)	$L_{sen,corr,\lambda} = L_{sen,\lambda}\cos\beta\left(\frac{\cos\vartheta_s}{\cos\gamma_i\cos\beta}\right)^{k_\lambda}$	Smith et al. (1980)
Pixel-based Minnaert (PBM)	$L_{sen,corr,\lambda} = L_{sen,\lambda}\frac{\cos\beta}{(\cos\beta\cos\gamma_i)^{k_\lambda *}}$	Lu et al. (2008)
Modified Minnaert (MM)	$L_{LAMB,\lambda} = L_{sen,\lambda}\frac{\cos\vartheta_s}{\cos\gamma_i}$ $L_{sen,corr,\lambda} = L_{LAMB,\lambda}\left(\frac{\cos\gamma_i}{\cos\beta_t}\right)^b = L_{LAMB,\lambda}\cdot G$	Richter (1998)
Two stage normalization (2SN)	1F: $L_{sen,corr,\lambda} = L_{sen,\lambda} + \left[L_{sen,\lambda}\cdot\left(\frac{\mu_k - X_{ij}}{\mu_k}\right)\right]$ 2F: $L_{sen,corr,\lambda} = L_{sen,\lambda} + \left[L_{sen,\lambda}\cdot\left(\frac{\mu_k - X_{ij}}{\mu_k}\right)\cdot c_{2sn,\lambda}\right]$	Civco (1989)
Slope-Matching (SM)	1F: $L_{sen,corr,\lambda} = L_{sen,\lambda} + \left(L_{sen,max,\lambda} - L_{sen,min,\lambda}\right)\left(\frac{\mu_w - X_{ij}}{\mu_w}\right)$ 2F: $L_{sen,corr,\lambda} = L_{sen,\lambda} + \left(L_{sen,max,\lambda} - L_{sen,max,\lambda}\right)\left(\frac{\mu_w - X_{ij}}{\mu_w}\right)\cdot c_{sm,\lambda}$	Nichol et al. (2006)

In the calculation of TOC parameters, flat pixels were excluded, i.e., $\beta < 5°$. Also pixels occluded by surrounding topography, that is, cast shadowed pixels and self-shadowed pixels (i.e., pixels where $\cos\gamma_i < 0$) were masked out for that purpose, although TOC algorithms were later applied image-wide with no mask used. Additionally, BRDF was not considered, as this information is rarely if ever available, and is extremely difficult to obtain for regional studies (Goslee 2012). Moreover, for high spatial resolution sensors with a small field of view the solar viewing geometry is approximately constant in flat surfaces. Therefore, BRDF variations for a certain cover type due to geometry changes are small (Richter 1998). Finally, no corrections were made in the view direction as little impact of sensor viewing angle on reflectance in temperate latitudes was reported in the literature (Nagol et al. 2014).

Table 6.5. Nomenclature

Symbol	Description
$L_{sen,\lambda}$	Original radiance for band λ
$L_{sen,corr,\lambda}$	Corrected radiance for band λ
θ_s	Solar zenith angle
γ_i	Solar incidence angle
c_λ	Empirical coefficient used by the CC, sCC3 and SCS+C methods for band λ
β	Terrain slope
β_t	Threshold angle introduced by MM correction
γ'_i	Solar incidence angle obtained from smoothed slope
$\overline{L_{sen,\lambda}}$	Mean radiance of the image for band λ
k_λ	Constant of Minnaert for band λ
k_λ*	Pixel-based k_λ for band λ obtained stratifying the image by terrain slope ranges
$L_{LAMB,\lambda}$	Radiance of band λ after a Lambertian correction, i.e., COS method
G	Correction factor introduced to avoid the overcorrection of poorly illuminated pixels
μ_k	Mean value of the scaled (0–255) cosγ_i for the main cover type
X_{ij}	Scaled (0–255) cosine of γ_i for pixel ij for the main cover type
$c_{2sn,\lambda}$	Empirically-derived calibration coefficient for band λ
$L_{sen,max,\lambda}$ and $L_{sen,min,\lambda}$	Maximum and minimum radiance value for main cover type
μ_w	Mean value of the scaled cosγ_i for the main cover type on sunny slopes
$c_{sm,\lambda}$	Modified correction coefficient for band λ

6.2.4. Evaluation strategies

6.2.4.1. TOC ranking based on multi-criteria

To have a general overview of the performance of the TOC algorithms tested over the three case studies, a multi-criteria ranking was performed, based on seven evaluation procedures. For each assessment technique, TOC methods were ranked from best to worst and then the average of different criteria rankings was performed, leading to a final multi-criteria ranking.

6.2.4.2. Visual analysis

The comparative visual analysis of TOC methods for the three case studies was carried out by ranking topographic methods from the best to the worst. This visual evaluation was performed independently by 10 RS scientists and engineers, who were asked to compare pairs of images, with no information about the TOC method used to correct each one. Then based on those 1350 pairwise comparisons (i.e., 45 comparisons x 3 zones x 10 participants), where each method was compared a total of 90 times for each zone (i.e., 9 comparisons x 10

participants), a ranking of TOC methods was built, considering the number of times each TOC was considered visually better than the other one in the pair comparisons.

6.2.4.3. Correlation analysis

The quantification of the reduction of the dependence between $\cos\gamma_i$ and the radiance of each spectral band after the correction was computed by fitting a linear regression, and analyzing its slope and correlation coefficient (r).

6.2.4.4. Stability of land cover radiometry

In this work the three study areas were classified in 8 broad land cover classes based on local cartography (see Table 6.2), and the median (more reliable than mean value, when outliers appear) of each class was measured before and after the correction. Strictly speaking, this should not be considered a criterion to assess the performance of the correction, but a measure of stability.

6.2.4.5. Intraclass IQR reduction

The reduction of intraclass variance after correction was measured. The major flaw on this procedure is that the presence of statistical outliers generated by TOC algorithms on unfavorable conditions could produce non reliable results. This effect could be minimized substituting the commonly used SD, by the interquartile range (IQR) (i.e., the difference between the upper (Q3) and lower (Q1) quartiles) which is much less sensitive to outliers. Consequently, this modification was proposed by the authors and implemented in this paper. To calculate IQR, images were stratified in the eight land cover classes explained in Section 6.2.2, and all the pixels of the scene were included, that is, no mask was applied.

The main statistics (i.e., minimum, Q1, median, Q3 and maximum radiance) of each land cover class before and after the correction were calculated, and afterwards the IQR was obtained for each land cover. An advantage of this criterion is the per class analysis to evaluate the influence of correction on different land cover, more or less affected by topography (see Table 6.1). For that purpose, the relative reduction of IQR of each land cover

after topographic correction was calculated, and then the area weighted average of all land cover was obtained.

6.2.4.6. Comparison of coniferous forest radiometry between sunlit and shaded slopes

In this work 2000 pixels of coniferous forest were randomly selected for each zone, where half of them were located in sunlit slopes (i.e., slope aspect = solar azimuth ± 10º) and the other half in shaded slopes. Then the radiance difference between sunlit and shaded slopes was computed.

6.2.4.7. Percentage of outliers

Most previous evaluation of TOC algorithms in the literature were carried out on quite favorable conditions and the few problematic pixels located on weakly illuminated slopes, (i.e., $\cos\gamma_i \leq 0$), were masked and excluded from the evaluation. Consequently, it is normally deemed better to left these pixels uncorrected than to correct them. However, it seems interesting to assess the performance of TOC algorithms on the whole image, without including any masks and therefore correcting even those extreme pixels located on weakly illuminated slopes. But when a TOC algorithm fails at correcting those pixels and creates too many outliers then this method cannot be recommended either. In this work, pixels of TOC-corrected scenes with radiance values higher than the maximum original radiance or lower than the minimum were considered statistical outliers, and their percentage in the image was calculated.

6.2.4.8. Synthetic images

Sola et al. (2014a) proposed a novel evaluation strategy of the performance of TOC based on the comparison between synthetic horizontal images (SH) and TOC-corrected synthetic real images (SR). The latter were generated considering the real DEM of an area, while the former were obtained running the simulation model over an ideal flat DEM. SH corresponds to the ideal situation, i.e., the at-sensor radiance with no influence of topography. Therefore, this image was used as a reference to compare how close the corrected image to the ideal correction was, by using image quality indexes such as the

Structural SIMilarity index (SSIM) proposed by Wang et al. (2004). As an example, the obtained synthetic images, both SH and SR, for case study 2 are shown in Fig. 6.S1.

6.3. Results

6.3.1. Visual analysis

In Fig. 6.2, false color composite of TOC corrected images of case study 2 is displayed (the corrected images of cases 1 and 3 are displayed in supplementary results, i.e., Figs. 6.S2 and S3). In case study 1 the topographic effect in the original image (Fig. 6.S2a) was minor, so differences between methods were also slight in most cases (Figs. 6.S2b-k).

In the case study 2 the topographic effect was stronger (Fig. 6.2a) and differences between TOCs were clearly more noticeable (Figs. 6.2b-k). In this particular case, and on the contrary of case 1, SM performed visually very well, while CC and SCS+C corrected most of the shadowed areas. In turn, sCC3 showed a corrected image where shadows were just partially removed. On the other hand, methods based on Minnaert (i.e., MIN, EMIN and PBM) successfully corrected the differences on radiance introduced by the topography in most of the areas but the visual evaluation was negatively affected by the presence of outliers in some pixels. Besides, the latter modified the mean brightness of the original image (Fig. 6.2h). At last, 2SN and MM failed again at correcting the topography, and yielded unreliable results.

Finally, case study 3 corresponded to an extreme scenario, as the image was acquired in December, with a solar elevation angle as low as 21°, and in an area of rough relief (Fig. 6.S3). The topographic effect of the original image was tremendous (Fig. 6.S3a) and none of the tested TOC algorithms achieved to correct it completely (Figs. 6.S3b-k). For instance, the shadowed area in the bottom-left corner of the original image (Fig. 6.S3a) was only partially corrected with CC, SCS+C, SE and SM, while in the other methods outliers in this area were clearly noticeable. Minnaert based methods (MIN, EMIN, PBM, MM) did not extract reliable spectral information from those areas either, while MM had a dramatically poor performance in this case study.

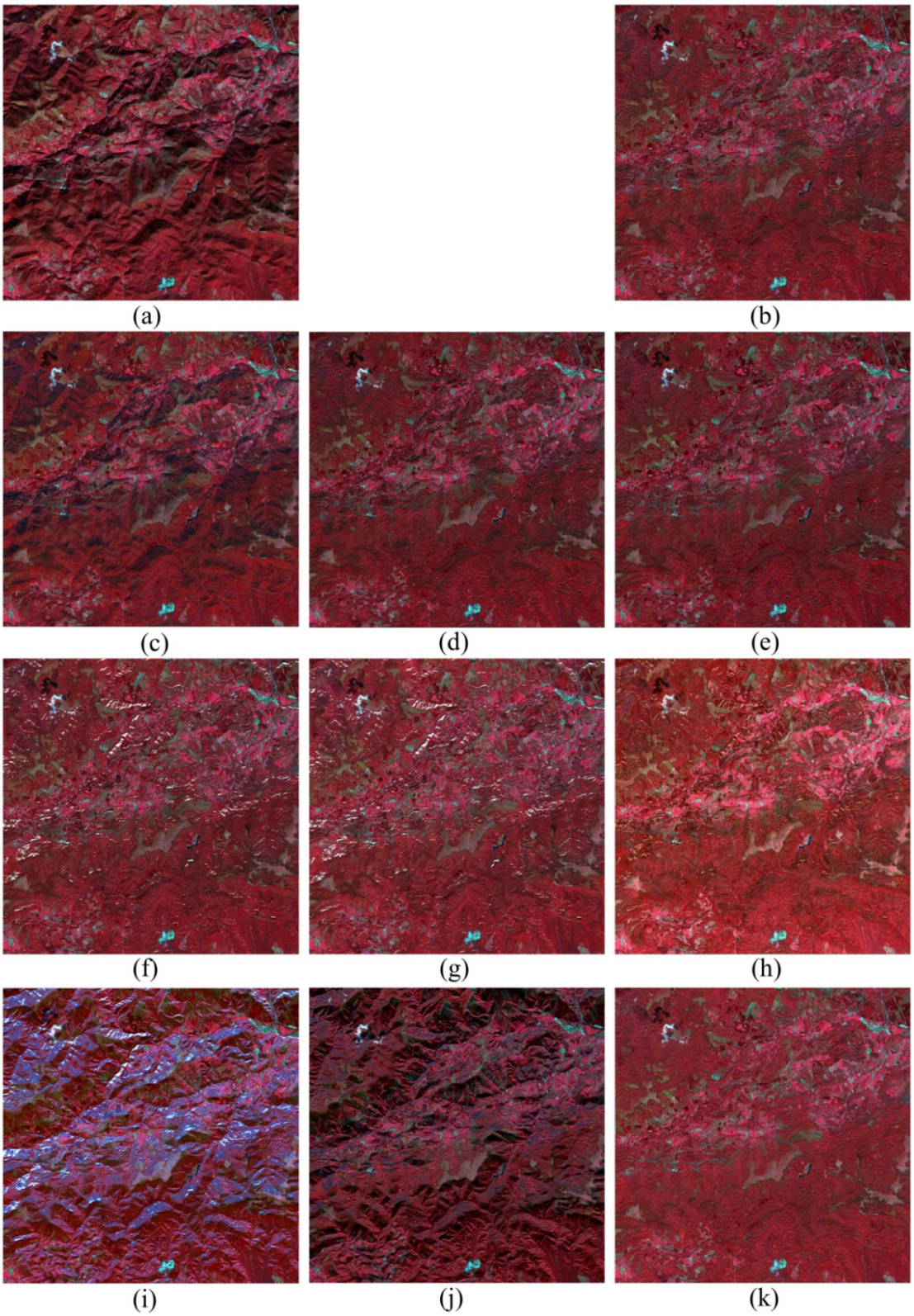

Fig. 6.2. Original (a) and corrected images of case study 2 with TOCs (b) CC (c) sCC3 (d) SCS+C (e) SE (f) MIN (g) EMIN (h) PBM (i) MM (j) 2SN (k) SM

The number of times each TOC method was superior in pairwise comparison according to the 10 participants in this analysis and the consequent visual ranking are shown in Table 6.6. The ranking of methods according to the subjective visual appearance of topographic effect correction provide preliminary results of the quality of each TOC, although in some cases the evaluation was limited by the slight differences among methods to compare.

Table 6.6. Number of times each TOC method was superior (out of 90) and average ranking of methods by visual analysis for the 3 case studies (1= best, 10 = worst)

NUMBER OF TIMES EACH TOC IS SUPERIOR				VISUAL RANKING			
TOC	Z1	Z2	Z3	Z1	Z2	Z3	OVERALL
CC	73	69	73	3	3	2	3
sCC3	31	36	52	7	6	5	6
SCS+C	78	69	70	2	3	3	2
SE	52	79	90	4	1	1	1
MIN	45	22	19	5	8	9	8
EMIN	37	31	26	6	7	7	7
PBM	85	57	25	1	5	8	4
MM	0	1	0	10	10	10	10
2SN	22	9	40	9	9	6	9
SM	27	77	55	8	2	4	5

As seen in Table 6.6, the ranking of methods varied from one case to another, i.e., the method that ranked first was different for each case. PBM, SCS+C and CC, in that order, performed the best in case 1, with minor differences among them in term of votes. In case 2 SE ranked first, with results slightly superior than SN, SCS+C and CC. Finally, in case 3 the differences between methods were more significant, showing a superior performance of SE, that was capable of extracting spectral information even from shadowed slopes. CC, SCS+C, SM and sCC3, performed well too, with similar results among them. MIN, EMIN and PBM gave intermediate results and ranked very similar in the three cases, with some problems of overcorrection in weakly illuminated slopes (see Figs. 6.3f, 6.3g & 6.3h), while MM and 2SN ranked the last in the three cases, showing a poor correction of the topographic effect.

6.3.2. Correlation analysis

In Fig. 6.3 the slope and the correlation coefficient (r) of the regression between $\cos\gamma_i$ and the radiance of each spectral band are shown for the original image (left) and then for the ten

TOC-corrected images for the three case studies. As seen in Fig. 6.3, positive slopes and high r values were observed for the original images, due to the topographic effect, especially in NIR band of cases 2 and 3. According to this criterion, CC, SE, SCS+C and MIN, were the best methods reducing the dependence of spectral radiance on illumination in the three studied scenarios, with minimum slopes and r values. EMIN and PBM also performed well in cases 2 and 3, but in case 1 the former showed negative correlation while the latter had positive correlation, sign of an incomplete removal of the topographic effect. Finally, sCC3 only reduced partially the correlation between radiance and illumination, while MM, 2SN, and to a lesser extent SM, overcorrected the original image, showing a negative slope between corrected radiance and $\cos\gamma_i$.

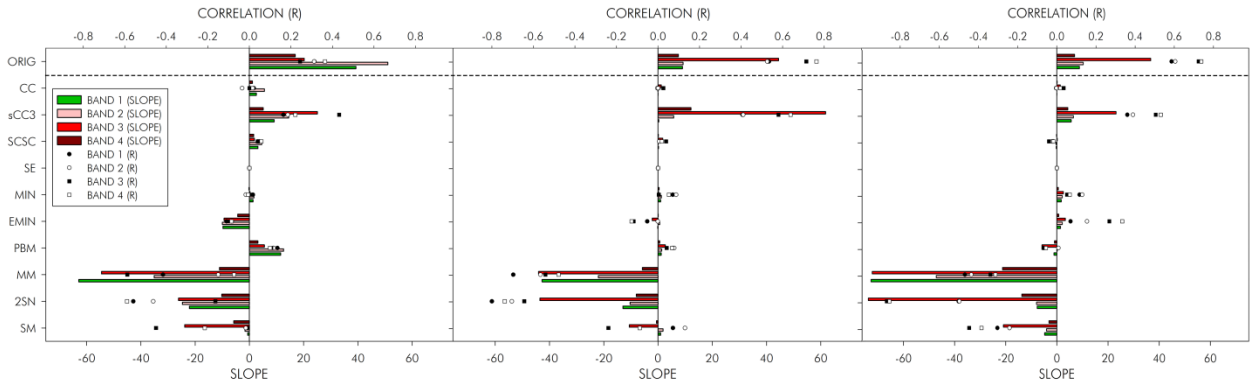

Fig. 6.3. Slope and correlation coefficient of regression between $\cos\gamma_i$ and the radiance of each spectral band. The closer slope and r are from 0, the better

6.3.3. Radiometric stability of land covers

In order to quantitatively evaluate the radiometric stability of land covers band-wise, the relative radiance difference before and after TOC for land covers medians, averaged considering the area occupied by each land cover, are shown in Fig. 6.4 in a specific plot for each case study.

As seen in Fig. 6.4, the original radiometry of land covers was strongly modified by some TOCs, especially by PBM method, with a relative difference of median radiance of land covers up to 100% in the hardest scenario for the IR bands. It is noticeable that most methods increased the original radiance of land covers to a greater or lesser extent, and only 2SN

decreased the original median radiance. As expected, results were generally worse in case study 3. Overall, sCC3, SCS+C, SE and CC, in this order, were the TOCs that altered the radiometry the least.

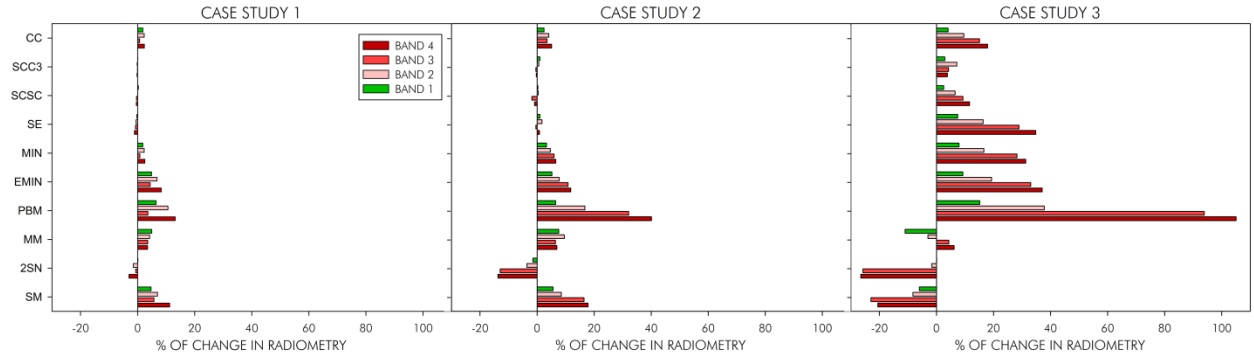

Fig. 6.4. Radiometric stability of land cover represented by the weighted average of % of change in land cover radiometry after TOC. The smaller percentage of change the better.

6.3.4. Intraclass IQR reduction

As explained above, case study 1 corresponded to an area where the influence of topographic effect was less pronounced due to its higher solar elevation angle. That means there was less to correct in this particular scenario, so as seen in Fig. 6.5, the IQR reduction of land cover was slight in CC, SCS+C, SE and MIN, while the other six methods even increased the original IQR. Negative IQR reduction rates means overcorrection, resulting in more heterogeneous land covers after correction.

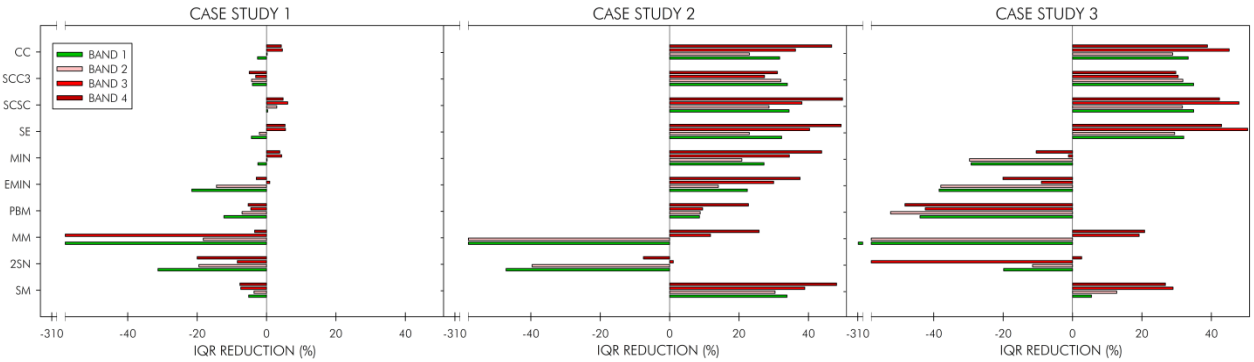

Fig. 6.5. Intraclass IQR reduction. Weighted average of 8 land covers. The biggest positive IQR reduction (%) the better

On the contrary, in case 2 the IQR reduction was much higher, and more TOC algorithms were successful in homogenizing land covers: 8 out of 10 in case 2, all of them except MM and 2SN. Finally, in case 3, CC, sCC3, SCS+C, SE and SM reduced the original IQR of land covers in all the spectral bands in a range of 20% to 50%, while methods such as MIN, EMIN and PBM, that performed well in case 2, increased the original IQR of land covers in this scenario. The results of MM and SM were surprising, with good results for the latter in IR bands in cases 2 and 3, but the worst performance of all the tested methods in the visible bands. On the contrary, SM performed better when illumination conditions were weaker, (i.e., case studies 2 and 3), with an increase of original IQR up to 20-40%.

6.3.5. Comparison of conifer forests radiometry between between sunlit and shaded slopes

The radiance difference between pixels of conifer forests located on sunlit slopes and shaded slopes increased when the topographic effect was more severe, i.e., case study 3 (see Fig. 6.6 on the right). Again, MM and 2SN had a poor performance, showing a clear overcorrection, resulting in pixels of shaded slopes with much higher radiance than in sunlit slopes.

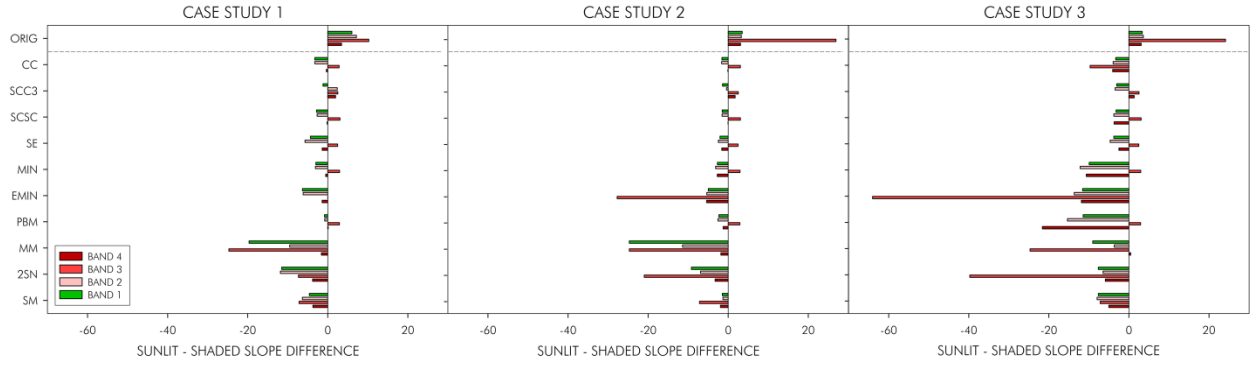

Fig. 6.6. Radiance difference of conifer forest on sunlit-shaded slopes (W. m^2. $sr.^{-1}.\mu m^{-1}$). The closer to zero the difference is, the better

Even if most TOC methods showed an overcorrection in some spectral bands (i.e., b1 and b2), especially in case study 3, the results of CC, sCC3, SCS+C and SE were much better than the original image in the three study cases, as pixels located on sunlit and shaded slopes got closer after the correction. There were only slight differences among them. Some other

methods showed a good performance only in the first two cases, with a reduction of the difference between sunlit and shaded slopes, but not in the third case, i.e., MIN or PBM.

6.3.6. Percentage of outliers

As seen in Fig. 6.7, the percentage of outliers was low for CC, sCC3, SCS+C and SE in all the case studies, increasing in the NIR and SWIR for the other methods. In particular, they rose dramatically in case study 3 for some of the methods (SM, 2SN, MM) in all the spectral bands. On the other hand, some other methods produced outliers in this case study only in band 4, such as PBM, MIN and EMIN. According to this criterion the best method was the sCC3.

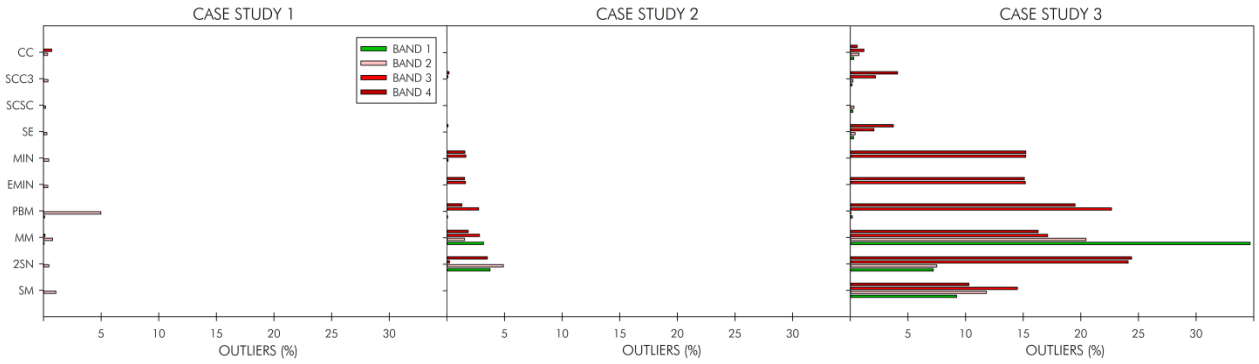

Fig. 6.7. Percentage of outliers generated by the TOCs tested for the different case studies and spectral bands. The smaller percentage, the better

6.3.7. Evaluation using synthetic images

The Mean Structural SIMilarity index (MSSIM) between the ideal situation (i.e., Synthetic Horizontal (*SH*) image) and the TOC-corrected Synthetic Real (SR_{corr}) images were used as a quantitative measure of the quality of the correction for each spectral band, case study and TOC algorithm. The results are shown in Fig. 6.8, where MSSIM values are depicted for each case. The closer the compared images were, the higher the MSSIM was. The lowest MSSIM values in the original image appeared in case 3, as this was the case where the topographic effect was more severe, and thus SR and SH were less similar. Besides, MSSIM values were lower in band 4 comparing to the other spectral bands.

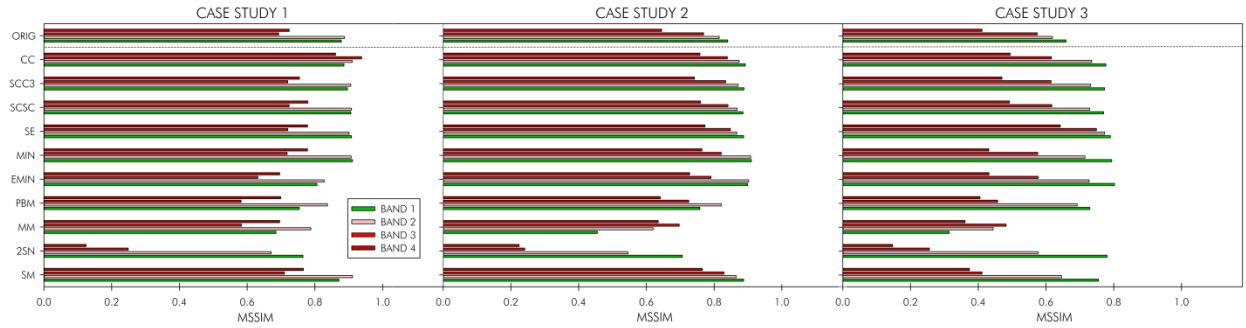

Fig. 6.8. MSSIM of TOC algorithms for each spectral band and case study. Ranks from 0 (worst) to 1 (best)

It is easily observed how most TOCs improved the original situation. Among the ten TOC methods SE ranked first. This algorithm achieved a successful correction in all the bands and case studies. Furthermore, sCC3, CC and SCS+C performed well in most cases but the correction was poorer in b4 and case study 3. Methods such as MIN, EMIN, PBM or SM performed better in visible bands in cases 1 and 2 but failed in infrared bands (b3 and b4), mainly in case 3. Finally MM and 2SN resulted in a poor performance, with even worse MSSIM indexes than the original image in most cases.

6.3.8. TOC ranking based on multi-criteria

In brief, the results obtained through the seven different evaluation procedures were grouped in a multi-criteria ranking of TOC methods (see Table 6.7). Among the tested methods, SCS+C could be considered the best, performing well in the three case studies considering all the criteria (i.e., it ranked among the first 4 positions according to the seven considered criteria for the three tested case studies) being the differences between the best-performing TOCs minor. SE and CC also obtained good results, improving their performance in cases 2 and 3, where there was more topographic effect to correct.

Other methods, such as MIN, EMIN, PBM or SM had inconsistent results, with good performances according to some criteria and poor results according to others. For instance, SM ranked in the first positions in visual evaluation for cases 2 and 3, and was the method that reduced the most the IQR of land covers in case 2, but in terms of stability the results were poor, modifying the radiometry of land covers and generating too many outliers in cases 1 and 3. In general, Minnaert-based methods (i.e., MIN, EMIN and PBM) performed better in

case 1 than in cases 2 and 3. Finally, MM and 2SN had the worst results, both visually and statistically, as they were not able to properly correct the topographic effect.

Table 6.7. Multi-criteria ranking of TOC methods (1= best, 10 = worst)

CASE	Z1								Z2								Z3								AVERAGE
TOC	VISUAL	CORR	STABILITY	IQR RED	SUNLIT/SHADED	OUTLIERS	SR/SH	MEAN	VISUAL	CORR	STABILITY	IQR RED	SUNLIT/SHADED	OUTLIERS	SR/SH	MEAN	VISUAL	CORR	STABILITY	IQR RED	SUNLIT/SHADED	OUTLIERS	SR/SH	MEAN	
CC	3	2	5	2	4	8	1	3.57	3	2	4	4	3	3	3	3.14	2	2	4	3	4	2	2	2.71	3.14
sCC3	7	8	1	5	5	3	5	4.86	6	8	1	6	1	5	6	4.71	5	9	1	4	1	4	4	4.00	4.52
SCS+C	2	4	2	1	2	1	2	2.00	3	3	2	2	2	1	4	2.43	3	3	3	1	3	1	3	2.43	2.29
SE	4	1	3	4	6	2	4	3.43	1	1	3	3	4	4	2	2.57	1	1	8	2	2	3	1	2.57	2.86
MIN	5	3	6	3	3	6	3	4.14	8	5	5	5	6	7	1	5.29	9	5	7	6	6	6	6	6.43	5.29
EMIN	6	5	8	8	7	4	7	6.43	7	7	8	7	9	6	7	7.29	7	6	9	8	10	5	5	7.14	6.95
PBM	1	6	10	7	1	10	8	6.14	5	6	10	8	5	8	8	7.14	8	4	10	9	8	7	7	7.57	6.95
MM	10	9	7	10	10	7	9	8.86	10	9	6	10	10	9	9	9.00	10	8	2	10	7	10	10	8.14	8.67
2SN	9	10	4	9	9	5	10	8.00	9	10	7	9	8	10	10	9.00	6	10	5	7	9	9	9	7.86	8.29
SM	8	7	9	6	8	9	6	7.57	2	4	9	1	7	2	5	4.29	4	7	6	5	5	8	8	6.14	6.00

Table 6.7 also showed that some TOC evaluation criteria gave very similar results, while there were great contrasts among other criteria. For instance, SE ranked the first in case study 3 considering some of the tested criteria. To sum up, it provided a corrected image with a good visual effect of flat appearance, removed the correlation between radiance and illumination, and the highest similarity between TOC corrected SR and SH was obtained, but ranked only 8th in stability. Related to this, the criteria that show the highest correlation between them in the three cases, and also with the final multi-criteria analysis are the reduction of intraclass IQR and the similarity index measured through synthetic images (SR/SH), as a clear signal of their usefulness to assess the performance of TOC methods.

6.4. Discussion

Of the ten TOC methods compared in this study, CC, SCS+C and SE seemed to perform slightly better than others, compensating the differences between shaded and sunlit slopes to a higher extent. On the contrary, the worst corrections were performed by MM and 2SN,

which overcorrected poorly illuminated areas and modified the original radiometry of the image. These results contrast with Richter et al. (2009), who claimed MM achieved the best visual ranking compared with other frequently used TOC methods. This could be due to the inconsistent nature of these methods, where it is necessary to tune and optimally select a number of empirical parameters to each particular case or dataset.

The results obtained by the best TOC methods, i.e., SCS+C, SE and CC, are in line with Soenen et al. (2008), who claimed SE, CC, MIN and SCS+C corrections all reduced the topographic effect to a similar extent, but they still had an overcorrection feature for shaded slopes. sCC3 just performed well in terms of stability, but due to the smoothed slope, it was not able to completely remove the dependence of radiance on illumination, so there was still a visual appearance of topography in TOC-corrected images and a positive correlation coefficient. Consequently this method had a poor rank on those criteria. In line with the results of Riaño et al. (2003), sCC3 retained best the spectral characteristics of each band, but this method did not provide a successful removal of the dependence of radiance on illumination like the authors suggested. It could be concluded that this method performed well only under good illumination conditions, such as those considered by Riaño.

In general, Minnaert-based methods performed better in case 1 than in cases 2 and 3. This was in line with previous investigations, where some authors (e.g., Hantson and Chuvieco 2011) claimed better performances under lower solar zenith angle, while other authors claimed a poor performance (Gao and Zhang 2009b) under large solar zenith angle about 65°, similar to our case 3. Finally, the poor results of MM and 2SN could be partly due to an inadequate implementation of these methods to our specific datasets, eventually due to a non-optimum tuning of empirical parameters.

Summing up, the performance of 10 widely used TOC methods were assessed through multi-criteria analysis on three different case studies, covering a range of illumination conditions from moderate to severe. The obtained results have been used to provide some basic guidelines of the use of TOCs for different statistics, summarized in a table of pros and cons (see Table 6.8):

Table 6.8. Pros and cons of TOC methods for different characteristics

TOC	Pros	Cons
CC	Good performance in all conditions according to most criteria	Not the best in intraclass IQR reduction and comparison between sunlit and shaded slopes
sCC3	Stable LC radiometry in all conditions	Topographic effect is not completely removed
SCS+C	Good performance in all conditions, very stable and without outliers	Originally designed only for forested areas
SE	Good performance in all conditions. The best according to the visual and correlation analysis, specially in severe conditions	LC radiometry not completely stable in severe conditions
MIN	Good or moderate performance in favorable conditions	Problems of overcorrection in poorly illuminated areas. Presence of outliers in poorly illuminated areas
EMIN	Good or moderate performance in favorable conditions	No improvement observed when compared to MIN
PBM	Good performance in favorable or moderate conditions	LC radiometry not stable. Presence of outliers in poorly illuminated areas. Open to users' arbitrary decisions
MM	LC radiometry stable in severe conditions	Poor performance in moderate and severe conditions. Open to users' arbitrary decisions
2SN	Reasonable performance in terms of LC radiometric stability	Poor performance in moderate and severe conditions. Presence of outliers. Open to users' arbitrary decisions
SM	Reasonable performance according to the visual analysis in severe conditions. Improves the performance of 2SN	LC radiometry not stable and high percentage of outliers. Presence of outliers. Open to users' arbitrary decisions

In this work seven different evaluation criteria have been considered to assess the performance of TOC. The results are generally consistent with previous findings in the literature, but not in every case. For instance, the results of SM in visual assessment (Table 6.6) are surprising, since it ranked higher in cases 2 and 3 than in 1. This might be explained by the weaker topographic effect to correct in case 1, which resulted in less differences between TOC methods, revealing a drawback of this evaluation criterion. According to the correlation criterion, CC, SE, SCS+C and MIN, were the best methods reducing the dependence of spectral radiance on illumination in the three studied scenarios, with minimum slopes and r values. This results are in line with the conclusions from previous studies (Gao et

al. 2014; Soenen et al. 2008; Wu et al. 2008). But land covers behave differently when topographic corrections are applied due to their degree of non-Lambertian behavior (Mariotto and Gutschick, 2010), so it is interesting to analyze the results by land cover. When some particularly sensitive land covers (i.e., grasslands and conifers) were analyzed, the results were clearly better for grasslands (Fig 6.S4). This could be due to this land cover's structure being more homogeneous, and consequently their reflective behavior more controled by the topography. Besides, this land cover is frequently located in gentler slopes than coniferous forests, more present in steeper areas. Consequently, the successful removal of the topographic effect on the latter is particularly useful for forestry applications. Nevertheless, differences in forest structure and resulting differences in canopy self-shadowing would also be a major problem to take into account in future developments in this field (Gu and Gillespie, 1998; Soenen et al., 2005; Kane et al. 2008). When the reduction of land covers' IQR is analyzed the result of 2SN and SM are in line with Nichol et al. (2006), who concluded that SM was able to reduce intra-class variance significantly more than 2SN. When this reduction was analyzed for grasslands and conifers, (see Fig. 6.S5), trends similar to those of Fig. 6.5 were depicted, with a higher IQR reduction in cases 2 and 3 for the best TOC algorithms. In most methods results were similar for both land covers in case 1 and 2, but in case 3 the IQR reduction was clearly higher for grasslands in all the TOCs tested. This could be due to the distribution of each land cover, as coniferous forest were mainly located in steeper slopes.

Regarding to the difference between shaded and sunlit slopes, among the spectral bands, the NIR (b3) was the one where this difference was higher, probably due to a particularly strong topographic effect on this spectral band, in line with previous studies (Nichol et al. 2006). Similar to Balthazar et al. (2012), statistical outliers were found mostly in very low-illuminated areas, generally shaded slopes, i.e., with low values of $\cos\gamma_i$. Consequently their amount increased dramatically in case 3 (Fig. 6.7). Finally, the use of synthetic images suggested a good performance of CC, SCS+C and SE, which is consistent with the results obtained through other criteria.

6.5. Conclusions

This paper aimed to perform a multi-criteria analysis of different topographic correction methods, applied under different conditions, and including advantages and shortcomings of each TOC algorithm. The multi-criteria analysis showed that the use of a unique evaluation procedure to assess the quality of topographic correction algorithms appeared to be inappropriate, as the quality of the correction depended on several factors. Although some evaluation criteria provided similar TOC rankings (e.g., intraclass IQR reduction vs. the strategy based on synthetic images, i.e., SR/SH), there were great contrasts among some others (e.g., stability of land cover radiometry vs. visual analysis). Consequently, the use of different criteria to assess the performance of topographic correction algorithms is strongly recommended. If a single evaluation criterion was to be recommended, the intraclass IQR reduction or the strategy based on synthetic images should be used, since they gave TOC rankings most similar to the overall multi-criteria ranking.

TOC performance depended strongly on the magnitude of the topographic effect to correct, that is, on the topography of the area and the illumination conditions of the acquisition. In favorable conditions (case study 1), most TOC algorithms performed adequately and the differences between the best TOCs (i.e., SCS+C, SE and CC) were minor. Therefore, in these conditions the selection of one algorithm or another seemed to have little impact in the outcome of the correction. However, as the topographic effect became stronger differences between TOC algorithms became more apparent. According to our results, methods including slope smoothing (i.e., sCC3), or based on Minnaert approach (i.e., MIN, EMIN or PBM) should be avoided when poor illumination conditions were considered. The former was unsuccessful reducing the intraclass IQR, while the latter introduced too many artifacts and failed in terms of stability.

Table 6.8 provides a list of advantages and shortcomings of each TOC algorithms, which can be interpreted as practical recommendations based on the results of this study. Overall, the TOC algorithms that achieved a best performance were SCS+C, CC and SE, so these could be recommended for most situations. Other methods such as SM performed

inconsistently, with results varying from good to moderate depending on the case study, illumination conditions or method implementation.

Finally, some methods were found to be too complex to apply (since they required many parameters) and some others were open to users' arbitrary decisions (i.e., PBM, MM, 2SN and SM) to adapt the correction to each specific dataset. These issues are not minor, since every processing algorithm should be as simple as possible to facilitate its use and implementation in automated image processing chains.

Acknowledgments

The authors gratefully acknowledge the financial support provided by the Public University of Navarre (UPNA). The authors would also like to thank the Spanish National Geographic Institute (IGN) for providing the test data. Part of the research presented in this paper is funded by the Spanish Ministry of Economy and Competitiveness in the frame of the ESP2013-48458-C4-2-P project.

Supplementary figures

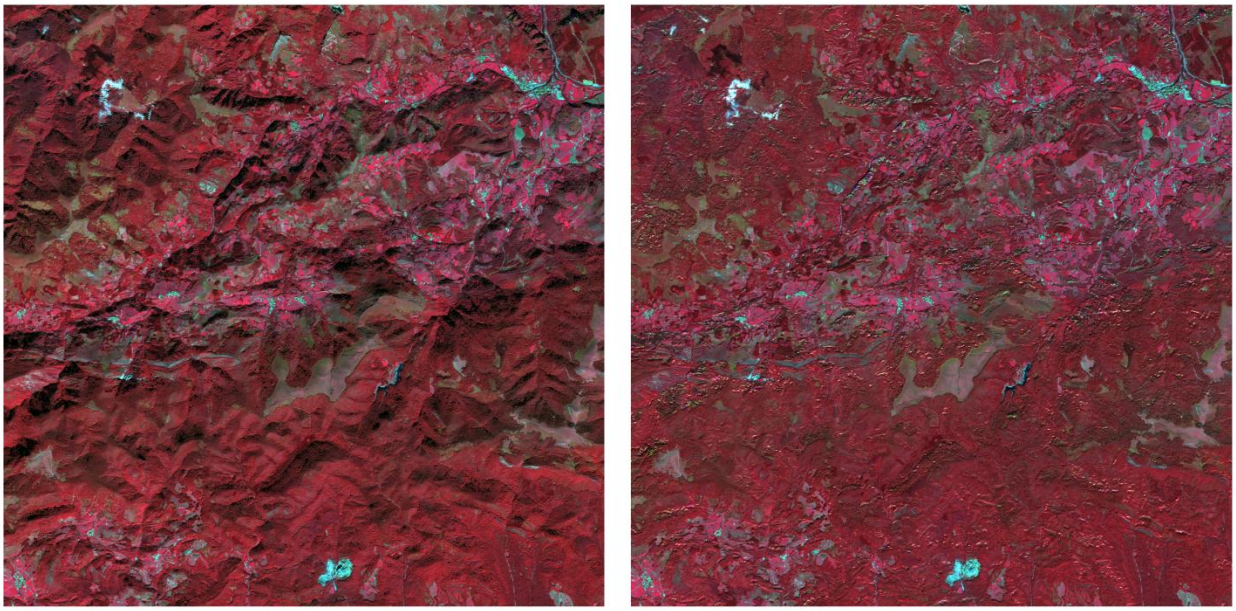

Fig. 6.S1. (**a**) Synthetic real (SR) and (**b**) Synthetic horizontal (SH) images for case study 2

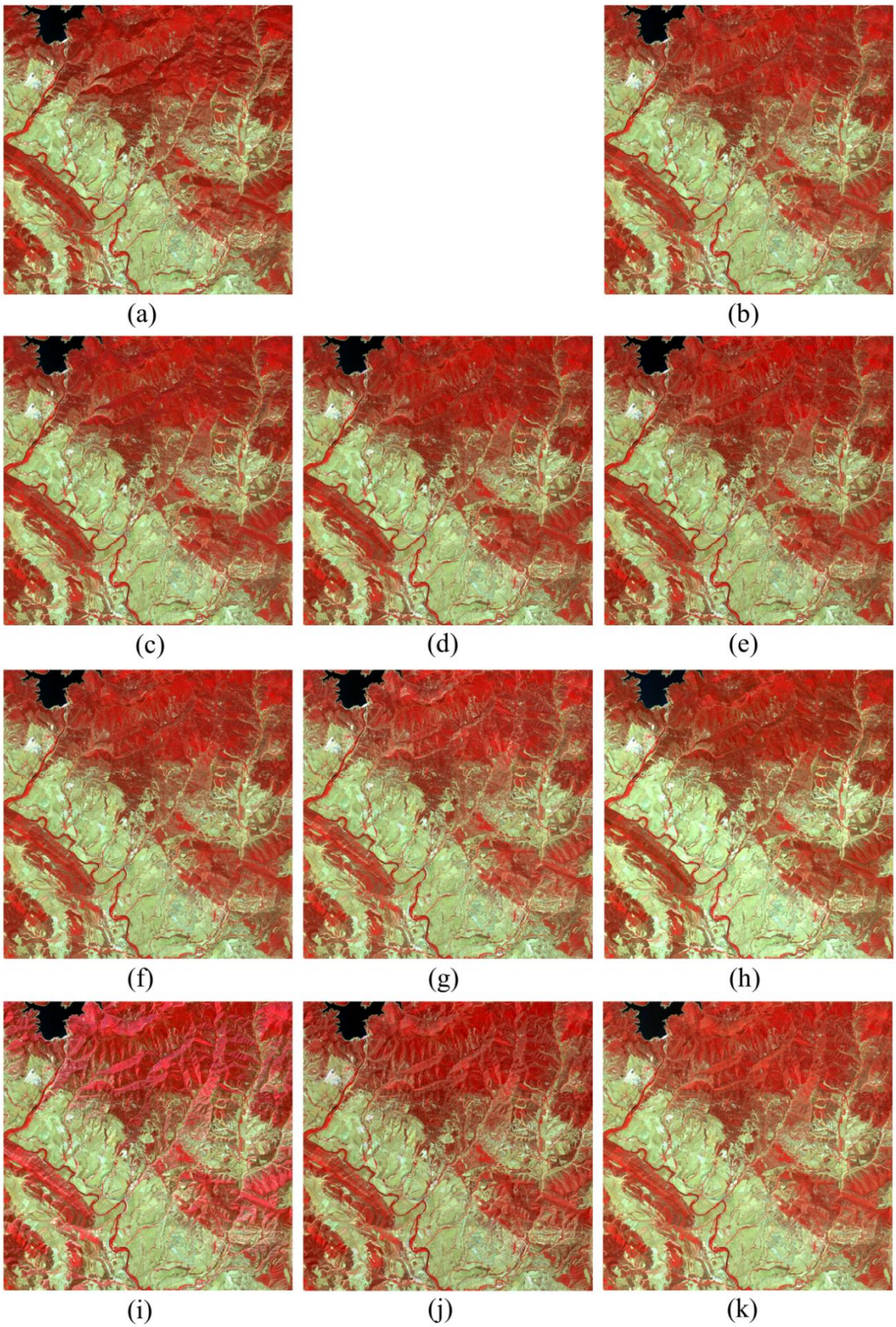

Fig. 6.S2. Original **(a)** and corrected images of case study 1 with TOCs **(b)** CC **(c)**SCS+C **(e)** SE **(f)** MIN **(g)** EMIN **(h)** PBM **(i)** MM **(j)** 2SN **(k)** SM

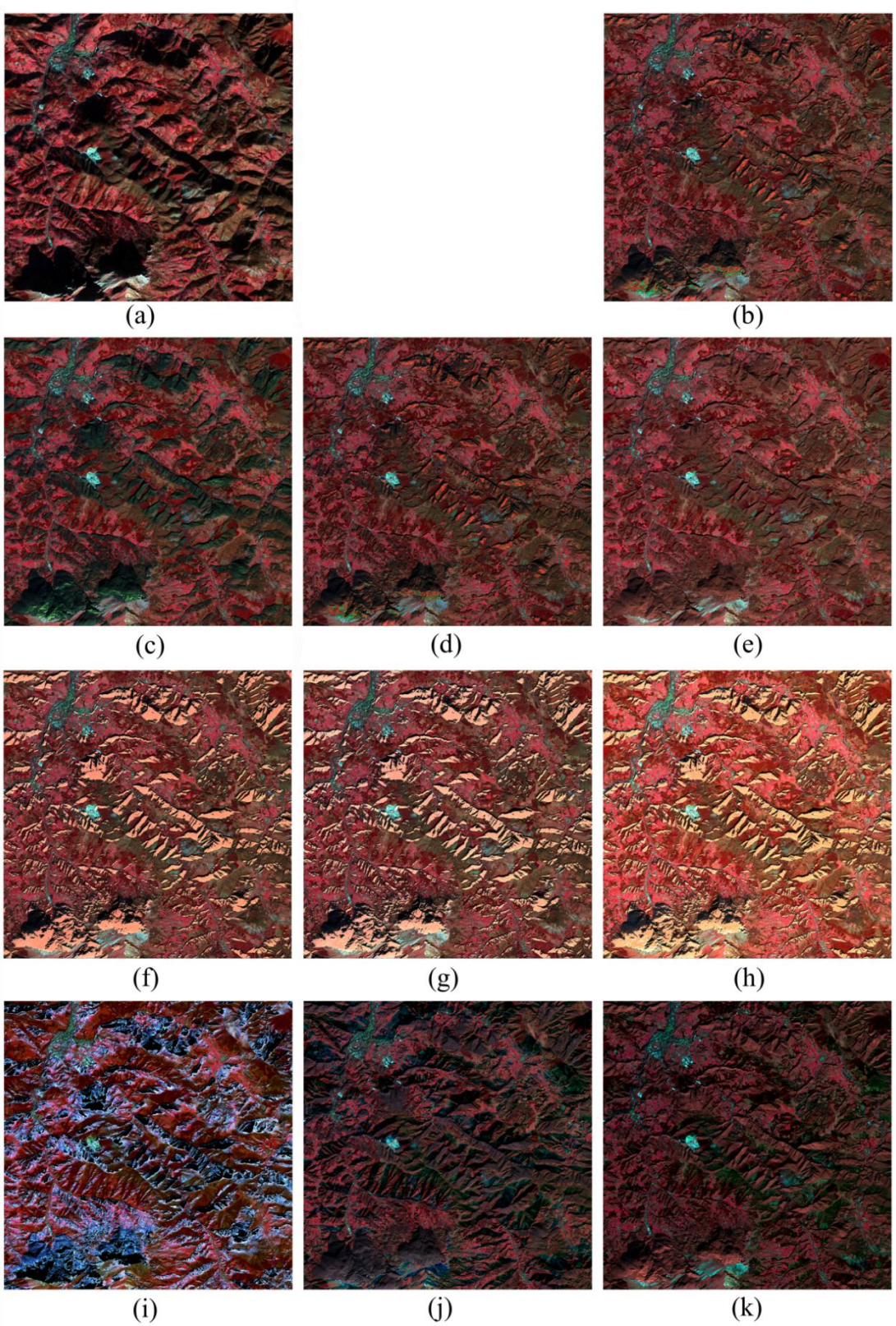

Fig. 6.S3. Original **(a)** and corrected images of case study 3 with TOCs **(b)** CC **(c)**SCS+C **(e)** SE **(f)** MIN **(g)** EMIN **(h)** PBM **(i)** MM **(j)** 2SN **(k)** SM

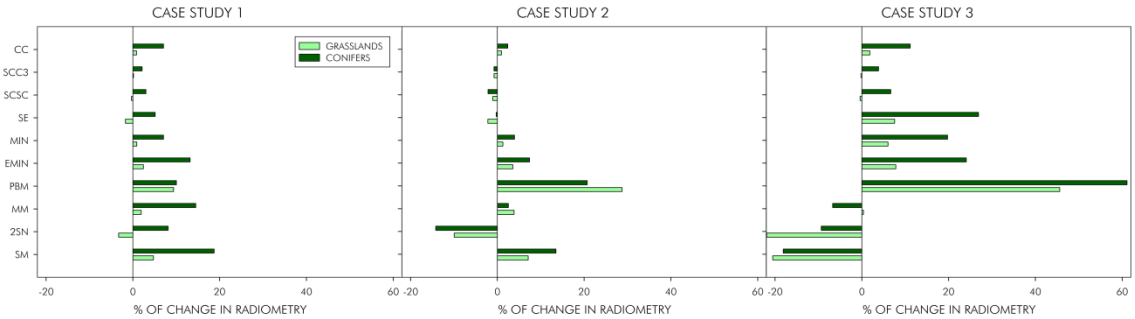

Fig. 6.S4. Stability of original radiometry of grasslands and conifers

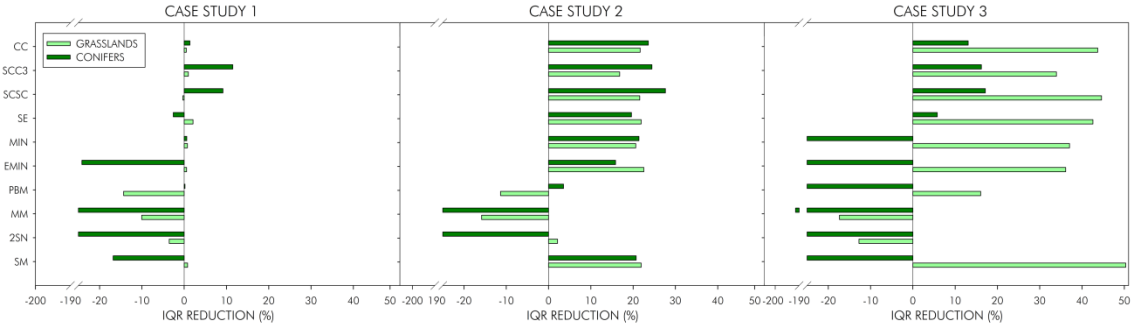

Fig. 6.S5. IQR reduction of grasslands and conifers

CHAPTER 7

STRATIFICATION: On the added value of stratified topographic correction of multispectral images

Published in:

- Sola, I.; González-Audícana M.; Álvarez-Mozos, J. (2015). On the added value of stratified topographic correction of multispectral images. *Remote Sensing*. Manuscript ID: remotesensing-109302

Abstract — Satellite images in mountainous areas are strongly affected by topography. Topographic correction techniques aim to normalize the radiometric differences between slopes of different aspect and are an important pre-processing step for RS applications over mountain areas. Different studies demonstrated that the results of semi-empirical topographic correction algorithms improved when a stratification of land covers was carried out first. Stratification allows for computing per each stratum the empirical coefficients needed in most algorithms, so that the different behavior of land covers can be effectively taken into account in the correction. However, differences in the stratification strategies proposed and also in the evaluation of the results obtained make it unclear how to implement them. The objective of this study was to compare two stratification strategies with a non-stratified approach using several evaluation criteria. For that purpose, the SCS+C algorithm was applied and six different stratification approaches, based on vegetation indices and land cover maps, where implemented and compared with the non-stratified traditional option. The results, evaluated with different statistical criteria did not show a drastic improvement on the performance of topographic correction when stratification approaches were implemented. Stratification approaches based on land cover maps (considering 2, 4 and 8 strata) yielded a slightly better performance in some evaluation criteria (mostly related to radiometric stability and land cover variability) but these differences were rather minor. Therefore, the non-stratified option proved to be mostly effective in removing the topographic effect. Furthermore, it does not require any ancillary information and it is easier to implement in automatic image processing chains. In any case, further research is necessary to evaluate other stratification strategies and confirm these results.

Keywords — Topographic correction; stratification; NDVI; land cover; evaluation; quality assessment

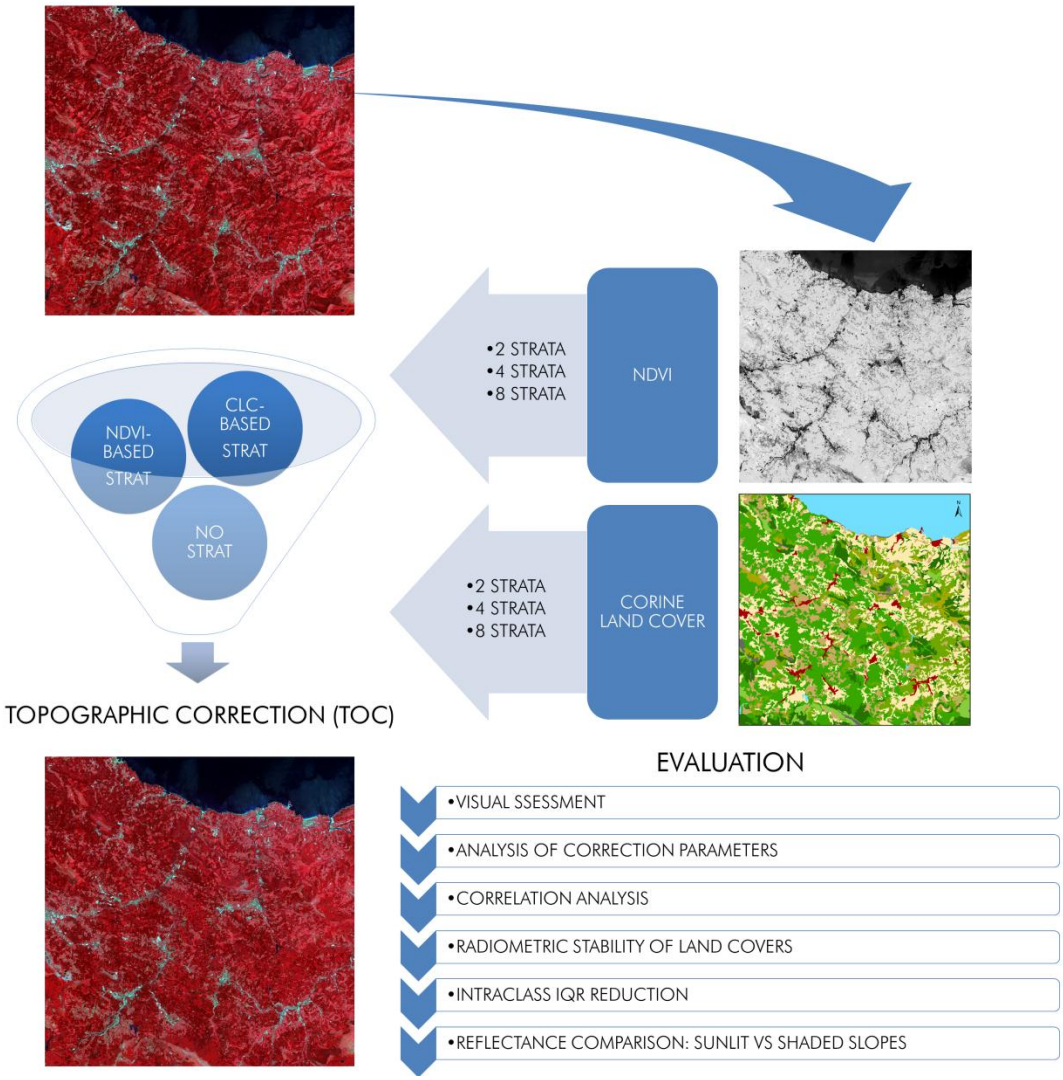

Graphical abstract

7.1. Introduction

Land cover classification and quantitative analysis of multispectral data in flat or gently undulating terrain have become routine practice. However, these applications can still remain a challenge in mountainous regions, due to the so called topographic effect (Leprieur and Durand 1988; Richter et al. 2009). The solar irradiance impinging on the Earth surface and, consequently, the radiance detected by remote sensors can vary significantly depending, not only on the reflectance of land covers, but also on the slope and aspect of the areas where they are located (Riaño et al. 2003). The objective of topographic correction (TOC) is thus to compensate the differences in solar irradiance between slopes with differing aspect and,

ultimately, to obtain the radiance values the sensor would have obtained in case of a perfectly flat surface (Sola et al. 2014a). The topographic effect has long been recognized as a problem for quantitative analyses of RS data, and during the last two decades notable advancements have been made to develop TOC methods. Therefore, topographic correction has become an important image pre-processing step in the application of RS data in mountain areas (Lu et al. 2008; Tokola et al. 2001).

A variety of TOC algorithms have been proposed in the last decades to correct or attenuate the topographic effect on the radiance measured by satellite sensors. These methods can be grouped into three categories based on their degree of complexity and data requirements (Balthazar et al. 2012): Simple empirical methods, semi-empirical methods, and physically-based methods. Semi-empirical methods consist of a photometric function tuned by an empirical coefficient (Reese and Olsson 2011), they have gained popularity because of their balance between complexity and performance. Methods of this type are the Cosine method (COS), Statistic-Empirical method (SE), Minnaert method (MIN), Enhanced Minnaert (EMIN), C-Correction (CC), or Sun-Canopy-Sensor+C (SCS+C) (Teillet et al. 1982; Smith et al. 1980; Soenen et al. 2005). All of them are based on the cosine of the solar incidence angle ($\cos\gamma_i$), a key factor representing the illumination conditions for each pixel, which is calculated from the acquisition geometry (sun angles) and a Digital Elevation Model (DEM) of at least the same spatial resolution of the satellite image (Richter and Schläpfer 2015). Fitting a regression between spectral reflectance and $\cos\gamma_i$, the empirical coefficients required by these methods are calculated, i.e., c_λ parameter or k_λ constant. These coefficients modulate the degree of topographic correction needed for each case, and therefore vary for each area, spectral band, and acquisition geometry considered.

Previous studies evaluated the performance of semi-empirical TOC methods through different criteria, concluding that there is no clear agreement on which method to use for specific combinations of topography, vegetation, and illumination (Goslee 2012). Furthermore, in favorable conditions most semi-empirical TOC algorithms successfully corrected the topographic effect and the differences between the best TOCs were minor (Sola et al. 2015b). Therefore, in these conditions the selection of one algorithm or another seemed to have little impact in the outcome of the correction.

Nevertheless, most of these assessments only considered a single scene generally acquired under favorable illumination conditions and with relatively homogeneous land cover type, which rarely occurs for large mapping projects (Hantson and Chuvieco 2011). Thus, the impact of diverse land cover types on the TOC-corrected images had to be assessed. In the case of heterogeneous land cover within a study site, some authors (Bishop and Colby 2002; Bishop et al. 2003; Szantoi and Simonetti 2013) stated that the estimation of coefficients c_λ (for CC and SCS+C methods) or k_λ (for Minnaert-based methods) individually for each land cover class resulted in enhanced results and were more suitable than the generalized form.

In theory, the correction parameters used in semi-empirical TOC methods depend on the lambertianity of surfaces, which varies due to the roughness and structure of land covers. Thus, TOC methods should be best applied separately to each land cover to account for their different spectral behavior (Richter and Schläpfer 2015; Baraldi et al. 2010; Twele et al. 2006; Blesius and Weirich 2005), this is referred to as stratified topographic correction (STOC). In practice, this is done by dividing the different land cover types into strata that are then corrected separately (i.e., based on empirical parameters calculated for each stratum) with the selected TOC method to achieve better reduction of the topographic effect. The stratification can be carried out using different criteria and considering a different number of classes (Table 7.1).

As seen in Table 7.1, most stratification methods were based on the LULC of the area and their outcome were different strata that corresponded to specific LULC classes or class groups (Tokola et al. 2001; Blesius and Weirich 2005; McDonald et al. 2002, Marioto and Gutschick 2010; Ediriweera el al. 2013; Kobayashi and Sanga-Ngoie 2009), but this approach might not be easily generalized because it requires ancillary information on LULC cartography. Moreover, Hantson and Chuvieco (2011) claimed that the use of land-cover maps was not adequate for an operative stratification of time series of scenes, due to important seasonal and temporal variability of land-covers. In order to overcome this limitation, some authors proposed automated image-classification approaches previous to the topographic correction (Szantoi and Simonetti 2013, Baraldi et al. 2010) while some others decided to stratify by thresholding vegetation indexes, such as the NDVI (Hantson and Chuvieco 2011; Bishop and Colby 2002, Bishop et al. 2003; Adhikari et al. 2015).

Table 7.1. Stratification studies published in the literature

TOC method	Stratification criteria	No. of classes	Source	Ref.
EMIN	LULC/OTHER	2	Ground truth from aerial photographs	(Tokola et al. 2001)
EMIN	VI/OTHER	3/many	NDVI / sliding windows	(Bishop and Colby 2002)
SE, MIN, CC, others	LULC	2	Vegetation information derived from aerial photography	(McDonald et al. 2002)
SE, MIN, CC, EKS	VI	10	NDVI	(Törmä and Härmä 2003)
EMIN	OTHER	3	Interferometric coherence	(Twele and Erasmi 2005)
EMIN	LULC	3	Visually homogeneous regions	(Blesius and Weirich 2005)
EMIN	VI	3	NDVI	(Twele et al. 2006)
MIN, EMIN, CC, sCC	LULC	13 + outliers	Unsupervised classification	(Baraldi et al. 2010)
MIN	LULC	13	Land cover map	(Mariotto and Gutschick 2010)
SE, EMIN, CC, MM	VI	2	NDVI	(Hantson and Chuvieco 2011)
CC, MIN, SCS+C	LULC	3	Ground data and aerial photograph	(Ediriweera et al. 2013)
SE, CC, MIN, ICOS, VECA	VI+OTHER	3	NDVI + spectral decision rules	(Szantoi and Simonetti 2013)
EMIN, SCS+C, CC, others	OTHER	2	Main land cover	(Moreira and Valeriano 2014)
CC	VI	3	NDVI	(Adhikari et al. 2015)
MM	VI	2	Vegetation index	(Richter and Schläpfer 2015)

where, VI= Vegetation index, LULC = Land use/land cover cartography, EKS = Ekstrand correction, sCC = Smoothed C-Correction, MM = Modified Minnaert, ICOS = Improved Cosine method, VECA = Variable Empirical Coefficient Algorithm.

Land cover based STOC applications mostly used Minnaert based TOC methods (i.e., MIN or EMIN) (Bishop and Colby 2002; Blesius and Weirich 2005; Mariotto and Gutschick 2010; Gleriani et al. 2012), but some other methods (e.g., SE, SCS+C and CC methods) were also used, although less frequently (Hantson and Chuvieco 2011; Baraldi et al. 2010). For instance, Colby (1991) first derived the Minnaert k_λ constant for the entire scene, but then suggested that using a local k_λ could enhance analysis capabilities: However, their analysis was based on a small sample area, thus the authors recommended further testing using larger data (Colby 1991). Similarly, Moreira and Valeriano (2014), considering the unavailability of a detailed LULC cartography and the ease for implementation, decided not to stratify but used

only the main land cover type (masking out the rest) to estimate the correction parameters required by their TOC method (i.e., EMIN, 2SN, SE, CC, SCS+C and SM), which were then used to correct the whole image. On the other hand, Blesius and Weirich (2005) stratified the scene into three homogeneous regions based on their radiometric properties, taking random samples from visually distinct areas. The resulting classification was comparable with the results obtained from a traditional training-area approach.

Likewise, Bishop and Colby (2002) evaluated MIN method comparing a non-stratified approach using a single k_λ with two different stratification approaches: using locally computed k_λ-s applying a sliding window (Colby 1991), and using NDVI derived k_λ-s. The non-stratified option yielded low r^2 values in the regression analysis to obtain k_λ constant and consequently its use was not recommended, whereas the second option gave inconsistent results. Therefore, only the last option was recommended, that is, stratifying the scene into three primary classes (i.e., snow, vegetation, and non-vegetation) based on NDVI thresholding. Similarly, Hantson and Chuvieco (2011) proposed a NDVI threshold of 0.4 to divide the image in two strata that were separately corrected, with improved TOC results over their study site, while Törmä and Härmä (2003) proposed a stratification in ten classes according to different NDVI ranks. However, the use of NDVI to stratify the image into more than two classes is questionable as it is uncertain if NDVI values directly correlate with structural landscape characteristics, such as surface roughness, determining their lambertian behavior (Twele and Erasmi 2005). In this line, new TOC methods were also proposed, such as the MM of Richter (Richter 1998; Richter et al. 2009; 2015), including empirical rules that stratified the scene in two vegetation classes based on a simple vegetation index threshold. However, one must bear in mind that NDVI (or any other VI) values obtained from non TOC corrected imagery are incorrect, since the topographic effect is not the same in the different spectral bands, so in order to obtain realistic NDVI values imagery needs to be TOC corrected first, leading to an ill-posed problem, that can only be solved using iterative techniques.

Finally, some other stratification approaches have been based on unsupervised classification of land covers. For instance, Baraldi et al. (2010) proposed a novel stratification strategy combining solar illumination features and image radiometry using a spectral-rule-based decision-tree preliminary classifier (SRC), which resulted in 14 strata. Equivalently,

Szantoi and Simonetti (2013) developed a stratification approach based on spectral decision rules using as input NDVI data. These authors compared their TOC results with and without stratification over several study sites, showing that topographic effects were further removed when stratification was done.

In the light of all these studies, stratification might be understood as a basic requirement for an improved topographic correction. But, some studies pointed out it might not always be necessary, basically depending on the heterogeneity of the study site (Hantson and Chuvieco 2011), or on the TOC method used and the evaluation technique considered (Törmä and Härmä 2003). In many occasions, published studies only compared STOC with no correction at all, which seems a somehow biased comparison that does not allow to extract any conclusions with regard to the convenience or not of stratifying. All in all, the degree of improvement of TOC due to stratification seems at least unclear, as many stratification strategies (with different options and variants) have been proposed in the literature with unsteady and not easily comparable results. Also, if automated image processing chains are to be designed and routinely applied to large areas, stratification adds significant complexity to the whole process. Therefore, more research on this topic has been strongly encouraged (Baraldi et al. 2010).

The objective of this work is to evaluate the added-value of STOC when compared with a non-stratified (or traditional) correction. With this aim, two stratification criteria were evaluated, one based on ancillary LULC information and another one based on NDVI ranks, with a different number of strata tested on each. Furthermore, the results obtained were thoroughly assessed using six different evaluation strategies. This study aims to perform an objective comparison of stratified vs. non stratified strategies and to provide a guideline on the use of topographic correction in both cases.

7.2. Material and methods

7.2.1. Study area

The study area is located on the Atlantic coast of northern Spain (see Fig. 7.1). The mean altitude of the study area is 354 m, ranging from 0 to 1369 m, and the maximum and mean

slopes are 82.1° and 20.1°, respectively. These figures show a rough topography, with a great topographic effect to correct, especially for images acquired under low solar elevation angles. The landscape is highly fragmented in a mosaic of forested areas, pastures, urban areas etc. (see more details in Section 7.2.3).

According to the Köppen climate classification (Köppen 2015), this area belongs to Littoral Oceanic Climate (C_{fb}), characterized by relatively mild winters and warm summers. The climate and landscape are determined by the Atlantic Ocean winds whose moisture gets trapped by the mountains circumventing the Spanish Atlantic coast. The annual average temperature ranges from 8.5 to 14.5° C and the mean annual precipitation is 1100-2500 mm, depending on the altitude and location.

7.2.2. Data acquisition and Processing

A SPOT 5 scene acquired the 30th of August of 2008 was orthorectified and converted from digital numbers (DN) to top of atmosphere radiance (TOARD), in $W \cdot m^{-2} \cdot sr^{-1} \cdot \mu m^{-1}$ units, by using the gain and offset values provided in the metadata for each spectral band. Afterwards, TOARD was converted to ground reflectance (ρ_t) including atmospheric correction based on dark object subtraction method (Chavez 1996). The study site had an extension of 44 x 44 km, and the SPOT 5 scene a spatial resolution of 10 m with four spectral bands, i.e., green: 0.50 – 0.59 μm, red: 0.61 – 0.68 μm, NIR (near infrared): 0.78 – 0.89 μm and SWIR (short-wave infrared): 1.58 – 1.75 μm.

As seen in Table 7.2, the solar geometry (i.e., solar elevation angle) is typical of an end of summer scene, when topographic effect is not that severe, but it still leads to interpretation errors unless efficiently removed. Moreover, this date was selected as most RS applications use images acquired in summer months.

Table 7.2. Configuration of the SPOT 5 scene used

Parameters	Values
Date	30/08/2008
Time	11:11
Solar elevation	53.53
Solar azimuth	155.02

7.2.3. Ancillary information

The LULC information was obtained from Corine Land Cover (CLC) cartography, levels 1, 2 and 3 (EEA 2015), of 2006, easily available for Europe. The area is heterogeneous and can be deemed representative of the most common land cover classes in Spain and Europe, especially in mountainous areas. For instance, six out of the eight most common land cover classes in Spain were present in the study area, while the other two (i.e., non-irrigated arable land and complex cultivation patterns) are not frequent in mountainous areas.

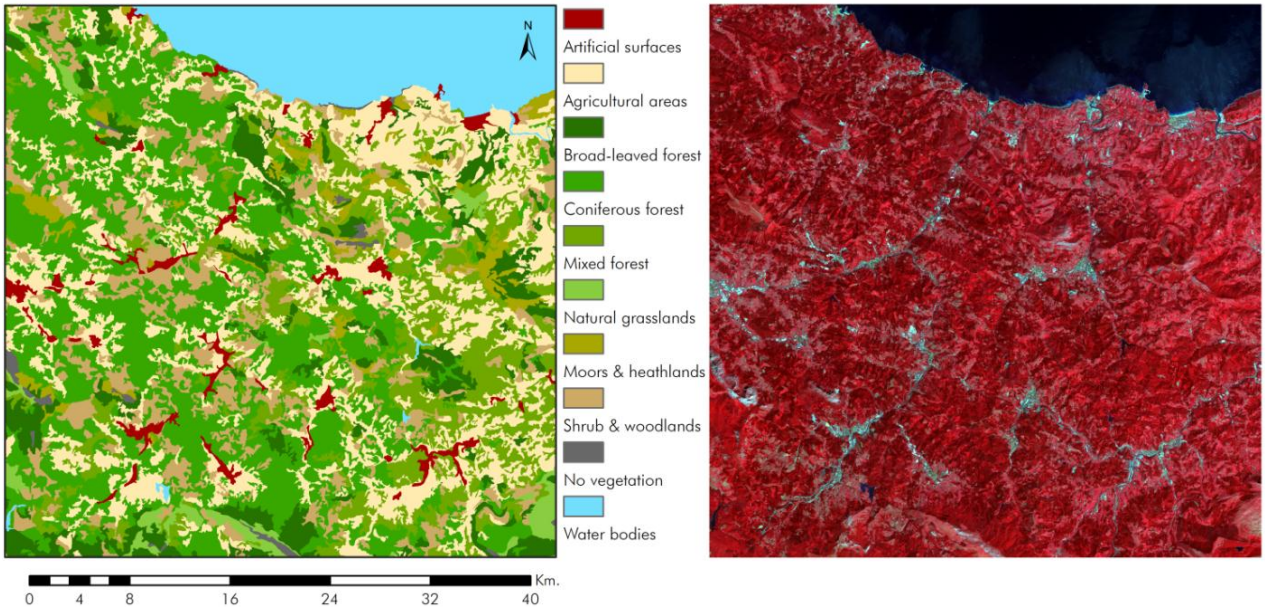

Fig. 7.1. Corine Land Cover (CLC) information (level 3) and SPOT 5 scene of the study site.

The study area is covered in more than 60% by forest and pastures (within agricultural areas according to CLC level 1), but other land covers such as shrubs, sclerophyllous vegetation, moors or bare soil (no vegetation) have an important coverage within the study site. Besides, more than 10% of the area is associated to water bodies that have been masked out in this work.

NDVI was obtained from the topographically corrected ground reflectance obtained from the SPOT 5 scene. As explained in the introduction, vegetation indices are affected by topography (Matsushita et al. 2007). Consequently topographic correction is a required pre-processing step to obtain reliable NDVI values. For that purpose a traditional non-stratified SCS+C was applied previous to the NDVI calculation.

The characteristics of topography ($\cos\gamma_i$) were computed at the original 5 m resolution of the available DEM and then resampled to 10 m to have the same spatial resolution of SPOT 5 images. The DEM, provided by the Spanish National Geographic Institute (IGN), was obtained from cubic convolution of LIDAR point cloud, with a density of 0.5 points m^{-2}.

7.2.4. Stratification strategies

The information provided by CLC cartography and NDVI data was used to generate land cover strata following different strategies (Table 7.3).

Table 7.3. Stratification approaches

Approach	Number of strata	Land cover	Code	Coverage (%)	Masked
No stratification	1	All land covers	ALL	100.00	---
CLC-2	2	Artificial surfaces	ARTIF	2.14	YES
		Agricultural areas (pastures)	AGRIC	21.04	NO
		Forest and semi natural areas	FOREST	65.34	NO
		Water bodies (+wetlands)	WATER	11.48	YES
CLC-4	4	Artificial surfaces	ARTIF	2.14	YES
		Agricultural areas (pastures)	AGRIC	21.04	NO
		Forests	FOREST-L2	49.83	NO
		Scrub and/or herbaceous vegetation associations	SHRUB	14.91	NO
		Open spaces with little or no vegetation	NOVEGET	0.60	NO
		Water bodies (+ wetlands)	WATER	11.48	YES
CLC-8	8	Artificial surfaces	ARTIF	2.14	YES
		Agricultural areas (pastures)	AGRIC	21.04	NO
		Broad-leaved forest	BROAD	7.48	NO
		Coniferous forest	CONIF	28.95	NO
		Mixed forest	MIXED	13.40	NO
		Natural grasslands	GRASS	1.83	NO
		Moors and heathland	MOORS	2.48	NO
		Transitional woodland-shrub + sclerophyllous veget.	SHRUB-L3	10.60	NO
		Open spaces with little or no vegetation	NOVEGET	0.60	NO
		Water bodies (+ wetlands)	WATER	11.48	YES
NDVI-2	2	0<NDVI<0.4	NDVI 0-4	13.30	NO
		0.4<NDVI<1	NDVI 4-1	86.70	NO
NDVI-4	4	0<NDVI<0.4	NDVI 0-4	13.30	NO
		0.4<NDVI<0.6	NDVI 4-6	5.91	NO
		0.6<NDVI<0.8	NDVI 6-8	23.32	NO
		0.8<NDVI<1	NDVI 8-1	57.47	NO
NDVI-8	8	0<NDVI<0.2	NDVI 0-2	4.54	NO
		0.2<NDVI<0.4	NDVI 2-4	8.77	NO
		0.4<NDVI<0.5	NDVI 4-5	2.50	NO
		0.5<NDVI<0.6	NDVI 5-6	3.40	NO
		0.6<NDVI<0.7	NDVI 6-7	7.32	NO
		0.7<NDVI<0.8	NDVI 7-8	16.00	NO
		0.8<NDVI<0.9	NDVI 8-9	55.32	NO
		0.9<NDVI<1	NDVI 9-1	2.15	NO

Six different stratification approaches were considered and compared with the traditional non-stratified approach. On the one hand, CLC classes from level 1, 2 and 3 were used to divide the images in 2, 4 and 8 strata respectively, while flat areas, cast shadows, water bodies and wetlands, and artificial surfaces were masked out. On the other hand, arbitrary NDVI thresholds were used (Hantson and Chuvieco 2011, Törmä and Härmä 2003), to split the scene in 2, 4 and 8 strata, masking again flat areas and cast shadows, as well as pixels where NDVI < 0.

7.2.5. Selected topographic correction algorithm

Based on a previous multi-criteria evaluation (Sola et al. 2015b) the Sun-Canopy-Sensor+C (SCS+C) algorithm was selected to correct the topographic effect both in the non-stratified and the stratified approaches. This method was originally proposed by Soenen et al. (2005) as a modification of the SCS algorithm previously designed by Gu and Gillespie (1998). Besides of being ranked the first in the evaluation among ten of the most widely-used TOC methods (Sola et al. 2015b), the SCS+C algorithm was originally designed for forested areas, which are predominant on tilted slopes in the study area where the topographic effect is more severe.

$$\rho_{corr,\lambda} = \rho_{\lambda} \frac{cos\,\beta cos\,\vartheta_s + c_{\lambda}}{cos\,\gamma_i + c_{\lambda}} \qquad (7.1)$$

where, $\rho_{corr,\lambda}$ is the corrected ground reflectance of band λ, ρ_{λ} is the ground reflectance of band λ in rugged terrain, β is the terrain slope computed from the DEM, ϑ_s is the solar zenith angle, and c_{λ} is the empirical coefficient of band λ, calculated as the ratio between the intercept and the slope of the regression of $cos\gamma_i$ against the reflectance of each band. In the calculation of c_{λ}, flat pixels (i.e., $\beta < 5°$), cast shadowed pixels and self-shadowed pixels, (i.e., pixels where $cos\gamma_i < 0$), were masked out.

7.2.6. Evaluation strategies

The performance of the different stratification types tested needs to be evaluated using objective strategies. Different evaluation strategies have been proposed in the literature and six of them were used in this study.

7.2.6.1. Analysis of correction parameters

As explained above, c_λ is obtained through a linear regression between reflectance and $\cos\gamma_i$ values. The coefficient of correlation of the fitted regression illustrates the robustness and reliability of the topographic correction. Therefore, it is interesting to evaluate this correlation and also how values change for each stratum when different stratification strategies are applied. In order to help interpreting these values, the standard deviation (SD) of $\cos\gamma_i$ for each stratum was also considered, as it might impact the regressions fitted.

7.2.6.2. Correlation analysis

Probably the most used criteria to evaluate the performance of TOC is the correlation of $\cos\gamma_i$ against the radiance/reflectance of each spectral band after the correction (Riaño et al. 2003; Szantoi and Simonetti 2013; Gao and Zhang 2009b; Vincini and Frazzi 2003). In general, the higher the reduction of this correlation, the better the performance of TOC algorithm. This was measured through the correlation coefficient (r) of the linear regression between $\cos\gamma_i$ and the TOC corrected reflectance.

7.2.6.3. Stability of land cover radiometry

Ideally, the original median reflectance of each land cover should not change after TOC; otherwise the TOC method would have introduced a bias (Goslee 2012; Moreira and Valeriano 2014). Strictly speaking, this should not be considered a criterion to assess the performance of the correction, but a measure of its stability. In this work, the stability was assessed by splitting the image in the eight land cover classes of CLC-8 (masking water, wetlands and artificial surfaces) and comparing the median of each class before and after TOC.

7.2.6.4. Intraclass IQR reduction

A widely used procedure to evaluate the performance of TOC algorithms is to measure the reduction of intraclass variance after correction. Ideally, topographic correction should result in more homogeneous land covers, i.e., independent of illumination, aspect or slope. For that purpose, instead of the commonly used SD (Riaño et al. 2003; Lu et al. 2008; Shepherd and

Dymond 2003), the inter quartile range (IQR) was used in this work. IQR measures the difference between quartile 3 (Q3) and quartile 1 (Q1) for each land cover, and it is less sensitive to outliers than SD. For each land cover the IQR was calculated before and after the correction, and subsequently the area weighted IQR average was calculated.

7.2.6.5. Comparison of reflectance between sunlit and shaded slopes

In the study area, coniferous forests take the steepest slopes, and thus are particularly affected by the topographic effect. A successful TOC should reduce the differences in radiometry between forests located on sunlit and shaded slopes (Shepherd and Dymond 2003). Two random samples of 1000 pixels of coniferous forest were extracted from sunlit and shaded slopes, respectively. Then, the reflectance difference between these two samples was computed before and after TOC. Ideally, pixels of the same land cover class should be more homogeneous after the correction, with reflectance difference values close to zero.

7.2.6.6. Synthetic images

Synthetic images can be used to evaluate topographic correction algorithms by comparing a TOC corrected scene with a synthetic image generated assuming a completely flat topography and considered an ideal reference (Sola et al. 2014a; 2015a). In this study synthetic images were generated for the same acquisition time and study area of the SPOT 5 image using the model developed in (Sola et al. 2014a; 2015a), and then TOC corrected Synthetic Real (SR) images were compared with the Synthetic Horizontal (SH) reference. This comparison was quantitatively carried out by calculating the Mean Structural SIMilarity index (MSSIM) (Wang et al. 2004), which measures how similar two scenes are according to three different components, i.e., luminance, structure and contrast comparison.

7.3. Results and discussion

7.3.1. Visual analysis

The visual analysis of the TOC and STOC approaches suggest a successful removal of the topographic effect over the vast majority of the study site regardless of the stratification option.

Differences between traditional and stratified corrections were minor. While shadowed slopes in mountainous areas, mainly covered by forest, grasslands, shrubs and bare soil were topographically corrected, flat areas, water bodies and artificial surfaces remained uncorrected as they were masked out. Similarly, agricultural areas, frequently located on gentler slopes, were not strongly affected by topography. A detail zone of the scene is shown in Fig. 7.2 for further information.

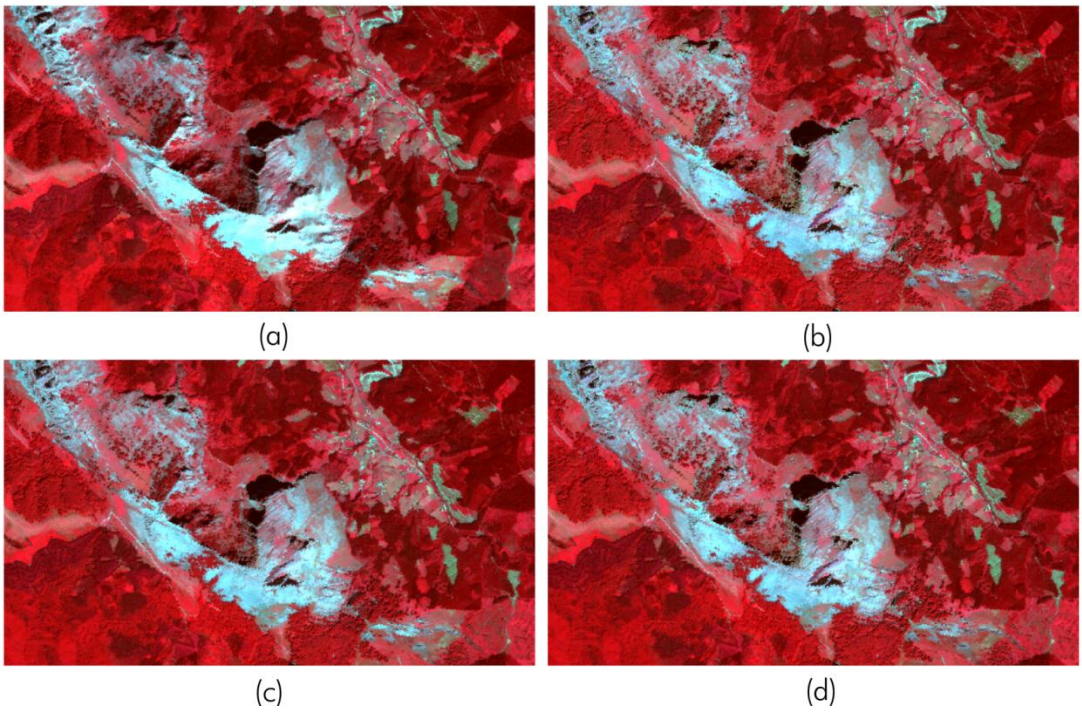

Fig. 7.2. Detail zone with **(a)** Non-corrected scene (**b)** TOC-corrected scene with no stratification **(c)** TOC-corrected scene with CLC-8 stratification and **(d)** TOC-corrected scene with NDVI-8 stratification.

The detail zone in Fig. 7.2 corresponds to an extremely abrupt topography mainly covered by broad-leaved and conifer forests, pastures and bare soil. The area is good example of the limits of semi-empirical corrections, unable to fully correct shadowed areas where no direct irradiance is impinging on the surface (Goslee 2012). All in all, the traditional SCS+C correction (see Fig. 7.2b) performed adequately in the vast majority of the area, while CLC-8 and NDVI-8 stratification approaches (see Figs. 7.2c and 7.2d) were visually very similar to the traditional correction. Fig. 7.2 also shows areas where shaded slopes had been slightly overcorrected. This effect was less apparent in CLC-8 approach.

7.3.2. Analysis of correction coefficients

In Fig. 7.3 the c_λ values obtained for each stratum and spectral band of the image are displayed. There were great differences for this value when the traditional, non-stratified approach was compared with the different stratifications.

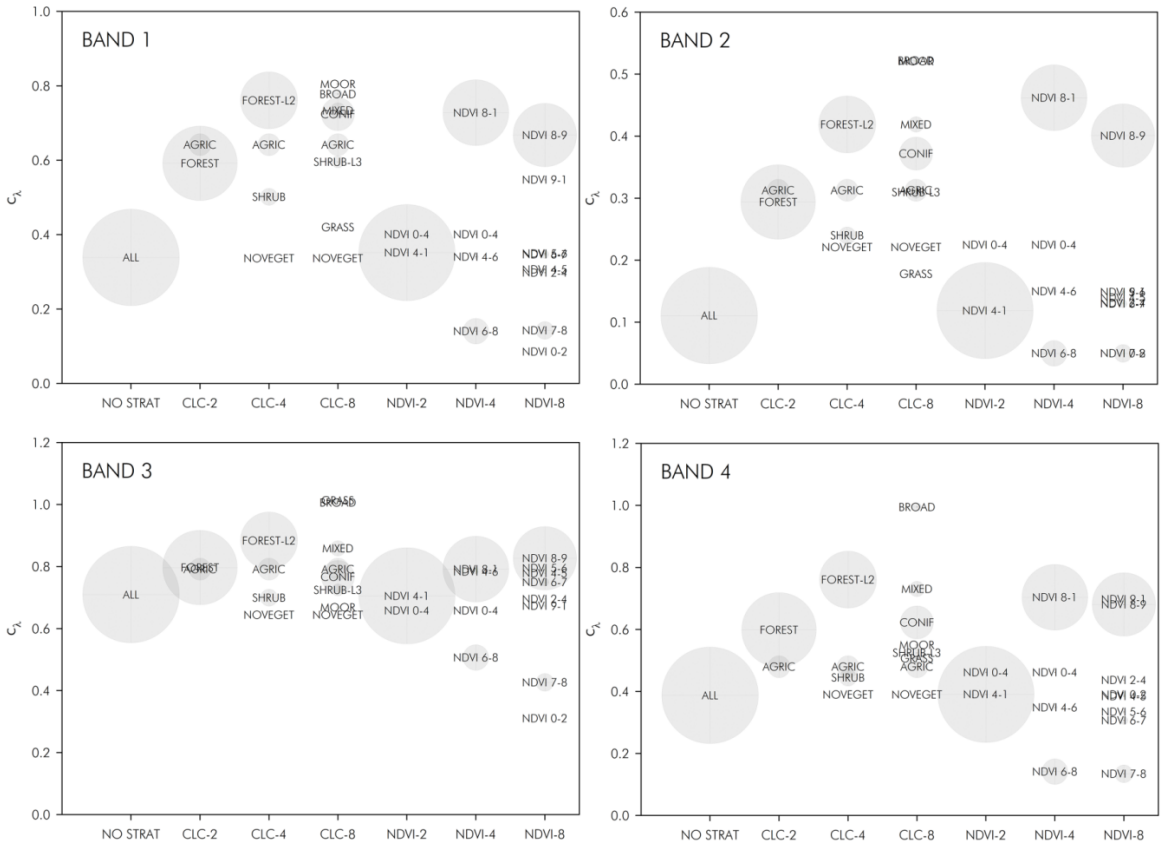

Fig. 7.3. c_λ coefficient obtained for each spectral band on the different stratification approaches evaluated. Circle sizes represent the proportion of each stratum in the study area.

In general parameter c_λ was higher for high NDVI values (i.e., NDVI>0.8) and forested land covers. Due to the role of this parameter in the SCS+C method, the higher c_λ is, the smoother the correction. That is, high c_λ values soften topographic correction and thus avoid overcorrection on poorly illuminated slopes. All in all, Pons et al. (2014) suggested that this adverse effect, commonly reported on COS and SCS method (Soenen et al. 2005; Fan et al. 2014), could be avoided if pixels under an incidence angle higher than 70° were discarded.

These results are similar to those obtained by Ediriweera et al. (2013) who found a considerable variation in the c_λ parameters by vegetation type, but contrast with McDonald et

al. (2002) who found that in flat terrain the empirical coefficients obtained for agricultural land covers were very small and consequently CC tended toward a COS correction. Although our results are not directly comparable to this study, the same effect is expected on strata with low c_λ (i.e., NDVI 6-8 or NDVI 7-8), thus SCS+C tends towards SCS on these strata.

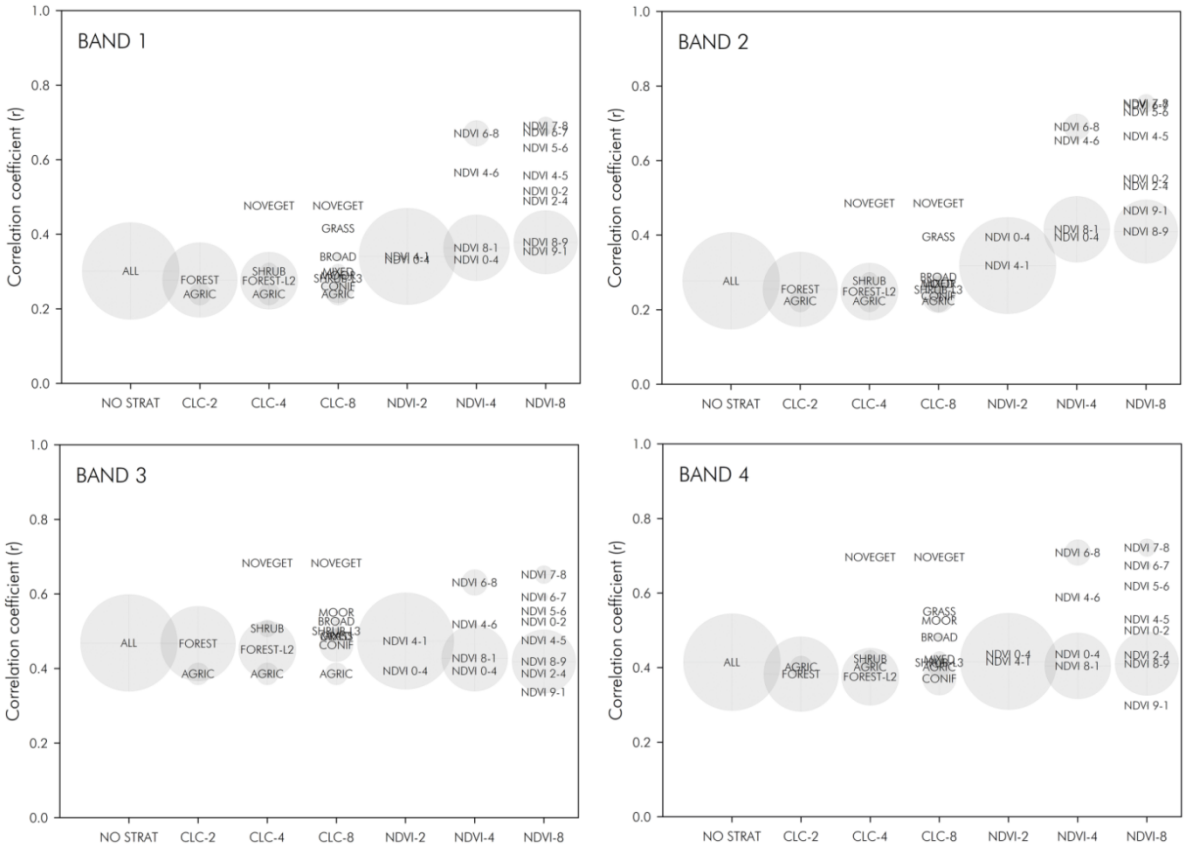

Fig. 7.4. Correlation coefficient between $\cos\gamma_i$ and the reflectance of spectral bands for each stratum. Circle sizes represent the proportion of each stratum in the study area.

In Fig. 7.4 the correlation between $\cos\gamma_i$ and the reflectance of spectral bands (for each land cover) is depicted. Although r values did not change dramatically in the different stratifications tested, in bands 1 and 2 there was a clear trend of higher correlation for NDVI-based stratifications, with higher r values for every NDVI strata compared with the non-stratified approach. In these two bands, the lowest correlation among the NDVI strata was achieved by the NDVI 0.9-1 strata, but it was still higher than the correlation for the non-stratified option. LULC based stratifications lead to slightly lower correlation than the non-stratified option in bands 1 and 2 when only two strata were considered and also with four strata. When eight strata were considered, NOVEGET and GRASS lead to improved

correlations but the rest obtained similar or lower correlations. As expected, agricultural areas showed the lowest correlation as they mainly corresponded to flat areas so the correlation with $\cos\gamma_i$ was less reliable.

For bands 3 and 4 obtained r were different trends for the different stratification options evaluated (Fig. 7.4). In band 3 the non-stratified option already yielded quite a high r value that then increased or decreased after stratification depending on the particular NDVI or LULC class considered. Generally, NDVI strata with moderate-high NDVI values (>0.4) yielded higher r values. In band 4, after stratification r values did not change significantly in most cases, but in some LULC (NOVEGET, GRASS, BROAD and MOORS) and NDVI classes (NDVI 4-6, NDVI 6-8, etc.) r value increased. These results contrast with previous findings, where higher correlations were reported after stratification (Tokola et al. 2001; Bishop and Colby 2002). In our study this was only true in some cases, depending on the particular land cover and spectral band considered.

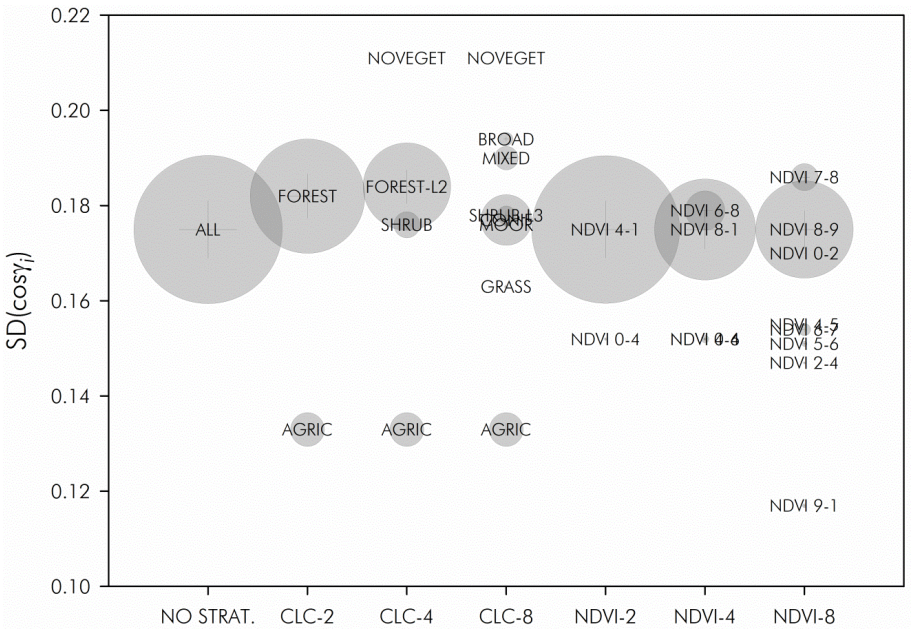

Fig. 7.5. SD of $\cos\gamma_i$ for each stratum. Circle sizes represent the proportion of each stratum in the study area.

In Fig. 7.5 the SD of $\cos\gamma_i$ is displayed for each stratum in every stratification approach. Looking at Fig. 7.4 and Fig. 7.5, there seems to be a coincidence in some bands. For instance in band 2 the stratum AGRIC had low SD and low r, and the opposite occurred for

NOVEGET, with high SD and high r. The results in other LULC strata were not so clear, probably because their SD values were very similar to the non-stratified case.

These results uncover that for some particular strata the c_λ values were obtained from regressions fitted with quite low correlations, so TOC in these conditions could be unstable. This issue seems to be intrinsic to the stratified approach, and in particular, for strata with a small area in the image either because they are minority or because a high number of strata is considered. In this cases it is unlikely that a sufficient variability in $\cos\gamma_i$ values is guaranteed so as to lead to strongly correlated regressions and solid c_λ values.

7.3.3. Correlation analysis

In Fig. 7.6 the correlation coefficient (r) of the regression between $\cos\gamma_i$ and the reflectance of each spectral band are shown for the original image (top) and then for the TOC-corrected images on the seven stratification strategies evaluated. In the original non-corrected image r ranged from 0.25 to 0.50, being higher in the infrared bands (i.e., b3 and b4).

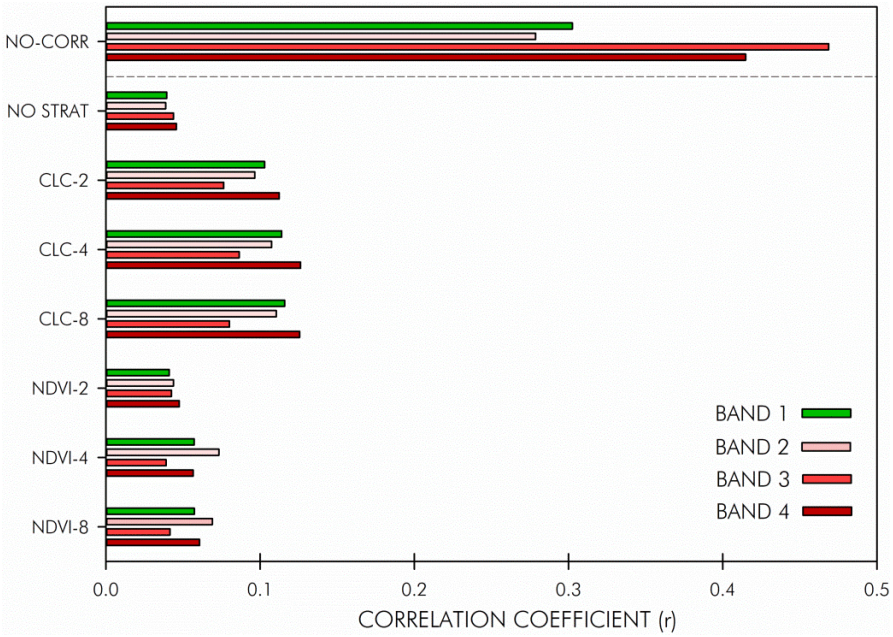

Fig. 7.6. Correlation coefficient of the regression between $\cos\gamma_i$ and the reflectance of each spectral band for the original image (NO-CORR) and the different strategies tested.

All topographic corrections were successful in removing this correlation to a certain extent in all the bands. Notwithstanding that, all the topographic corrections showed slightly positive values of residual correlation, proof of an incomplete removal of the topographic effect, in

line with the findings of Gao and Zhang (2009b). All in all, these low values (i.e., $r < 0.1$) are not significant if compared to the r values of the original image. It must be taken into account that the successful removal of the topographic effect does not necessarily mean $r = 0$, there could be a residual correlation due to the presence of areas where slope orientation determines the land cover (e.g., Fig. 7.2a). According to this evaluation criterion there was not a clear improvement of the correction when stratification was applied. Furthermore, the CLC-based stratification approaches performed slightly worse (higher correlation) than the non-stratified option, while minor differences were observed between the NDVI-based stratifications and the non-stratified TOC.

7.3.4. Radiometric stability of land covers

In Fig. 7.7 the area weighted average of the relative difference of land covers' median reflectance before and after TOC is shown, comparing corrected and original scenes band-wise.

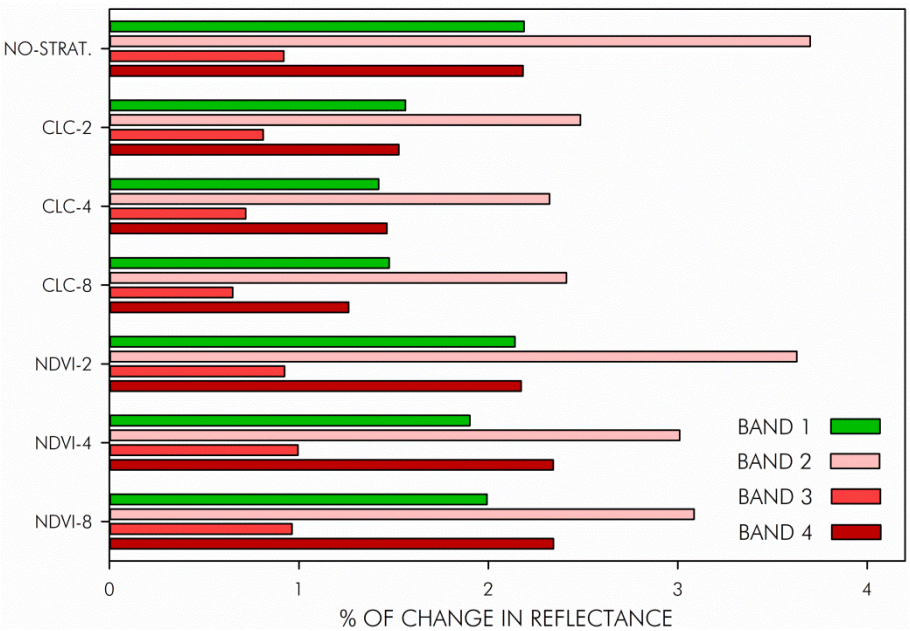

Fig. 7.7. Radiometric stability of land covers represented by the weighted average of % of change in land cover reflectance after TOC.

The figure shows a clear increase in the original reflectance of land covers in all the bands. This increase of 1-4% of the original reflectance was already observed by other authors

applying the SCS+C method, and also the CC method (Moreira and Valeriano 2014; Gao and Zhang 2009b), probably due to the formulation of both methods. Although, this bias was consistent, its magnitude suggests it to be negligible and besides, very similar when different stratification approaches were compared. In a comparable study, Moreira and Valeriano (2014) observed that SCS+C correction increased the original radiometry of forests compared to uncorrected data, as the forest samples were more concentrated in shaded slopes.

7.3.5. Intraclass IQR reduction

In Fig. 7.8 the IQR reduction of land covers performed by each correction is shown. IQR reduction was the lowest for band 3, this can be explained by the overall higher radiometry in this band for vegetated covers, which caused IQR reduction (measured in %) to be relatively small if compared to the other bands. Small differences were observed between stratification approaches.

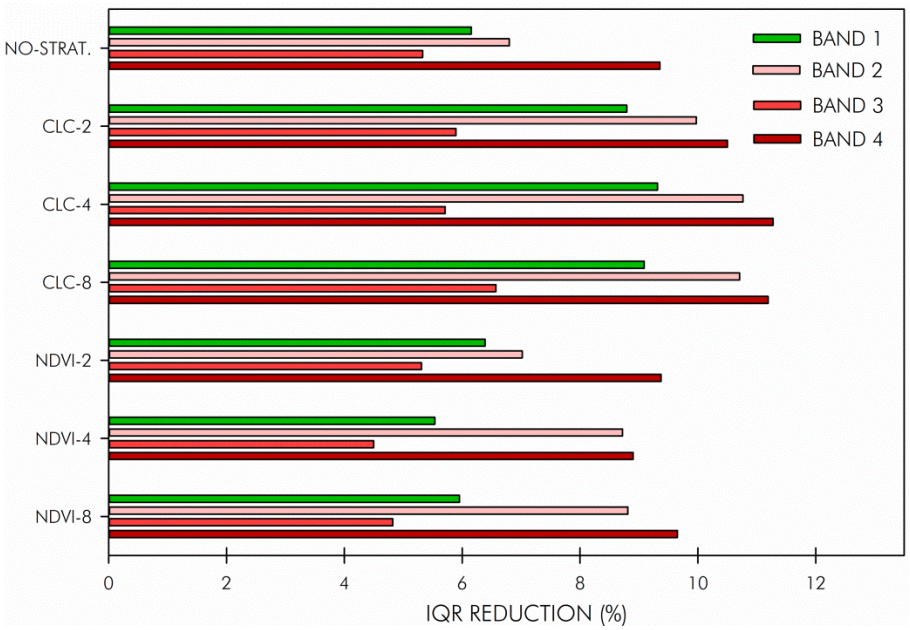

Fig. 7.8. Mean intraclass IQR reduction. Measured as the weighted average of IQR reduction for eight land covers.

Fig. 7.8 clearly shows that stratification did not significantly improve the IQR reduction rate achieved by the non-stratified SCS+C correction. Some improvements were observed in bands 1 and 2 for the CLC based stratifications, but differences with the other configurations were not that marked.

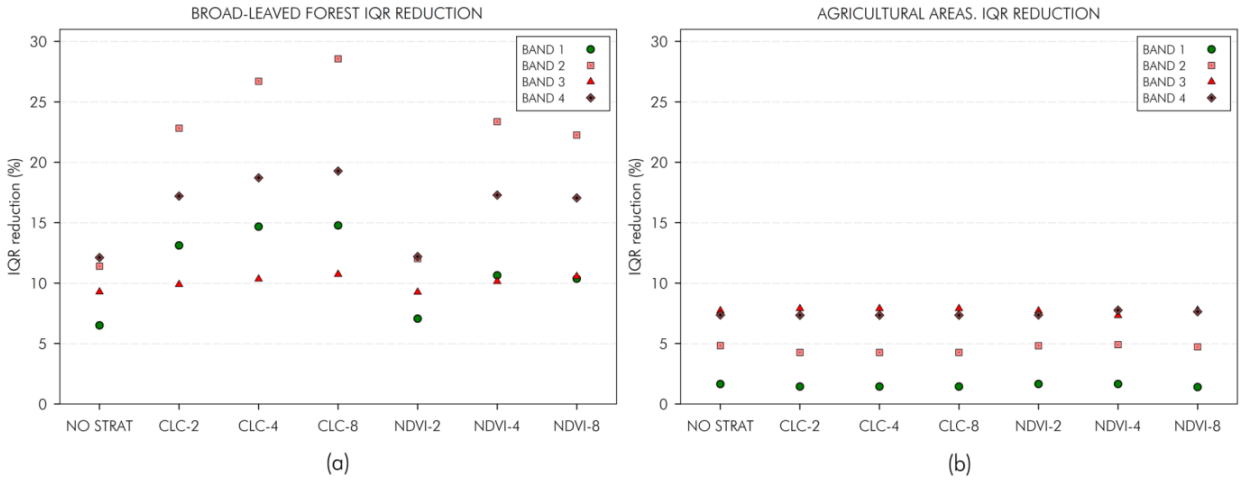

Fig. 7.9. Intraclass IQR reduction of **(a)** broad-leaved forest and **(b)** agricultural areas for each spectral band

If the results showed in Fig. 7.8 are analized by land cover, additional information is obtained. For instance, in the non-stratified option, broad-leaved forests (see Fig. 7.9a) showed a greater reduction of IQR up to 7-13% than in general (Fig. 7.7). This means that this land cover was particularly homogenized after TOC. Besides, this reduction significantly increased for the different stratification approaches, especially the CLC-based ones. In fact, the higher the number of strata consider the better. These results demonstrate a clear improvement of topographic correction of broad-leaved forest when it is applied separately per land cover. On the other hand, agricultural areas (pastures in a vast majority), were less affected by the topography (i.e., low SD($\cos\gamma_i$)) and had low correlation between $\cos\gamma_i$ and reflectance (Figs. 7.4 and 7.5). This land cover showed a lower IQR reduction, and differences among stratification approaches were inappreciable and clearly not significant.

7.3.6. Comparison of reflectance between sunlit and shaded slopes

When the non-corrected scene was analyzed, the reflectance difference between pixels of conifer forests located on sunlit slopes (facing the sun) and shaded slopes (facing away from the sun) was up to 30-40% due to the topographic effect (see Fig. 7.10).

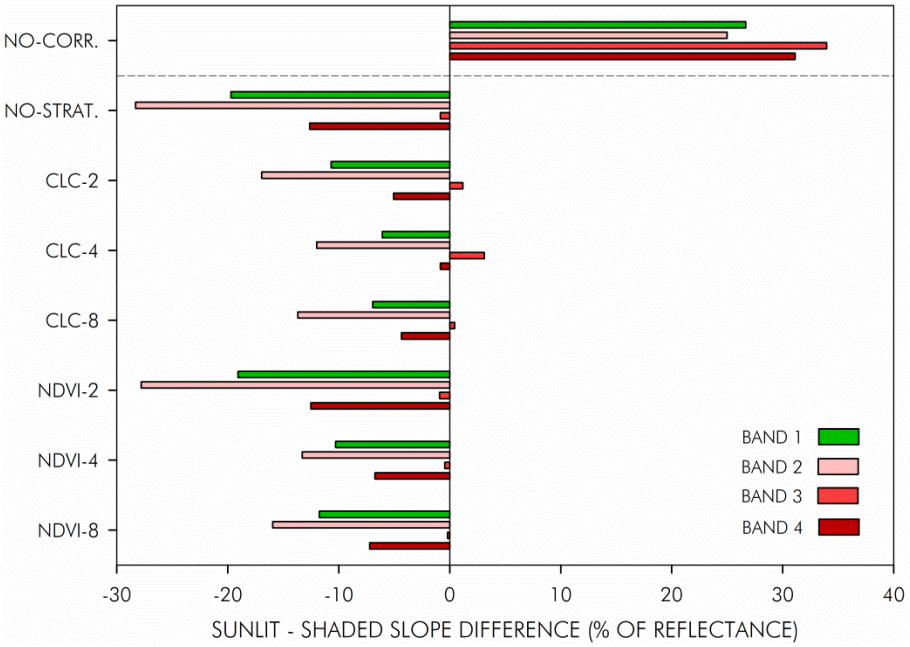

Fig. 7.10. Reflectance difference between sunlit and shaded slopes for conifer forests

Among spectral bands this difference was again higher for infrared bands. After the correction, no matter which stratification approach was tested, this positive difference between sunlit and shaded slopes was completely removed, and what is more, a systematic overcorrection was observed mostly in visible bands, i.e., b1 and b2. This effect was clear in the non-stratified correction, and it was also apparent in the forested areas of the detail zone in Fig. 7.2b. Overcorrection was not that strong in the CLC-based stratifications, particularly in CLC-4 and CLC-8. However, NDVI based stratifications, and in particular NDVI-2 lead to strong overcorrection in this land cover.

Our results are similar to those presented by Ediriweera et al. (2013) who observed that SCS+C method seemed to overcorrect reflectance on very steep slopes. This result is in line with the radiometric stability criterion (see Section 7.3.4), where band 2, and to a lesser extent bands 1 and 4, showed a systematic increase in radiometry after correction. Also the lower correlation values reported in Fig. 7.6 could be partly explained because the non-stratified and the NDVI based stratified options overcorrected some land covers. It should be noted that the NDVI-2 stratification yields very similar values to the non-stratified alternative (in all the different criteria), this could be due to the arbitrary NDVI threshold of 0.4 selected (following Hantson and Chuvieco (2011)), as most of the pixels were located within the NDVI 4-1 strata.

A more effective stratification could be based on ISODATA cluster analysis of NDVI, in line with previous studies of other authors (Bishop and Colby 2002; Bishop et al. 2003).

7.3.7. Evaluation using synthetic images

The results obtained with this technique are shown in Table 7.4, where MSSIM values are depicted for each case. Higher MSSIM values correspond to a closer match between the TOC corrected scene and the ideal reference (SH), and thus to a better reduction of the topographic effect. The MSSIM value for the original (uncorrected) image is also depicted in Table 7.4 as a reference for interpreting the other cases.

Table 7.4. MSSIM of the different stratification approaches for each spectral band

TOC	B1	B2	B3	B4
NO-CORR	0.801	0.794	0.720	0.612
NO-STRAT.	0.890	0.885	0.882	0.857
CLC-2	0.888	0.881	0.881	0.843
CLC-4	0.884	0.875	0.880	0.835
CLC-8	0.885	0.876	0.880	0.836
NDVI-2	0.891	0.885	0.884	0.859
NDVI-4	0.872	0.868	0.882	0.840
NDVI-8	0.877	0.874	0.878	0.841

It is easily observed that all TOCs improved the MSSIM value of the original scene, and this was particularly true for infrared bands. Among the different stratification approaches tested, no clear differences in MSSIM were observed, and in fact, none of them improved the performance of the non-stratified correction.

To sum up, the visual assessment of the globally applied SCS+C correction revealed a successful removal of the topographic effect. Moreover, the results have been shown to reduce spectral variance of land covers, remove the dependence of reflectance on $\cos\gamma_i$, a better balancing between sunlit and shaded slopes and an increase on SSIM indices of every spectral band. Nevertheless, a side effect of this correction is the increase in the mean reflectance of land covers and the slight overcorrection in forested areas. These findings differed from some studies that attributed a poor performance of topographic correction to SCS+C (Ediriweera et al. 2013; Gao and Zhang 2009b); but were in line with some others (Moreira and Valeriano 2014; Sola et al. 2015b).

The stratification approaches further corrected the topographic effect, improving the performance of non-stratified option in some evaluation criteria, i.e., IQR reduction of land covers, and removal of the difference between sunlit and shaded slopes. This superior performance is clearer in some particular land covers, such as broad-leaved forest, where CLC-based stratification provided much higher IQR reduction. In the literature, the stratified approaches yielded results with varying degrees of success for the respective investigated study site, depending on the stratification strategy, land cover distribution and selected TOC method.

7.4. Conclusions

The empirical coefficient c_λ required in the SCS+C method, changed clearly between the different stratification options and took different values for each strata (in many cases higher than the c_λ value obtained for the non-stratified option). However, these c_λ variations did not necessarily result from a more robust correlation and issues such as the relative size of the stratum or the variability of $\cos\gamma_i$ therein played an important role here. In some evaluation criteria CLC-based stratifications yielded slightly better results than the non-stratified or the NDVI based stratification options, particularly in the stability of land cover radiometry, intraclass IQR reduction or sunlit-shaded slope difference. The non-stratified and NDVI based stratifications (in particular NDVI-2) showed a tendency to slightly overcorrect the topographic effect of steep slopes, but this effect was removed when CLC-based stratifications were applied.

All in all, even if in some criteria, CLC-based approaches performed slightly better than the non-stratified correction, the latter proved to be mostly effective in removing the topographic effect. This conclusion is deemed important, because the non-stratified option can be applied without a priori knowledge or ancillary information of the scene. Furthermore, it can be implemented in a much easier way in automatic image processing chains. In any case, future research is necessary on stratification strategies based on a priori unsupervised classifications of the scene to correct, so as to check whether better results are achieved following this approach. Moreover, further studies on different study sites and image acquisition dates are necessary to confirm the conclusions drawn here.

After the evaluation of different stratification strategies (based on land cover and NDVI) and their comparison with a non-stratified SCS+C correction, the results obtained did not show a drastic improvement on the performance of topographic correction when stratification approaches were implemented.

Acknowledgments

The authors gratefully acknowledge the financial support provided by the Public University of Navarre (UPNA). The authors would also like to thank the Spanish National Geographic Institute (IGN) for providing the test data. Part of the research presented in this paper is funded by the Spanish Ministry of Economy and Competitiveness in the frame of the ESP2013-48458-C4-2-P project.

Author Contributions

Ion Sola, María González-Audícana and Jesús Álvarez-Mozos provided the overall conception of this research, designs the methodologies and experiments, and wrote the majority of the manuscript; Ion Sola carried out the implementation of proposed algorithms, conducted the experiments and performed the data analyses.

CONCLUSIONS

Terrain shape causes solar illumination to change markedly between areas with different slope and aspect. These illumination differences cause radiometric variations in optical Remote Sensing images, which can be erroneously interpreted as changes in land cover or in bio-geophysical parameters of the terrain, severely affecting the viability of remote sensing applications in mountain areas. A thorough literature survey revealed that a large number of topographic correction methods exist, ranging from simple empirical relations to complex physically based models. Semi-empirical methods achieve a good balance between complexity and performance, and thus have become the most popular and appropriate to correct satellite images in a simple and extensive way. Yet, a very significant number of semi-empirical topographic correction algorithms and variants exist and there seem to be no clear rules on which algorithm to apply for each particular case (in terms of terrain and scene acquisition conditions). What is more, it is not straightforward to tell which algorithm is "the best" for a particular case because there is no standard evaluation criterion to apply. Hence, the results of each topographic correction algorithm depend on the evaluation criterion used, but none of the widely used criteria can be considered simple and objective. These issues

have been addressed in this thesis and the results obtained shed some light, and open new questions, on this topic.

Firstly, a topographic correction algorithm evaluation technique has been proposed, which is based on synthetic images generated with a simplified simulation model. Synthetic images provide an objective and rigorous means of assessing the performance of topographic correction algorithms, by comparing corrected images to the ideal situation of no topographic effect. This technique has a number of advantages when compared to traditional evaluation techniques: it is quantitative, it does not require ancillary information on land covers and it can be used to objectively compare topographic correction algorithms for different terrain and scene acquisition conditions. The evaluation is performed globally and locally, thus problematic areas can be easily detected. Moreover, the model proposed to generate synthetic images was validated using real imagery over four different test areas showing a reasonable agreement in all spectral bands.

The evaluation of topographic correction algorithms using synthetic images showed best results for C-Correction, Statistic-Empirical and Enhanced Minnaert methods, in this order, while the Cosine method had a poor performance, with clear signs of overcorrection in poorly illuminated slopes. C-Correction ranked first, but differences among the best methods were minor. Shaded areas, corresponding to slopes where $\cos\gamma_i$ is close to zero or negative, were a great challenge for topographic correction methods, as it was very difficult to extract reliable spectral information from them, and none of the tested semi-empirical methods achieved to completely correct these areas of the scene.

Topographic correction algorithm performance depends strongly on the magnitude of the topographic effect to correct, that is, on the topography of the area and the illumination conditions of the acquisition. In extreme conditions, the topographic correction is even more important, as the radiometric distortions introduced by topography are more severe. However, most of the algorithm evaluations performed in the literature only considered images acquired under good illumination conditions. The new evaluation technique proposed here was applied on a multitemporal study to analyze the performance of topographic correction algorithms along the year. As expected, worse results were obtained for winter dates, when the solar elevation angle was lower. Regarding to the tested methods our findings showed that the C-

Correction slightly outperformed other methods between March and August, but the Statistic-Empirical performed slightly better in December. On the contrary, the Cosine method performed the worst, no matter of the acquisition date.

As already explained, the number of topographic correction algorithms proposed in the literature is large, and so it is the number of evaluation strategies used. So, a thorough evaluation of ten algorithms was performed considering three different case studies and following a multi-criteria analysis based on seven evaluation strategies frequently used in the literature. The results obtained showed that Sun-Canopy-Sensor+C, C-Correction and Statistic-Empirical performed the best. Sun-Canopy-Sensor+C ranked first, with a performance slightly superior to Statistic-Empirical and C-Correction.

In contrast to previous results, Minnaert-based methods performed worse than the best methods mentioned, with signs of overcorrection on slopes facing away from the sun. These problems could be caused by weak regressions to calculate k_λ constant. Some other methods were not recommended either, such as the Two Stage Normalization or the Pixel Based Minnaert, because they were found too complex to apply or subject to users' arbitrary decisions. All in all, the results obtained highlight the benefits of a multi-criteria evaluation. The use of a single evaluation strategy might be insufficient, because the quality of the correction depends on several factors. If a single evaluation criterion was to be recommended, the intraclass interquartile range reduction or the strategy based on synthetic images should be used, since they gave algorithm rankings most similar to the overall multi-criteria ranking.

Lastly, the analyses performed in the stratified implementation of topographic correction algorithms showed that stratification tended to improve the degree of correlation between radiance/reflectance and $\cos\gamma_i$ in some cases, depending on the heterogeneity of the study site and the characteristics of the strata considered. However, the benefits of a stratified topographic correction observed here were only minor, so more research on stratification strategies is encouraged. In particular, to solve the circular problem caused by the need (in some cases) of land cover information to stratify and implement the correction, when this information is usually the final product sought after Remote Sensing image processing.

To sum up, topographic correction has proved to be an important pre-processing step of satellite imagery on mountainous areas, and an objective and quantitative evaluation of its performance is essential. The use of semi-empirical topographic correction methods enable a straightforward correction of the distortions introduced by topography to a great extent. Nevertheless, these methods failed in completely removing this effect under severe conditions. Thus, further research is encouraged to improve the performance of topographic correction in poorly illuminated areas in order to obtain high quality products from Remote Sensing data.

CONCLUSIONES

La topografía del terreno es responsable de profundos cambios en la iluminación entre áreas de distinta pendiente y orientación. Estas diferencias de iluminación ocasionan variaciones radiométricas en las imágenes captadas por sensores remotos, que pueden ser erróneamente interpretadas como cambios de cubierta o de parámetros bio-geofísicos del terreno, afectando severamente la viabilidad de las aplicaciones de teledetección en áreas de montaña. Una extensa revisión bibliográfica reveló la existencia de un gran número de métodos de corrección topográfica, que van desde relaciones empíricas simples a complejos modelos de base física. Los métodos semi-empíricos han conseguido un equilibrio entre sencillez y buen rendimiento, y por tanto se han convertido en los más populares y apropiados para corregir imágenes de satélite de una forma simple y extensiva. De todas formas, son muchos los métodos semi-empíricos existentes y no parece haber unas reglas claras acerca de qué algoritmos emplear para cada caso particular, en términos de tipo de terreno y condiciones de adquisición de la imagen. Es más, no es sencillo afirmar que un método es "el mejor" para un caso particular ya que no existe un criterio estándar de evaluación a aplicar. Por tanto, los resultados de cada algoritmo de corrección topográfica

dependen del criterio escogido para evaluarlo, pero ninguno de los comúnmente empleados puede considerarse simple y objetivo. Estas cuestiones han sido reseñadas en esta tesis, y los resultados obtenidos han arrojado algo de luz, pero igualmente han dado lugar a nuevas incertidumbres en este campo.

En primer lugar, se ha propuesta una nueva técnica para evaluar algoritmos de corrección topográfica, la cual está basada en imágenes sintéticas generadas mediante un modelo de simulación simplificado. Las imágenes sintéticas permiten evaluar de forma rigurosa y objetiva el rendimiento de los algoritmos de corrección topográfica, al comparar las imágenes corregidas con la situación ideal en ausencia de efecto topográfico. Esta técnica tiene un gran número de ventajas en comparación con las técnicas de evaluación tradicionales: Es cuantitativa, no requiere de información auxiliar de las cubiertas, y puede ser utilizada para comparar algoritmos de corrección topográfica para diferentes tipologías de terreno y diferentes condiciones de adquisición de la escena. Esta evaluación se lleva a cabo tanto de forma global como local, de manera que las zonas problemáticas son fácilmente detectadas. Además, el modelo propuesto para generar imágenes sintéticas fue validado utilizando imágenes reales para cuatro zonas de estudio mostrando una concordancia razonable en todas las bandas espectrales.

La evaluación de algoritmos de corrección topográfica utilizando imágenes sintéticas reflejó los mejores resultados para C-Correction, Statistic-Empirical y Enhanced Minnaert, en ese orden, mientras que el método del Coseno no corrigió adecuadamente, mostrando evidencias de sobrecorrección en las laderas pobremente iluminadas. El método que ofreció un mejor rendimiento fue el C-Correction, no obstante, las diferencias entre los tres mejores métodos fueron escasas. Las laderas en sombra, correspondientes a pendientes en las que el coseno del ángulo de incidencia solar es próximo a cero o negativo, supusieron un desafío para los métodos de corrección topográfica, ya que no es sencillo extraer información espectral fiable de las mismas. En consecuencia, ninguno de los métodos semi-empíricos testados consiguió corregir completamente el efecto topográfico en estas zonas.

La corrección topográfica depende en gran medida de la magnitud del efecto topográfico a corregir, y éste a su vez de la topografía del terreno y de las condiciones de iluminación en el momento de adquisición de la imagen. En condiciones extremas la corrección topográfica

adquiere una importancia mayor si cabe, ya que las variaciones radiométricas introducidas por la topografía son de mayor calado. La nueva técnica de evaluación propuesta aquí fue aplicada a un estudio multitemporal para analizar el rendimiento de los algoritmos de corrección topográfica a lo largo del año. Tal y como era de esperar, los resultados fueron claramente peores en fechas invernales, cuando el ángulo de elevación solar estaba más bajo. En cuanto a los métodos testados, los datos arrojaron resultados positivos para el método C-Correction, que superó ligeramente a otros métodos entre marzo y agosto, pero que fue superado por el método SE en diciembre. Por el contrario, el método del Coseno dio los peores resultados, independientemente de la fecha.

Como se ha dicho anteriormente, el número de algoritmos de corrección topográfica es elevado, y lo mismo ocurre con las estrategias de evaluación de los mismos. Es por ello que se llevó a cabo una completa evaluación de diez algoritmos de corrección, considerando tres zonas de estudio distintas, y llevando a cabo un análisis multi-criterio basado en siete estrategias de evaluación de entre las más empleadas en la literatura. Los resultados mostraron un mejor comportamiento de los métodos Sun-Canopy-Sensor+C, C-Correction y Statistic-Empirical, siendo el primero de estos el que mejores resultados ofreció, ligeramente por encima de los otros dos.

En contraste con estudios previos, los métodos basados en Minnaert funcionaron peor que los anteriormente citados, dando muestras de sobrecorrección en laderas poco iluminadas. Estos problemas pudieran deberse a regresiones poco significativas para obtener la constante k_λ de Minnaert. En base a los resultados obtenidos no cabría recomendar otros métodos, tales como el Two Stage Normalization o el Pixel Based Minnaert, al considerarse complejos o sujetos a decisiones arbitrarias a tomar por el usuario. De todas formas, los resultados obtenidos demuestran los beneficios de una evaluación multi-criterio. Al contrario, el uso de un único criterio de evaluación se antoja insuficiente, ya que la calidad de la corrección depende de varios factores. Si hubiera que recomendar un único criterio de evaluación, éste sería la reducción del rango intercuartil de las cubiertas o la metodología basada en imágenes sintéticas, ya que dieron lugar a un ranking de métodos similar al obtenido a partir del análisis multi-criterio general.

Por último, el análisis de la implementación de algoritmos de corrección topográfica de forma estratificada sugirió una mejoría en el grado de correlación entre radiancia/reflectividad y el coseno del ángulo de incidencia solar en algunos casos, dependiendo de la heterogeneidad del área de estudio y de las características de los estratos considerados. Sin embargo, la mejora de la corrección topográfica fruto de la estratificación fue limitada, de manera que se sugiere seguir investigando las distintas estrategias de estratificación. En concreto, se trataría de resolver este problema circular, ocasionado ya que la clasificación de cubiertas en zonas montañosas se ve beneficiada de una adecuada corrección topográfica, pero esta última a su vez es más eficaz si se aplica de forma estratificada (en algunos casos), para lo cual se requiere un conocimiento previo de las cubiertas.

En resumen, se ha demostrado la importancia de la corrección topográfica en la cadena de pre-procesamiento de imágenes de satélite en zonas de montaña, y una evaluación cuantitativa objetiva del rendimiento de la corrección es esencial. El empleo de métodos de corrección semi-empíricos permite corregir de forma sencilla y eficaz las distorsiones introducidas por la topografía en gran medida. Sin embargo, estos métodos no consiguen corregir por completo el efecto topográfico en condiciones severas. Por tanto, sería recomendable que los esfuerzos de investigación se dirigieran a mejorar el rendimiento de los métodos de corrección topográfica en estos casos, para así poder obtener productos de calidad derivados de la teledetección.

REFERENCES

Adhikari, H.; Heiskanen, J.; Maeda, E.; Pellikka, P. (2015). Does topographic normalization of landsat images improve fractional tree cover mapping in tropical mountains? In *International Archives of the Photogrammetry, Remote Sensing & Spatial Information Sciences*, Volume XL-7/W3, Berlin (Germany), 11–15 May 2015.

ASHRAE (1985). *ASHRAE Handbook of Fundamentals*. Atlanta: American Society of Heating, Refrigerating and Air-Conditioning Engineers.

Baldridge, A.M.; Hook, S.J.; Grove, C.I.,; Rivera, G. (2009). The ASTER spectral library version 2.0. *Remote Sensing of Environment, 113*, 711-715.

Balthazar, V.; Vanacker, V.; Lambin, E.F. (2012). Evaluation and parameterization of ATCOR3 topographic correction method for forest cover mapping in mountain areas. *International Journal of Applied Observation and Geoinformation, 18*, 436-450.

Baraldi, A.; Gironda, M.; Simonetti, D. (2010). Operational Two-Stage Stratified Topographic Correction of Spaceborne Multispectral Imagery Employing an Automatic Spectral-Rule-Based Decision-Tree Preliminary Classifier. *IEEE Transactions on Geoscience and Remote Sensing, 48*, 112-146.

Bird, R.E.; Hulstrom, R.L. (1981). A simplified clear sky model for direct and diffuse insolation on horizontal surfaces. In S.E.R. Institute (Ed.), *Technical Report SERI/TR* (pp. 642-761). Golden, CO.

Bird, R. E.; Riordan, C. (1986). Simple solar spectral model for direct and diffuse irradiance on horizontal and tilted planes at the earth's surface for cloudless atmospheres. *Journal of Climate and Applied Meteorology, 25(1),* 87-97.

Bishop, M.P.; Colby, J.D. (2002). Anisotropic reflectance correction of SPOT-3 HRV imagery. *International Journal of Remote Sensing, 23*, 2125-2131.

Bishop, M.P.; Shroder Jr. J.F.; Colby, J.D. (2003). Remote sensing and geomorphometry for studying relief production in high mountains. *Geomorphology, 55*, 345-361.

Blesius, L.; Weirich, F. (2005). The use of the Minnaert correction for land cover classification in mountainous terrain. *International Journal of Remote Sensing, 26*, 3831-3851.

Bo, L.; Rui, Y.; Hongxu, J. (2011). Remote-Sensing Image Compression Using Two-Dimensional Oriented Wavelet Transform. *IEEE Transactions on Geoscience and Remote Sensing , 49*, 236-250.

Borner, A.; Wiest, L.; Keller, P.; Reulke, R.; Richter, R.; Schaepman, M.; Schlapfer, D. (2001). SENSOR: a tool for the simulation of hyperspectral remote sensing systems. *ISPRS Journal of Photogrammetry and Remote Sensing, 55*, 299-312.

Brunet, D.; Vrscay, E.R.; Wang, Z. (2012). On the Mathematical Properties of the Structural Similarity Index. *IEEE Transactions on Image Processing, 21*, 1488-1499.

Chavez, P.S. (1988). An improved dark-object subtraction technique for atmospheric scattering correction of multispectral data, *Remote Sensing of Environment, 24,* 459-479.

Chavez, P.S. (1996). Image-based atmospheric corrections-revisited and improved. *Photogramm Eng Remote Sensing, 62,* 1025-1035.

Cihlar, J. (2000). Land cover mapping of large areas from satellites: status and research priorities, *International Journal of Remote Sensing, 21,* 1093-1114.

Civco, D.L. (1989). Topographic Normalization of Landsat Thematic Mapper Digital Imagery. *Photogrammetric Engineering & Remote Sensing, 55*, 1303-1309.

Clark, R.N.; Swayze, G.A.; Wise, R.; Livo, E.; Hoefen, T.; Kokaly, R.; Sutley, S.J. (2007). USGS digital spectral library splib06a: U.S. Geological Survey, Digital Data Series 231. Available online: http://speclab.cr.usgs.gov/spectral.lib06.

Colby, J.D. (1991) Topographic normalization in rugged terrain. *Photogrammetric Engineering and Remote Sensing, 57,* 531-537.

Conese, C.; Gilabert, M.; Maselli, F.; Bottai, L. (1993). Topographic normalization of TM scenes through the use of an atmospheric correction method and digital terrain models. *Photogrammetric Engineering and Remote Sensing, 59*, 1745-1753.

Couturier, S.; Gastellu-Etchegorry, J.P.; Martin, E.; Patiño, P. (2013). Building a Forward-Mode Three-Dimensional Reflectance Model for Topographic Normalization of High-Resolution (1-5 m) Imagery: Validation Phase in a Forested Environment. *IEEE Transactions on Geoscience and Remote Sensing, 51*, 3910-3921.

Datcu, M.; Holecz, F. (1993). Generation of synthetic images for the alleviation of radiometric influence induced by the topography. In, Proceedings of SPIE – The International Society for Optical Engineering (pp. 260-271).

Dozier, J.; Bruno, J.; Downey, P. (1981). A faster solution to the horizon problem. *Computers & Geosciences, 7*, 145-151.

Dumortier, D. (1995). Mesure, analyse et modélisation du gisement lumineux. Application à l'évaluation des performances de l'éclairage naturel des bâtiments. In, Université de Savoie, France.

Dumortier, D. (1998). The satellight model of turbidity variations in Europe In, *Report 6th SATELLIGHT meeting*. Freiburg (Germany).

Dymond, J.R.; Shepherd, J.D. (1999). Correction of the topographic effect in remote sensing. *IEEE Transactions on Geoscience and Remote Sensing, 37*, 2618-2620.

E.E.A. European Environmental Agency. Corine land cover. Available online: http://www.eea.europa.eu/publications/COR0-landcover (accessed 15 September 2015).

Ediriweera, S.; Pathirana, S.; Danaher, T.; Nichols, D.; Moffiet, T. (2013). Evaluation of different topographic corrections for Landsat TM data by prediction of foliage projective cover (FPC) in topographically complex landscapes. *Remote Sensing, 5*, 6767-6789.

Ehlers, M.; Klonus, S.; Johan Åstrand, P.; Rosso, P. (2010). Multi-sensor image fusion for pansharpening in remote sensing. *International Journal of Image and Data Fusion, 1*, 25-45.

Ekstrand, S. (1996). Landsat TM-based forest damage assessment: Correction for topographic effects. *Photogrammetric Engineering & Remote Sensing, 62*, 151-161.

Fan, Y.; Koukal, T.; Weisberg, P.J. (2014). A sun–crown–sensor model and adapted C-correction logic for topographic correction of high resolution forest imagery. *ISPRS Journal of Photogrammetry and Remote Sensing, 96*, 94-105.

Foody, G. M.; Mathur, A. (2004). A relative evaluation of multiclass image classification by support vector machines. *IEEE Transactions on Geoscience and Remote Sensing, 42,* 1335-1343.

Füreder, P. (2010). Topographic correction of satellite images for improved LULC classification in alpine areas. In, *10th International Symposium on High Mountain Remote Sensing Cartography* (pp. 187 - 194). Kathmandu, Nepal: Grazer Schriften der Geographie und Raumforschung.

Gao, M.L.; Zhao, W.J.; Gong, Z.N.; Gong, H.L.; Chen, Z.; Tang, X.M. (2014). Topographic Correction of ZY-3 Satellite Images and Its Effects on Estimation of Shrub Leaf Biomass in Mountainous Areas. *Remote Sensing, 6*, 2745-2764.

Gao, Y.N.; Zhang, W.C. (2007). Variable Empirical Coefficient Algorithm for removal of topographic effects on remotely sensed data from rugged terrain. In, IGARSS 2007. *International Geoscience and Remote Sensing Symposium* (pp. 4733-4736).

Gao, Y.N.; Zhang, W.C. (2009a). LULC Classification and Topographic Correction of Landsat-7 ETM+ Imagery in the Yangjia River Watershed: the Influence of DEM Resolution. *Sensors, 9*, 1980-1995.

Gao, Y.N.; Zhang, W.C. (2009b). A simple empirical topographic correction method for ETM plus imagery. *International Journal of Remote Sensing, 30*, 2259-2275.

Ghasemi, N.; Mohammadzadeh, A.; Reza Sahebi, M. (2013). Assessment of different topographic correction methods in ALOS AVNIR-2 data over a forest area. *International Journal of Digital Earth*, *6(5),* 504-520.

Gilabert, M.A.; Conese, C.; Maselli, F. (1994). An Atmospheric Correction Method for the Automatic Retrieval of Surface Reflectances from TM Images. *International Journal of Remote Sensing, 15*, 2065-2086.

Gleriani, J.M.; Homem, M.A.; Soares, V.P.; Ribeiro, C.A.A.S. (2012). Land cover variation of Minnaert constant for topographic correction on Thematic Mapper. In, IGARSS 2012. *International Geoscience and Remote Sensing Symposium* (pp. 2210-2212).

Gobierno de Navarra (2012). Mapa de Cultivos y Aprovechamientos de Navarra 1/25.000. (URL: http://www.cfnavarra.es/agricultura/informacion_agraria/MapaCultivos/index2.html (accessed 04/2015).

Gobierno Vasco (2007). Cartografía de hábitats, vegetación actual y usos del suelo de la Comunidad Autónoma del País Vasco. (URL: http://www.geo.euskadi.eus/geograficos/habitats-vegetacion-actual-y-usos-del-suelo/s69-geodir/es/ (accessed 04/2015).

Goslee, S.C. (2012). Topographic Corrections of Satellite Data for Regional Monitoring. *Photogrammetric Engineering and Remote Sensing, 78*, 973-981.

Gu, D.; Gillespie, A. (1998). Topographic normalization of Landsat TM images of forest based on subpixel Sun-canopy-sensor geometry. *Remote Sensing of Environment, 64*, 166-175.

Guanter, L.; Segl, K.; Kaufmann, H. (2009). Simulation of Optical Remote-Sensing Scenes With Application to the EnMAP Hyperspectral Mission. *IEEE Transactions on Geoscience and Remote Sensing, 47*, 2340 – 2351.

Gueymard, C. (1995). SMARTS2, a simple model of the atmospheric radiative transfer of sunshine: Algorithms and performance assessment. In, Florida Solar Energy Center, pp. 1-84.

Hantson, S.; Chuvieco, E. (2011). Evaluation of different topographic correction methods for Landsat imagery. *International Journal of Applied Observation and Geoinformation, 13,* 691-700.

Hay, J.E.; McKay, D.C. (1985). Estimating solar irradiance on inclined surfaces: a review and assessment of methodologies. *International Journal of Solar Energy, 3*, 230-240.

Hoshikawa, K.; Umezaki, M. (2014). Effects of terrain-induced shade removal using global DEM data sets on land cover classification. *International Journal of Remote Sensing, 35*, 1331-1355.

Hottel, H.C.; Whiller, A. (1958). Evaluation of fiat plate solar collector performance. In, *Conference on Use of Solar Energy, The Scientific Basis* (p. 74).

Ineichen, P. (1998). Report 6th SATELLIGHT meeting. In, *Radiation Derivation from Meteosat Counts*. Freiburg (Germany).

Itten, K.I.; Meyer, P.; Kellenberger, T.; Leu, R.; Sandmeier, S.; Bitter, P. (1992). Radiometric and Geometric Correction of TM-Data of Mountainous Forested Areas. *International Space Year: Space Remote Sensing, Vols 1 and 2*, 1650-1652.

Itten, K.I.; Meyer, P. (1993). Geometric and radiometric correction of TM-Data of mountainous forested areas. *IEEE Transactions on Geoscience and Remote Sensing, 31*, 764-770.

Jeromin, O.; Pattichis, M.S. (2012). Multiscale Sampling Geometries and Methods for Deterministic and Stochastic Reconstructions of Magnitude and Phase Spectra of Satellite Imagery. *IEEE Transactions on Geoscience and Remote Sensing, 50*, 3678-3692.

Kane V. R.; Gillespie A. R.; McGaughey R.; Lutz J. A.; Ceder K.; Franklin J. F. (2008). Interpretation and topographic compensation of conifer canopy self-shadowing. *Remote Sensing of Environment*, 112, 3820-3832.

Karathanassi, V.; Andronis, V.; Rokos, D. (2000). Evaluation of the topographic normalization methods for a Mediterranean forest area. *International Archives of Photogrammetry and Remote Sensing, 33,* 654-661.

Kasten, F. (1996). The Linke turbidity factor based on improved values of the integral Rayleigh optical thickness. *Solar Energy, 56*, 239-244.

Kasten, F.; Young, A.T. (1989). Revised optical air tables and approximation formula. *Applied Optics, 28*, 4735-4738.

Kobayashi, S.; Sanga-Ngoie, K. (2008). The integrated radiometric correction of optical remote sensing imageries. *International Journal of Remote Sensing, 29*, 5957-5985.

Kobayashi, S.; Sanga-Ngoie, K. (2009). A comparative study of radiometric correction methods for optical remote sensing imagery: The IRC vs. other image-based C-correction methods. *International Journal of Remote Sensing, 30*, 285-314.

Köppen climate classification. Available online: http://en.wikipedia.org/wiki/K%C3%B6ppen_climate_classification (accessed 10 November 2015).

Lambin, E. F.; H. J. Geist. (2008). Land Use and Land Cover Change, Local Processes and Global Impacts, *Springer Science & Business Media*.

Law, K.H.; Nichol, J. (2004). Topographic correction for differential illumination effects on IKONOS satellite imagery. In, *The International Archives of the Photogrammetry, Remote Sensing and Spatial Information Sciences* (pp. 641-646).

Leprieur, C.E.; Durand, J.M. (1988). Influence of topography on forest reflectance using Landsat Thematic Mapper and digital terrain. *Photogrammetric Engineering and Remote Sensing, 54,* 491-496.

Ling, Y.; Ehlers, M.; Usery, E.L.; Madden, M. (2007). FFT-enhanced IHS transform method for fusing high-resolution satellite images. *ISPRS Journal of Photogrammetry and Remote Sensing, 61*, 381-392.

Liu, B.Y.H.; Jordan, R.C. (1960). The interrelationship and characteristic distribution of direct, diffuse and total solar radiation. *Solar Energy, 4(3),* 1-19.

Louche, A.; Peri, G.; Iqbal, M. (1986). An analysis of the Linke turbidity factor. *Solar Energy, 37*, 393-396.

Lu, D.S.; Ge, H.L.; He, S.Z.; Xu, A.J.; Zhou, G.M.; Du, H.Q. (2008). Pixel-based Minnaert Correction Method for Reducing Topographic Effects on a Landsat 7 ETM+ Image. *Photogrammetric Engineering and Remote Sensing, 74*, 1343-1350.

Lunetta, R.S.; Elvidge, C.D. (1999) Remote sensing change detection: Environmental monitoring methods and applications. *Taylor & Francis Ltd*.

Ma, C.C.Y.; Iqbal, M. (1984). Statistical comparison of solar radiation correlation. Monthly average global and diffuse radiation on horizontal surfaces. *Solar Energy, 33(2),* 143-148.

Mariotto, I.; Gutschick, V.P. (2010). Non-Lambertian Corrected Albedo and Vegetation Index for Estimating Land Evapotranspiration in a Heterogeneous Semi-Arid Landscape. *Remote Sensing,* 2, 926.

Masek, J. G.; Huang, C.; Wolfe, R.; Cohen, W.; Hall, F.; Kutler, J. et al. (2008). North American forest disturbance mapped from a decadal Landsat record. *Remote Sensing of Environment, 112,* 2914–2926.

Matsushita, B.; Yang, W.; Chen, J.; Onda, Y.; Qiu, G. (2007). Sensitivity of the enhanced vegetation index (EVI) and normalized difference vegetation index (NDVI) to topographic effects: A case study in high-density cypress forest. *Sensors*, 7, 2636-2651.

McDonald, E.R.; Wu, X.; Caccetta, P.A. (2002). Illumination correction of Landsat TM data in south east NSW. In, *10th Australasian Remote Sensing Conference*.

Meyer, P.; Itten, K.I.; Kellenberger, T.; Sandmeier, S.; Sandmeier, R. (1993). Radiometric corrections of topographically induced effects on Landsat TM Data in an alpine environment. *ISPRS Journal of Photogrammetry and Remote Sensing, 48*, 17-28.

Minnaert, M. (1941). The reciprocity principle in lunar photometry. *Astrophysical Journal, 93*, 403-410.

Moran, M.S.; Jackson, R.D.; Slater, P.N.; Teillet P.M. (1992). Evaluation of simplified procedures for retrieval of land surface reflectance factors from satellite sensor output. *Remote Sensing of Environment, 41*, 169-184.

Moreira, E.P.; Valeriano, M.M. (2014). Application and evaluation of topographic correction methods to improve land cover mapping using object-based classification. *International Journal of Applied Earth Observation and Geoinformation, 32*, 208-217.

Mulder, N.J. (1988). Digital image processing, computer-aided classification and mapping. In *Vegetation Mapping*, A.W. Küchler and I.S. Zonneveld (Eds), pp. 269–316 ((Dordrecht: Kluwer Academic Press).

Nagol, J.R.; Sexton, J.O.; Kim, D.-H.; Anand, A.; Morton, D.; Vermote, E.; Townshend, J.R. (2014). Bidirectional effects in Landsat reflectance estimates: Is there a problem to solve? *ISPRS Journal of Photogrammetry and Remote Sensing, 103,* 129-135.

Nichol, J.; Hang, L.K.; Sing, W.M. (2006). Empirical correction of low Sun angle images in steeply sloping terrain: a slope-matching technique. *International Journal of Remote Sensing, 27*, 629-635.

Notarnicola, C.; Callegari, M.; De Gregorio, L.; Sonnenschein, R.; Remelgado, R.; Ventura, B. (2014). A novel topographic correction for high and medium resolution images by using combined solar radiation. In, IGARSS 2014. *International Geoscience and Remote Sensing Symposium* (pp. 1053-1056).

Ono, A.; Kajiwara, K.; Honda, Y. (2007). Development of Vegetation Index Using Radiant Spectra Normalized by their Arithmetic Mean. In, Proceedings *42nd Conference of the Remote Sensing Society of Japan*, (pp. 99–100).

Page, J. (1996). Algorithms for the SATELLIGHT programme. In, *Technical Report 2nd SATELLIGHT meeting* Bergen.

Parente, M.; Trevor Clark, J.; Brown, A.J.; Bishop, J.L. (2010). End-to-End Simulation and Analytical Model of Remote-Sensing Systems: Application to CRISM. *IEEE Transactions on Geoscience and Remote Sensing, 48,* 3877-3888.

Pons, X.; Pesquer, L.; Cristóbal, J.; González-Guerrero O. (2014). Automatic and improved radiometric correction of Landsat imagery using reference values from MODIS surface reflectance images. *International Journal of Applied Earth Observation and Geoinformation*, *33,* 243-254.

Proy, C.; Tanré, D.; Deschamps, P. Y. (1989). Evaluation of topographic effects in remotely sensed data. *Remote Sensing of Environment, 30*, 21-32.

Reese, H.; Olsson, H. (2011). C-correction of optical satellite data over alpine vegetation areas: A comparison of sampling strategies for determining the empirical c-parameter. *Remote Sensing of Environment, 115*, 1387-1400.

Rezazadeh, S.; Coulombe, S. (2009). A novel approach for computing and pooling Structural SIMilarity index in the discrete wavelet domain. In, *16th IEEE International Conference on Image Process* (pp. 2209-2212).

Riaño, D.; Chuvieco, E.; Salas, J.; Aguado, I. (2003). Assessment of different topographic corrections in Landsat-TM data for mapping vegetation types. *IEEE Transactions on Geoscience and Remote Sensing, 41*, 1056-1061.

Richter, R. (1998). Correction of satellite imagery over mountainous terrain. *Applied Optics, 37*, 4004-4015.

Richter, R.; Schläpfer, D. (2002). Geo-atmospheric processing of airborne imaging spectrometry data. Part 2: Atmospheric/topographic correction. *International Journal of Remote Sensing, 23*, 2631-2649.

Richter, R.; Kellenberger, T.; Kaufmann, H. (2009). Comparison of topographic correction methods. *Remote Sensing, 1*, 184-196.

Richter, R.; Schläpfer, D. (2015). ATCOR-2/3 User Guide, Version 9.0.0. Available online: http://www.rese.ch/pdf/atcor3_manual.pdf

Rodriguez-Galiano, V.F.; Pardo-Igúzquiza, E.; Chica-Olmo, M.; Mateos, J.; Rigol-Sánchez, J.P.; Vega, M. (2012). A comparative assessment of different methods for Landsat 7/ETM+ pansharpening. *International Journal of Remote Sensing, 33*, 6574-6599.

Sandmeier, S.; Itten, K.I. (1997). A Physically-Based Model to Correct Atmospheric and Illumination Effects in Optical Satellite Data of Rugged Terrain. *IEEE Transactions on Geoscience and Remote Sensing, 35*, 708-717.

Schulmann, T.; Katurji, M.; Zawar-Reza, P. (2015). Seeing through shadow: Modelling surface irradiance for topographic correction of Landsat ETM+ data. *ISPRS Journal of Photogrammetry and Remote Sensing, 99,* 14-24.

Shepherd, J.D.; Dymond, J.R. (2003). Correcting satellite imagery for the variance of reflectance and illumination with topography. *International Journal of Remote Sensing, 24*, 3503-3514.

Shepherd, J. D.; Dymond, J. R.; Gillingham, S.; Bunting, P. (2014). Accurate registration of optical satellite imagery with elevation models for topographic correction. *Remote Sensing Letters, 5,* 637-641.

Singh, M.; Mishra, V.; Thakur, N.; Sharma, J.D. (2015). Expansion of Empirical-Statistical Based Topographic Correction Algorithm for Reflectance Modeling on Himalayan Terrain using AWiFS and MODIS Sensor. *Journal of the Indian Society of Remote Sensing*, 1-10.

Smith, J.A.; Lin, T.L.; Ranson, K.J. (1980). The Lambertian Assumption and Landsat Data. *Photogrammetric Engineering and Remote Sensing, 46*, 1183-1189.

Soccorsi, M.; Gleich, D.; Datcu, M. (2010). Huber-2013; Markov Model for Complex SAR Image Restoration. *IEEE Geoscience and Remote Sensing Letters, 7*, 63-67.

Soenen, S.A.; Peddle, D.R.; Coburn, C.A. (2005). SCS+C: A modified sun-canopy-sensor topographic correction in forested terrain. *IEEE Transactions on Geoscience and Remote Sensing, 43*, 2148-2159.

Soenen, S.A.; Peddle, D.R.; Coburn, C.A., Hall, R.J.; Hall, F.G. (2008). Improved topographic correction of forest image data using a 3-D canopy reflectance model in multiple forward mode. *International Journal of Remote Sensing, 29*, 1007-1027.

Soenen, S.A.; Peddle, D.R.; Coburn, C.A.; Hall, R.J.; Hall, F.G. (2009). Canopy Reflectance Model Inversion in Multiple Forward Mode: Forest Structural Information Retrieval from Solution Set Distributions. *Photogrammetric Engineering and Remote Sensing, 75*, 361-374.

Sola, I.; González-Audícana, M.; Álvarez-Mozos, J.; Torres, J.L. (2011). Utilidad de las imágenes sintéticas para la determinación de la bondad de distintos algoritmos de corrección topográfica. In, XIV AET Congress (Mieres, Spain), 21-23 September 2011.

Sola, I.; González-Audícana, M.; Álvarez-Mozos, J.; Torres, J.L. (2012). Multitemporal evaluation of topographic correction algorithms using synthetic images. In, Proceedings of SPIE – *The International Society for Optical Engineering* (pp. 853706-853706).

Sola, I.; González-Audícana, M.; Álvarez-Mozos, J.; Torres, J.L. (2014a). Synthetic images for evaluating Topographic Correction Algorithms. *IEEE Transactions on Geoscience and Remote Sensing, 52*, 1799-1810.

Sola, I.; González-Audícana, M.; Álvarez-Mozos, J.; Torres, J.L. (2014b). Evaluación multitemporal de métodos de corrección topográfica mediante el uso de imágenes sintéticas multiespectrales. *Revista Teledetección, 41*, 71-78.

Sola, I.; González-Audícana, M.; Álvarez-Mozos, J. (2015a). Validation of a simplified model to generate multispectral synthetic images. *Remote Sensing*, 7, 2942-2951.

Sola, I.; González-Audícana, M.; Álvarez-Mozos, J. (2015b). Multi-criteria evaluation of topographic correction methods. *Remote Sensing of Environment*. Under review.

Sola, I.; González-Audícana, M.; Álvarez-Mozos, J. (2015c). Efecto de errores en el co-registro entre MDT e imagen de satélite en la calidad de la corrección topográfica. In, XVI AET Congress (Sevilla, Spain), 21-23 October 2015.

Sola, I.; González-Audícana M.; Álvarez-Mozos, J. (2015d). On the added value of stratified topographic correction of multispectral images. *Remote Sensing*. Under review.

Szantoi, Z.; Simonetti, D. (2013). Fast and Robust Topographic Correction Method for Medium Resolution Satellite Imagery Using a Stratified Approach. *Selected Topics in IEEE Journal of Applied Earth Observations and Remote Sensing, 6,* 1921-1933.

Tan, B.; Wolfe, R.; Masek, J.; Feng, G.; Vermote, E.F. (2010). An illumination correction algorithm on Landsat-TM data. In, IGARSS 2010. *International Geoscience and Remote Sensing Symposium* (pp. 1964-1967).

Tan, B.; Masek, J.G.; Wolfe, R.; Gao, F.; Huang, C.; Vermote, E.F.; Sexton, J.O.; Ederer, G. (2013). Improved forest change detection with terrain illumination corrected Landsat images. *Remote Sensing of Environment, 136*, 469-483.

Teillet, P.M.; Guindon, B.; Goodenough, D.G. (1982). On the slope-aspect correction of multispectral scanner data. *Canadian Journal of Remote Sensing, 8*, 84-106.

The DIRSIG User's Manual. In R.I.o. Technology (Ed.), *Digital Imaging Remote Sensing Laboratory. Available: http://dirsig.org/docs/manual/index.html Rochester Institute of Technology (2006)*.

Tokola, T.; Sarkeala, J.; Van der Linden, M. (2001). Use of topographic correction in Landsat TM-based forest interpretation in Nepal. *International Journal of Remote Sensing, 22*, 551-563.

Törmä, M.; Härmä, P. (2003). Topographic Correction of Landsat ETM images in Finnish Lapland. In, IGARSS 2003. *International Geoscience and Remote Sensing Symposium* (pp. 3629-3631).

Tukey, J.W. (1977). Box-and-whisker plots. In, *Exploratory Data Analysis* Reading. Addison-Wesley, MA, 39-43.

Twele, A.; Erasmi, S. (2005). Evaluating topographic correction algorithms for improved land cover discrimination in mountainous areas of central Sulawesi. In, S. Erasmi, B. Cyffka, & Kappas; (Eds.), *Remote Sensing & GIS for environmental studies*. Göttingen.

Twele, A.; Kappas, M.; Lauer, J.; Erasmi, S. (2006). The effect of stratified topographic correction on land cover classificacion in tropical mountainous regions. In, *ISPRS Technical Commission VII Symposium* (pp. 432-437).

Vanonckelen, S.; Lhermitte, S.; Van Rompaey, A. (2013). The effect of atmospheric and topographic correction methods on land cover classification accuracy. *International Journal of Applied Earth Observation and Geoinformation, 24*, 9-21.

Vanonckelen, S.; Lhermitte, S.; Balthazar, V.; Van Rompaey, A. (2014). Performance of atmospheric and topographic correction methods on Landsat imagery in mountain areas. *International Journal of Remote Sensing, 35*, 4952-4972.

Vanonckelen, S.; Lhermitte, S.; Van Rompaey, A. (2015). The effect of atmospheric and topographic correction on pixel-based image composites: Improved forest cover detection in mountain environments. *International Journal of Applied Earth Observation and Geoinformation, 35, Part B*, 320-328.

Veraverbeke, S.; Verstraeten, W.W.; Lhermitte, S.; Goossens, R. (2010). Illumination effects on the differenced Normalized Burn Ratio's optimality for assessing fire severity. *International Journal of Applied Observation and Geoinformation, 12*, 60-70.

Verhoef, W.; Bach, H. (2012). Simulation of Sentinel-3 images by four-stream surface-atmosphere radiative transfer modeling in the optical and thermal domains. *Remote Sensing of Environment, 120*, 197-207.

Vicente-Serrano, S.M.; Pérez-Cabello, F.; Lasanta, T. (2008). Assessment of radiometric correction techniques in analyzing vegetation variability and change using time series of Landsat images. *Remote Sensing of Environment, 112*, 3916-3934.

Vincini, M.; Reeder, D.; Frazzi, E. (2002). An empirical topographic normalization method for forest TM data. In, IGARSS 2002. *International Geoscience and Remote Sensing Symposium* (pp. 2091-2093).

Vincini, M.; Frazzi, E. (2003). Multitemporal evaluation of topographic normalization methods on deciduous forest TM data. *IEEE Transactions on Geoscience and Remote Sensing, 41,* 2586-2590.

Wang, Z.; Bovik, A.C. (2002). A Universal Image Quality Index. *IEEE Signal Processing Letter, 9,* 81-84.

Wang, Z.; Bovik, A.C.; Sheikh, H.R.; Simoncelli, E.P. (2004). Image Quality Assessment: From Error Visibility to Structural Similarity. *IEEE Transactions on Image Processing, 13*, 600-612.

Wang, Z.; Bovik, A.C.; Simoncelli, E.P. (2005). *Handbook of Image and Video Processing, 2nd edition*.

Wen, J.G.; Liu, Q.H.; Liu, Q.; Xiao, Q.; Li, X.W. (2009). Parametrized BRDF for atmospheric and topographic correction and albedo estimation in Jiangxi rugged terrain, China. *International Journal of Remote Sensing, 30,* 2875-2896.

Wu, J.; Bauer, M.E.; Wang, D.; Manson, S.M. (2008). A comparison of illumination geometry-based methods for topographic correction of QuickBird images of an undulant area. *ISPRS Journal of Photogrammetric Remote Sensing, 63*, 223-236.

Xiaolong, D.; Khorram, S. (1998) The effects of image misregistration on the accuracy of remotely sensed change detection. *IEEE Transactions on Geoscience and Remote Sensing, 36,* 1566-1577.

Yuan, Q.; Zhang, L.; Shen, H. (2012). Hyperspectral Image Denoising Employing a Spectral–Spatial Adaptive Total Variation Model. *IEEE Transactions on Geoscience and Remote Sensing, 50*, 3660-3677.

Yue, C.; Jiang, W. (2012). SAR image denoising in nonsubsampled contourlet transform domain based on maximum a posteriori and non-local constraint. *Remote Sensing Letters, 4*, 270-278.

Zakšek, K., Oštir, K., & Kokalj, Ž. (2011). Sky-View Factor as a Relief Visualization Technique. *Remote Sensing, 3*, 398-415.

Zhan, X.; Sohlberg, R.A., Townshend, J.R.G., DiMiceli, C., Carroll, M.L., Eastman, J.C., Hansen, M.C., & DeFries, R.S. (2002). Detection of land cover changes using MODIS 250 m data. *Remote Sensing of Environment, 83*, 336-350.

Zhang, W.C.; Gao, Y.N. (2011). Topographic correction algorithm for remotely sensed data accounting for indirect irradiance. *International Journal of Remote Sensing, 32*, 1807-1824.

Zhang, Y.; Yan, G.; Bai, Y. (2015). Sensitivity of Topographic Correction to the DEM Spatial Scale. *IEEE Geoscience and Remote Sensing Letters, 12*, 53-57.